

Università degli Studi di Milano
Dottorato di Ricerca in Chimica del Farmaco. Ciclo XV
Facoltà di Farmacia

**Synthesis, in silico and pharmacological
evaluation of 2-pyridin-acetamides as tyrosine
kinase inhibitors**

PhD Thesis of
Alessandro Contini
Matr. n. R03750

Docente Guida: chiar.ma prof. P. TRIMARCO
Coordinatore: chiar.mo prof. C. DE MICHELI

Index

Chapter 1

Organic Synthesis

1. Amidines as precursors for heterocycles synthesis	1
2. Synthesis of 2-pyridinacetamides	8
3. Experimental	18

Chapter 2

Pharmacology

1. Background	39
2. Receptors Tyrosine Kinases	40
3. Pharmacological methods and results	47

Chapter 3

Medicinal Chemistry

1. Structure-activity relationship	55
2. Docking of 2-pyridinacetamides to receptors tyrosine kinases	59
3. Docking of 2-pyridinacetamides to EGFRK	66
4. Docking of 2-pyridinacetamides to PDGFRK	81
5. Docking of 2-pyridinacetamides to VEGFR2K	92
6. Docking of 2-pyridinacetamides to FGFR1K	100
7. Experimental	106

Chapter 4

1. Conclusions	110
2. Acknowledgments	112

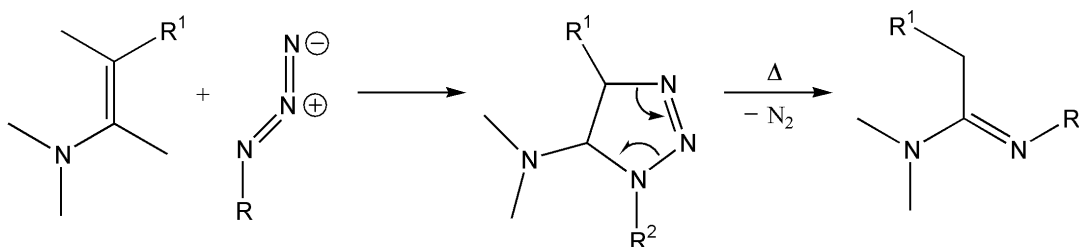
Chapter 1

Organic Synthesis

1. Amidines as precursors for heterocycles synthesis

Since several years in our laboratories we studied the role of amidines as precursors of heterocyclic compounds. The key step in the synthesis of such amidines is the 1-3 dipolar cycloaddition between an olefinic dipolarophile, usually an enamine, and a substituted azido derivative to yield a triazoline derivative that undergoes thermal rearrangement furnishing the corresponding amidine.

Scheme 1



Such rearrangement was observed for the first time by prof. Fusco¹ in 1961 making available a new route to amidinic synthones.

In our labs, tertiary amidines were successfully converted into several heterocyclic compounds, including substituted quinolines², quinoxalines³ and quinazoline⁴. Furthermore substituted amidines were used in the synthesis of amino-imidazolines and imidazoles⁵.

As could be noticed by *Scheme 2*, the synthetic versatility of tertiary amidines is strictly related to the functionalization of the azido precursor.

In a recent study we synthesized 5-amino- ν -triazolines bearing at N-1 a pyranonic ring. Thermal rearrangement of the investigated dihydro- ν -triazoles gave a mixture of nitrogen functionalized tertiary amidines and 1H-pyrano[4,3-b]pyrrol-4-ones. *Scheme 3* shows that by choosing the appropriate reaction conditions it was possible to achieve selectively one or the other product⁶.

1 R. Fusco, G. Bianchetti, D. Pocar, *Gazz. Chim. Ital.*, **1961**, 91, 933-957.

2 E. Beccalli, E. Erba, L.M. Gelmi, D. Pocar, *J.C.S. Perkins I*, **1996**, 1206.

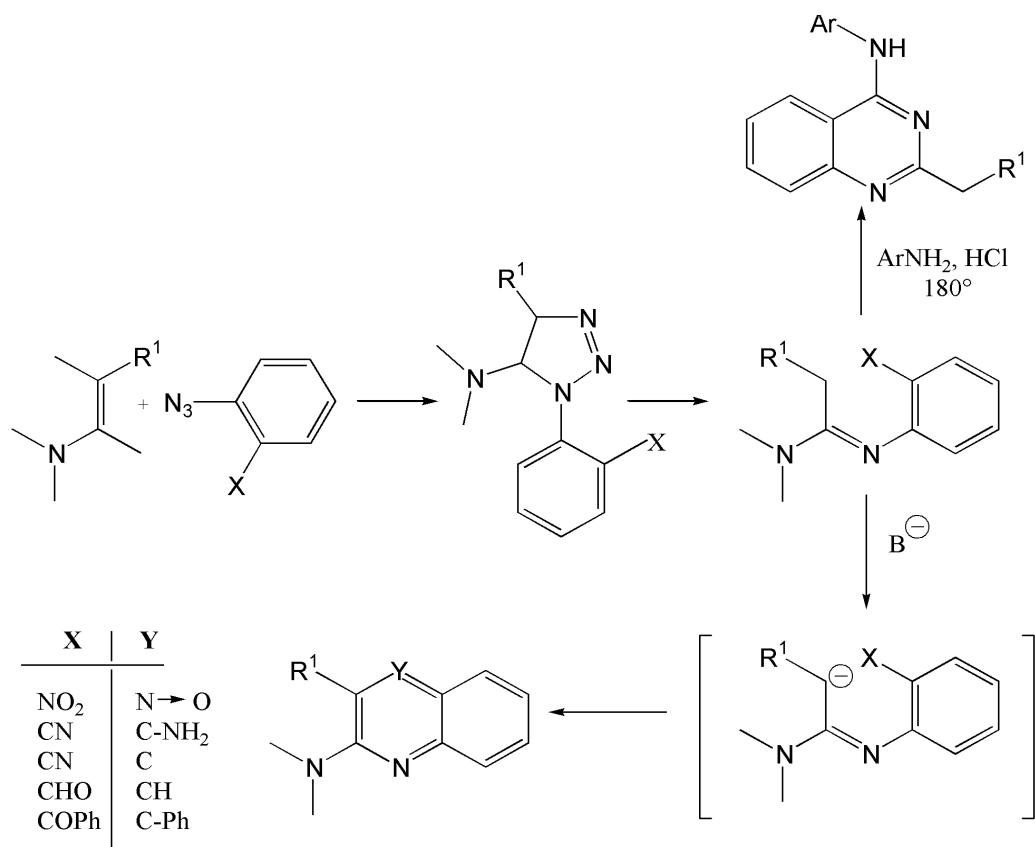
3 Battistini, E. Erba, *Synthesis*, **1992**, 1206.

4 E. Erba, D. Sporchia, *J.C.S. Perkins I*, **1997**, 3021.

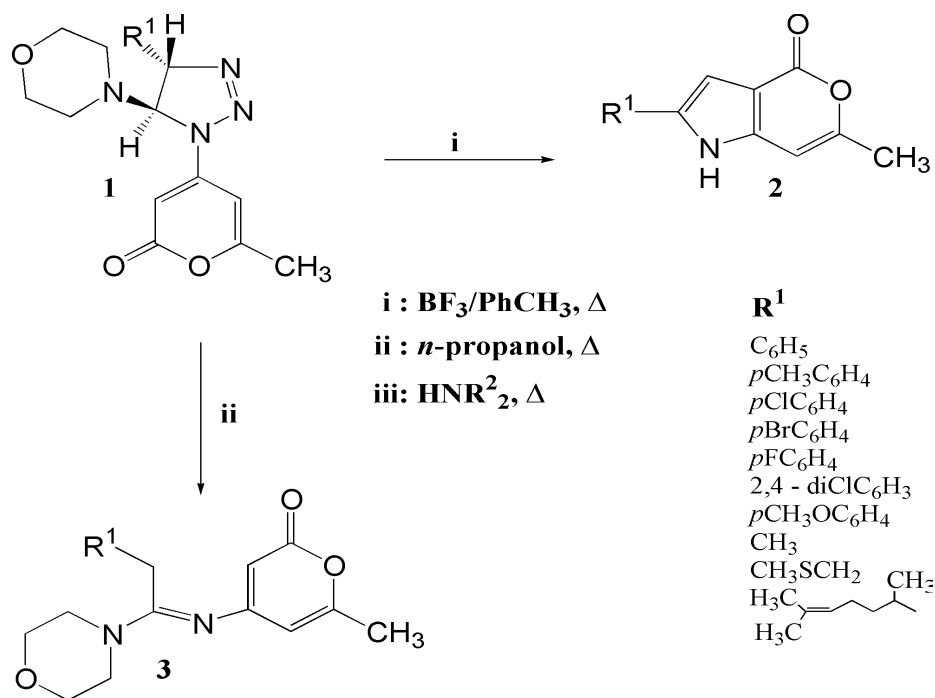
5 L. Citerio, D. Pocar, R. Stradi and B. Gioia, *J.C.S. Perkins I*, **1978**, 4, 309-314.

6 E. Erba, D. Pocar and P. Trimarco, *J.C.S. Perkins I*, **2001**, 14, 1723-1728.

Scheme 2



Scheme 3



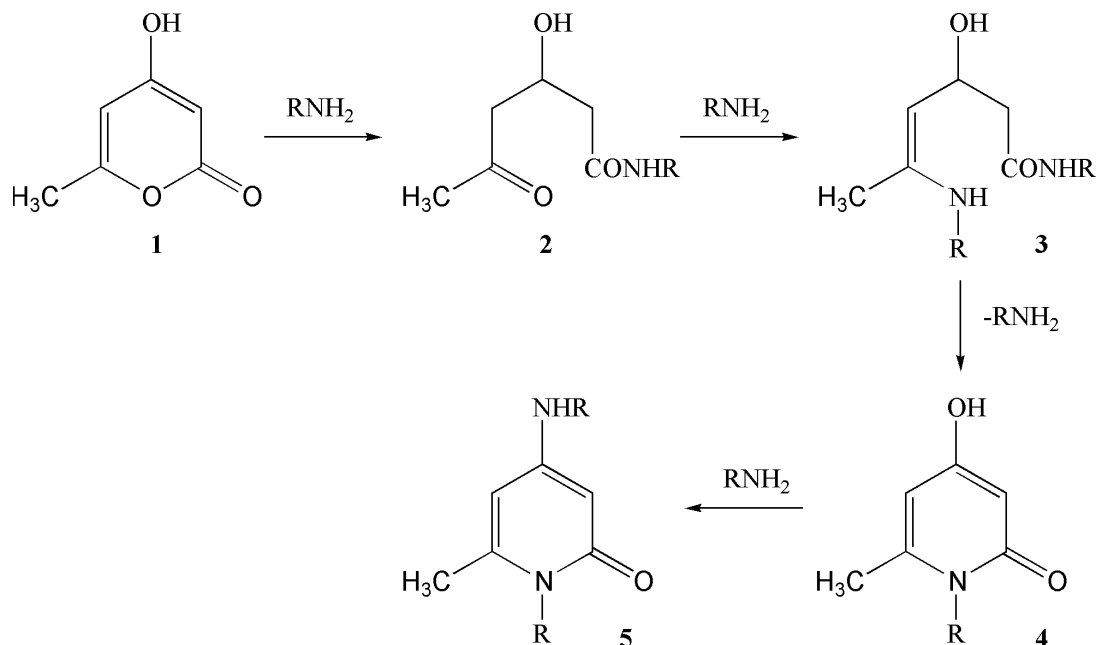
The choice of the pyrone substituent was made for mainly two reasons: it's occurrence in many natural products and it's peculiar reactivity. Specifically, it was our interest to explore the possibility of the triacetic lactone to react with nucleophiles. It is known that several kind of nucleophiles can react with pyran-2-one at C-2 and at C-6 causing initial ring opening⁷. However reactions resulting in opening of the pyrone ring without transformation into a different cyclic product are relatively uncommon, because highly functionalized open-chain compounds arising from pyronic ring opening exhibit a strong tendency to cyclize again into new heterocycles. Several examples of transformation of triacetic lactone into 4-hydroxy-2-pyridones by treatment with ammonia and primary amines have been reported. *Scheme 4* shows an example in which the treatment of triacetic lactone with an excess of primary amine results first in a nucleophilic attack at C-2, then enamine formation and ring condensation and finally nucleophilic substitution at

⁷ (a) G.P. Ellis, *Comprehensive Heterocyclic Chemistry*, A.J. Boulton, A. McKillop, Eds.; Pergamon: Oxford, 1984; Vol. 3, p 681 and references cited therein.

(b) M. Mañas, R. Pleixats, *Adv. Heterocycl. Chem.*, **1992**, 53, 59 and references cited therein.

C4.

Scheme 4



Diketoamide **2** and amidine **3** have been isolated, and independent conversion of **4** into **5** has also been reported, suggesting a ranking of electrophilic reactivity $\text{C-2} > \text{C-6} > \text{C-4}$.

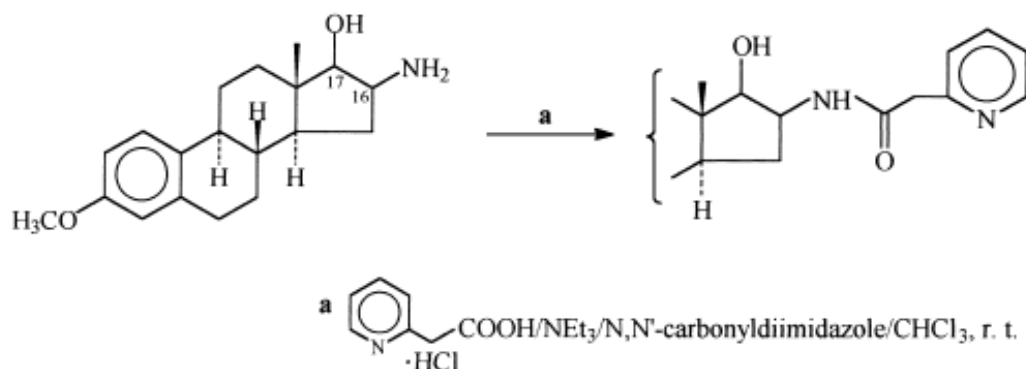
It has been reported that the methylene group linked to a amidine tertiary function is easily transformed into carbanion able to react in intra molecular nucleophilic condensations⁴. With the support of such theoretical preambles we decided to exploit either pyran-2-one nucleus reactivity and nucleophilic carbon atom on C- α to amidine group with the purpose to find a satisfactory route to synthesize functionalized 2-pyridinacetamides that are of general interest owing to the presence of similar structures in several compounds with antiarrhythmic⁸, anti HIV and enzymatic inhibitory activity⁹. Literature reports examples for the synthesis of amides derived from 2-pyridinacetic acid. For example M. Gonschior et. al reported the synthesis for N-[2-(2-pyridyl)ethyl]amino and N,N-bis[2-(2-pyridyl)ethyl]amino steroids, through an amidic intermediate¹⁰ (Scheme 5):

⁸ C. Bernhart et al., *J. Med. Chem.*, **1983**, 26, 451-455

⁹ D. R. Sliskovic et al, *J. Med. Chem.*, **1998**, 41, 682-690.

¹⁰ M. Gonschior et. al, *Tetrahedron: Asymmetry*, **2000**, 11, 2159-2182

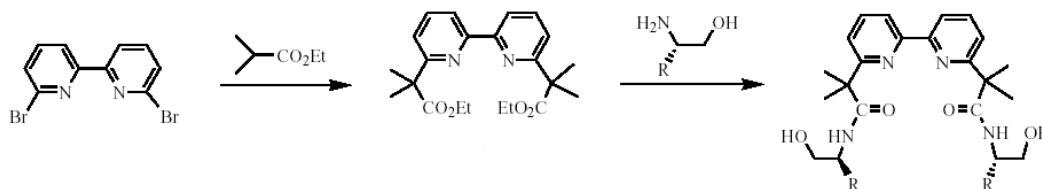
Scheme 5



Such synthetic scheme uses commercial 2-pyridinacetic acid hydrochloride, and therefore yields only unsubstituted amides.

More versatile could be the way adopted by Zhou et. al for the synthesis of chiral bis(oxazoliny)lbi pyridine ligands¹¹, in which the amide is obtained from directly from the ester (*Scheme 6*):

Scheme 6



Although the amidation step requires 7 days of reflux in xylene, and therefore is not so practical. For this reason we thought there was the need for new versatile synthesis for substituted 2-pyridinacetamides.

The first question that arose was if a pyrone ring substituted at C-5 with an amidinic moiety could maintain the same reactivity as unsubstituted triacetic lactone toward nucleophiles. Politzer et. al reported that *ab-initio* electrostatic potential calculations could help in identifying most reactive sites toward nucleophilic attacks, by mapping the calculated electrostatic potential on a $0.002 \text{ e}/\text{bohr}^3$ isodensity

¹¹ Qi-Lin Zhou et al, *Tetrahedron: Asymmetry*, **2002**, 13, 161-165

surface¹²; it has been shown, for a group of diatomic molecules and for methane, that this contour gives physically reasonable molecular dimensions, and encompasses at least 95% of the electronic charge. As shown in Equation 1, such potential derives from the difference between the positive nuclear contribution (first term) and the negative electronic contribution (second term). Equation 1 expresses rigorously the electrostatic potential $V(\mathbf{r})$ at any point \mathbf{r} in the space of a molecule.

Equation 1

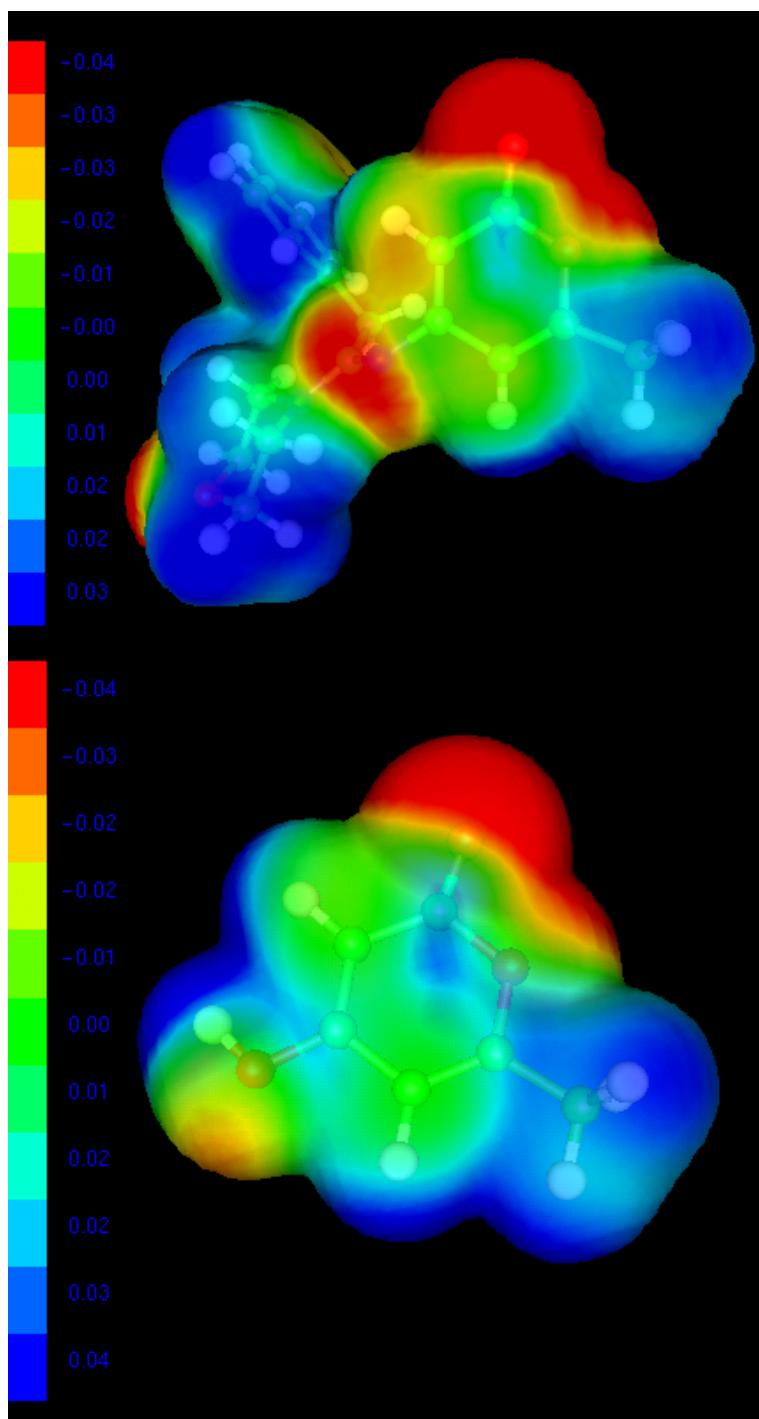
$$V(\mathbf{r}) = \sum_A \frac{Z_A}{|\mathbf{R}_A - \mathbf{r}|} - \int \frac{\rho(\mathbf{r}') d\mathbf{r}'}{|\mathbf{r}' - \mathbf{r}|}$$

Z_A is the charge on nucleus A , located at R_A , and $\rho(\mathbf{r})$ is the electronic density function of the molecule, which can be obtained by an *ab initio* self-consistent-field (SCF) molecular orbital approach. Then, in order to answer our question, we performed *ab initio* calculations at the HF/6-31G** level on both unsubstituted triacetic lactone and 5-amidino substituted pyrone. Figure 1 represents resulted electrostatic potential mapped on a 0.002 el/bohr³ isodensity surface; it's evident that the positive charge (blue) on the pyronic ring for both triacetic lactone and amidine is well localized mainly on carbons 2 and 6. However we notice a reduction of the positive potential intensity for amidine substituted pyronic C-2, with a value similar to that of C-6. This could result in lower selectivity between C-2 and C-6 nucleophilic attack. Must also be noted that the electrostatic potential on amidino-pyronic C-4 tends to be negative, while on pyronic C-4 is positive; this suggest us that nucleophilic substitution on amidino-pyronic C-4 should not happen.

Those preliminary data suggested us that the synthetic path designed to obtain 2-pyridineacetamides should be possible.

12 Politzer et al. *J. Phys. Chem.*, **1991**, 95, 844-848.

Figure 1

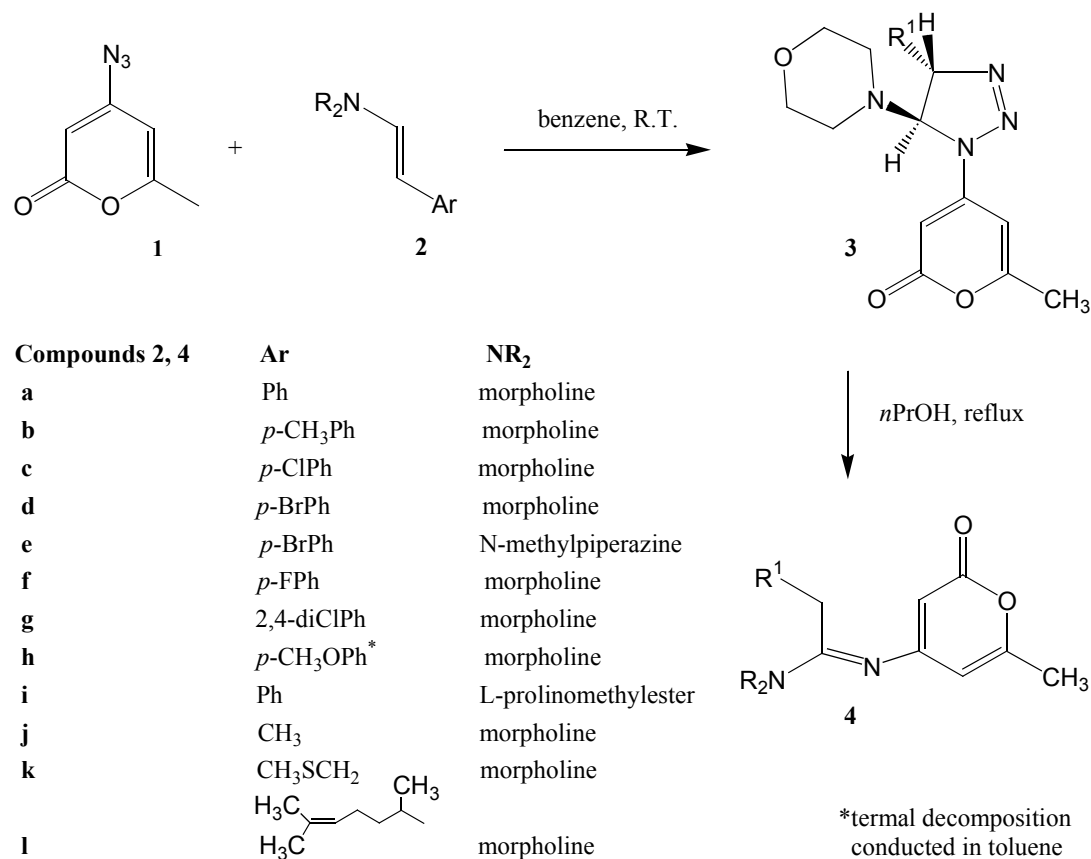


electrostatic potential calculations: positive potential values are distributed mainly on C-2 and C-6 of the pyranonic ring; C-2 and C-4 amidine values are lower compared with pyranonic C-2 and C-4

2. Synthesis of 2-pyridinacetamides

We recently described the preparation of 4,5-dihydro-*v*-triazoles **3a-d, f, h-j** from cycloaddition of azide **1** and appropriate enamines **2** in benzene solution⁶ (Scheme 1).

Scheme1

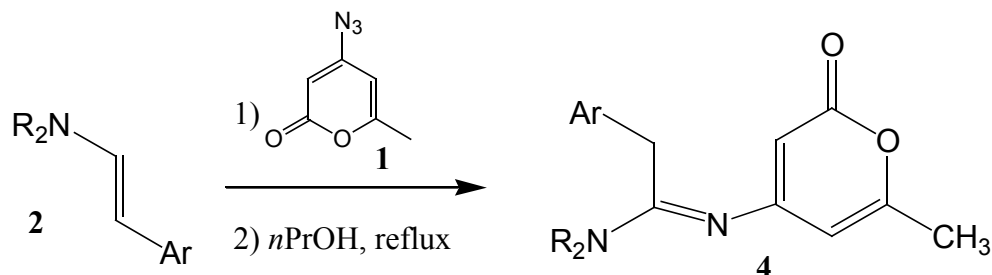


Compounds **3** have *trans* configuration, as they show a NMR coupling constant of about 3Hz. Compounds **3** when heated in boiling *n*-propanol or in toluene gave the corresponding amidines **4**. It is well known the cleavage of the N(1)-N(2) bond in the 4,5-dihydro-*v*-triazole nucleus is made easier by electron-withdrawing groups on N-1¹³. Concerning aromatic substituted amidines, further optimization of this reaction scheme resulted in not isolating the dihydro-*v*-triazoles **3** but reacting enamines **2** with the azido derivative **1** directly in *n*-propanol for 2 hours at room

13 P.K.B. Kadaba, B. Stanovnik, M. Tišler, *Adv. Heterocycl. Chem.*, **1984**, 37, 339 and references cited therein.

temperature and then refluxing the reaction mixture for 2 hours (*Scheme 2*).

Scheme 2

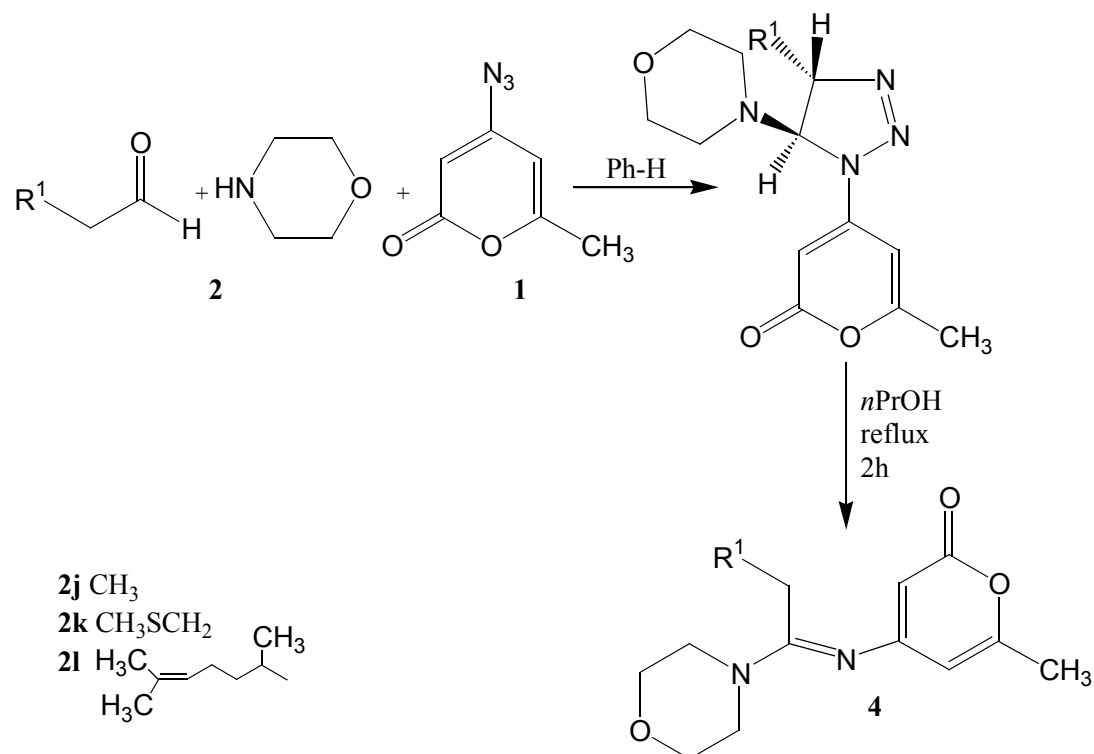


Compounds 2 , 4	Ar	NR ₂
a	Ph	morpholine
b	<i>p</i> -CH ₃ Ph	morpholine
c	<i>p</i> -ClPh	morpholine
d	<i>p</i> -BrPh	morpholine
e	<i>p</i> -BrPh	N-methylpiperazine
f	<i>p</i> -FPh	morpholine
g	2,4-diClPh	morpholine
h	<i>p</i> -CH ₃ OPh	morpholine
i	Ph	L-prolinomethylester

The amidino compounds, according to *Scheme 2* are collected as precipitate just by cooling the *n*-propanol solution. Enamines **2** has been prepared by reaction of the corresponding benzaldehyde and morpholine, N-methylpiperazine and L-prolinomethylester. We synthesized enamines bearing different amines, such as piperidine or pyrrolidine, but further reaction with azidopyrone **1** led to aromatic triazoles. This behavior has already been reported¹⁴ and it's probably due to the increased basicity of those amines. Alifatic amidines has been synthesized by one pot reaction between the corresponding aldehyde, morpholine and azidopyrone **1**. In this case, however, isolation of the triazoline intermediate **3** was necessary in order to obtain good yields in amidine **4** (*Scheme 3*)

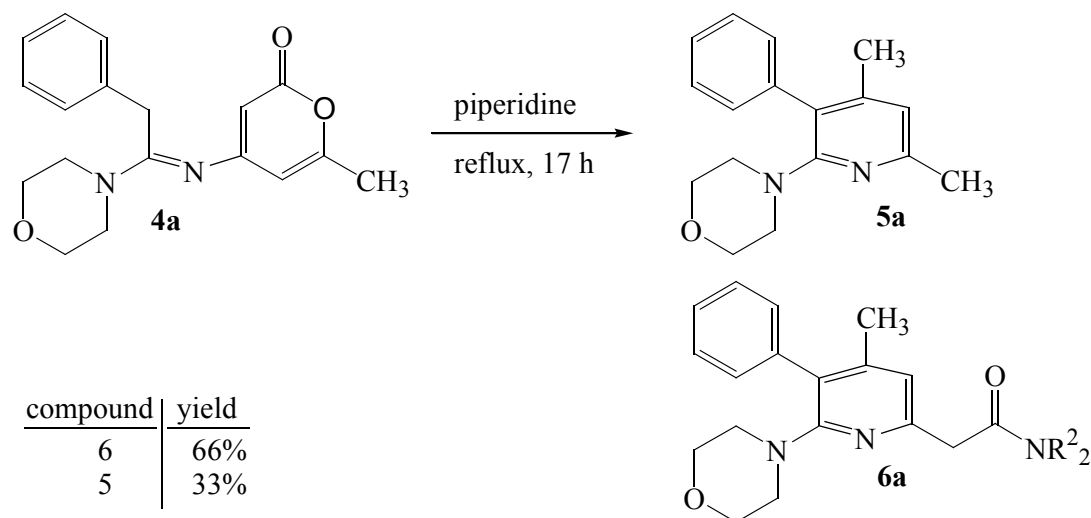
¹⁴ S. Cilloni, D. Pocar, L. M. Rossi and P. Trimarco, *Journal of Chemical Research, Synopses*, **1980**, *1*, 4

Scheme 3



During our preliminary experiment the 6-methyl-4-(1-morpholino-2-phenylethylideneamino)-2*H*-pyran-2-one **4** was refluxed in piperidine as solvent and after 17 hours turned into a mixture of substituted pyridines **5** and **6** in the ratio of 1:2 (*Scheme 4*).

Scheme 4

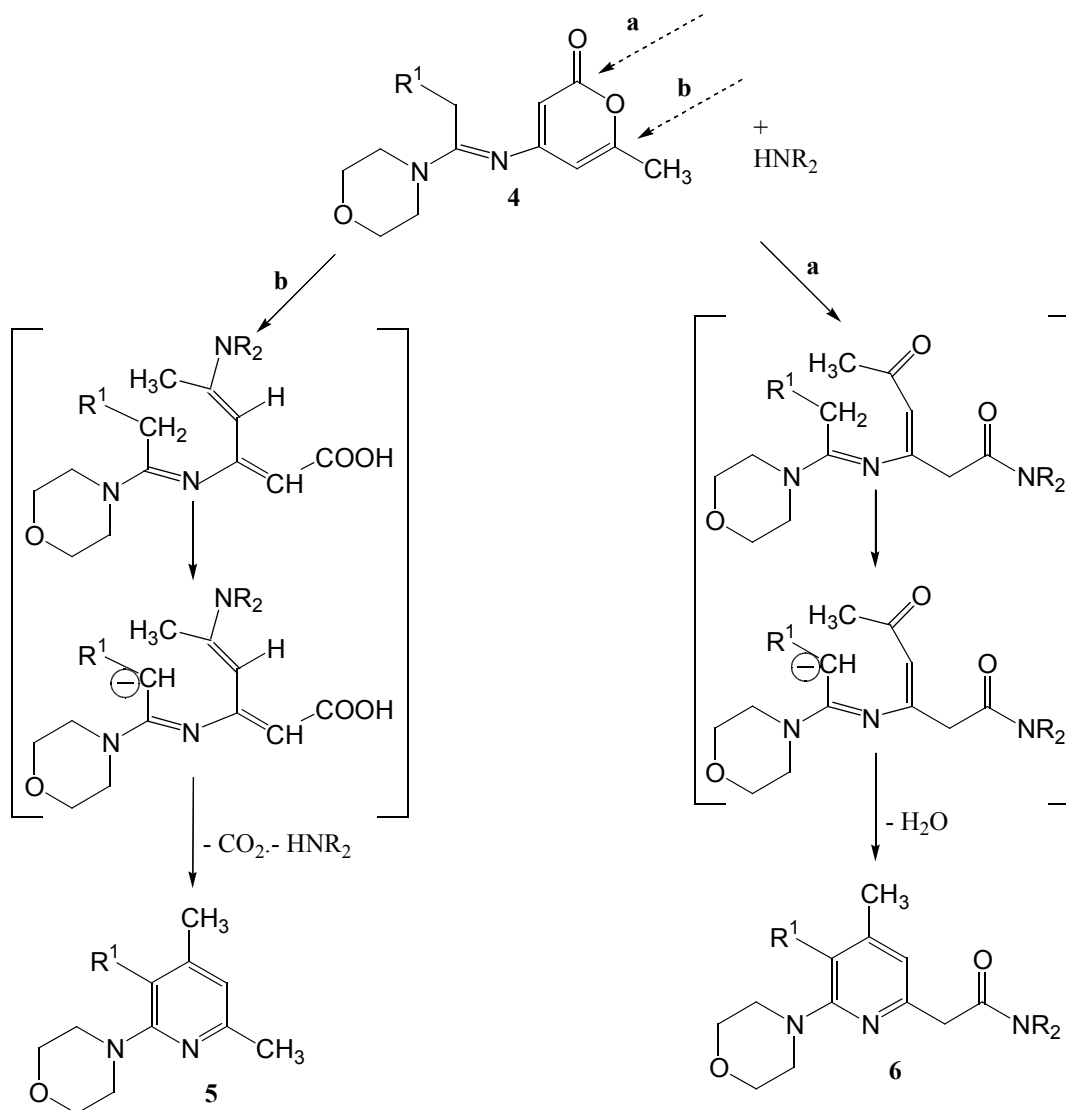


Their spectral data were in agreement with the proposed structures and with available data in literature for similar substitution pattern¹⁵. ¹³C-NMR spectrum of 2-pyridineacetamide **6** showed the signals related to CH-3 at about 119 ppm and to amide carbonyl group at 169 ppm, the latter was validated also by IR stretching at 1630 cm⁻¹. ¹H NMR was characterized by three singlets (2.06 δ, 3.80 δ and 6.87 δ) associated with CH₃ on C-4, CH₂ linked to amide carbonyl group on C-2 and H-3 on C-3, respectively. In ¹H NMR spectrum of 4,6-dimethylpyridine derivative **5** three singlets at 2.05, 2.44 and 6.70 δ associated respectively with the methyl groups linked to C-4 and C-2 and H-3 of the pyridine ring appeared diagnostic.

It can be quite reasonable to assume that **5** and **6** come from two different pathways, which seem competitive in these reaction conditions (*Scheme 5*).

15 (a) C.D. Johnson, *Comprehensive Heterocyclic Chemistry*, A. J. Boulton and A. Mc Killop, Ed, Pergamon, Oxford, **1984**, 2, 117-124 and ref. cited therein. (b) *Atlas of Spectral Data and Physical Constants for Organic Compounds*, 2nd Edition, J. G. Grasselli, and W. M. Ritchey, Ed. CRC Press, Cleveland, **1975**, 4, 373-408. (c) C. J. Pourchert, J. Behnke, *The Aldrich Library of ¹³C and ¹H FT-NMR Spectra*, 1st Edition, Aldrich Chemical Co., Milwaukee, **1993**. (d) E. Pretsch, J. Seibl, T. Clerc, W. Simon, *Tables of Spectral Data for Structure Determination of Organic Compounds*, 2nd Edition, Springer-Verlag, New York, **1989**.

Scheme 5

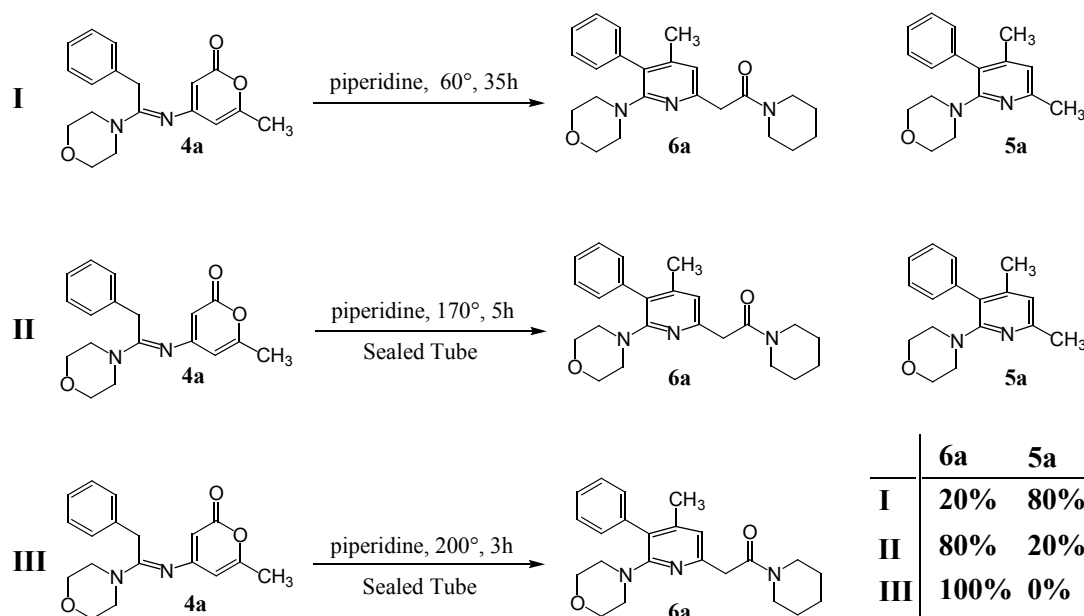


According to *path a* the pyridine amide derivative **6a** resulted from the nucleophilic attack of the amino group on the C-2 position of 2-pyranone nucleus followed by ring opening and intra molecular cyclization, by way of the C- α amidinic carbanion intermediate. According to *path b* the formation of 4,6-dimethylpyridine derivative **5a** is rationalized as follows: addition of the amino group on the C-6 position of the pyran-2-one nucleus, ring opening, followed by ring closure of the C- α amidinic carbanion intermediate. The final product **5a** was achieved after decarboxylation step, as it is well known on the pyridine nucleus¹⁶, and amino group elimination favored by aromatization to give pyridine ring.

16 T. Naito, R. Dohmori, T. Kotake, *Chem. Pharm. Bull.* **1964**, *12*, 588-90.

To confirm the proposed mechanism and to determine the best conditions to enhance the yield of amide derivatives **6** we decided to investigate the reaction closely (*Scheme 6*).

Scheme 6

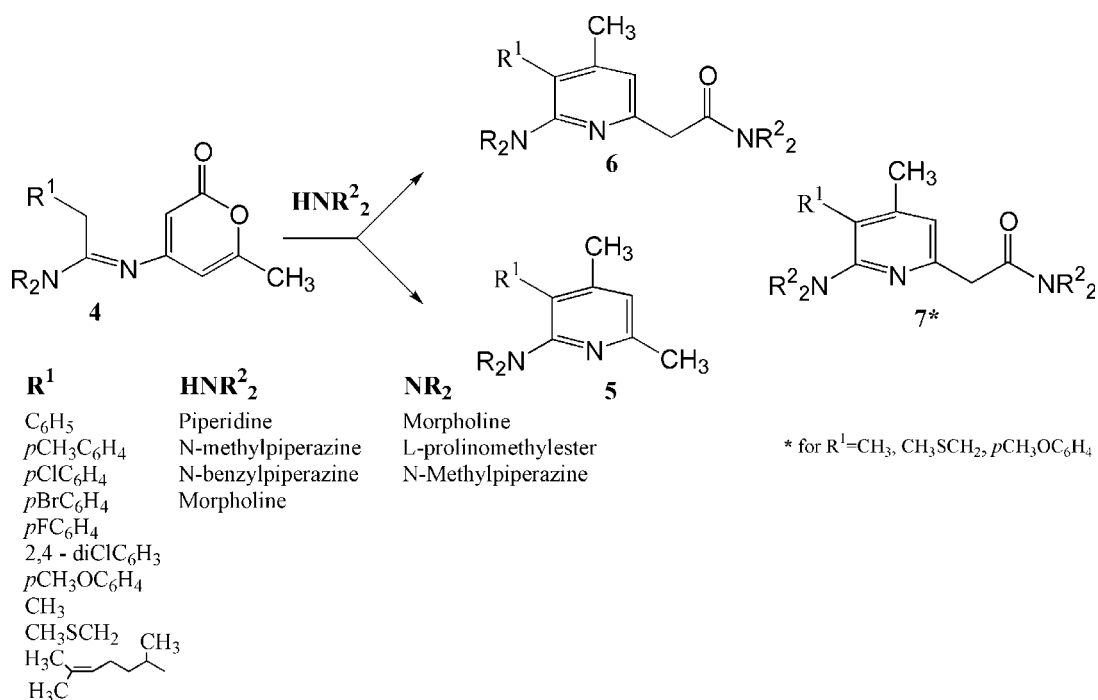


The reaction of the amidine **4** in piperidine as solvent at 60°C for 35 hours afforded a reaction mixture containing 15% of amide **6** and pyridine **5** in 85% yield. During subsequent experiments the piperidine and the amidine **4** were mixed in a sealed tube and put in a preheated oil bath at 170°C and then at 200°C. Significant improvements in yields were achieved by these reaction conditions. Just in 5 hours at 170°C the major isomer was shown to be the 2-pyridineacetamide **6** (88%) beside the 4,6-dimethylpyridine **5** in 12% yield. The ratio of **5** and **6** in the mixture was determined by ¹H-NMR analysis. In fact the different hydrogen shift on C-3 for **5** and **6** (6.70 δ and 6.87 δ respectively) allowed a clear difference between the two pyridines obtained. Performing the reaction at 200°C, the amide derivative **6** was only obtained.

These results point out that under mild conditions the nucleophilic addition on the C-6 (*path b*) prevails, but at higher temperatures the addition product to C-2 position (*path a*) is favored. In order to verify that **5** does not arise from hydrolysis

of amide **6**, this product was reacted 35 hours at 60°C under the most favorable conditions to **5** formation. The ¹H-NMR spectrum of the crude mixture showed only the signals of amide derivative **6a**, thus confirming the independence of paths leading to **5** and **6**, respectively. We thought therefore to extend the reaction to all the amidines reported in *Scheme 1* and perform the reaction at 200°C (*Scheme 7*)

Scheme 7

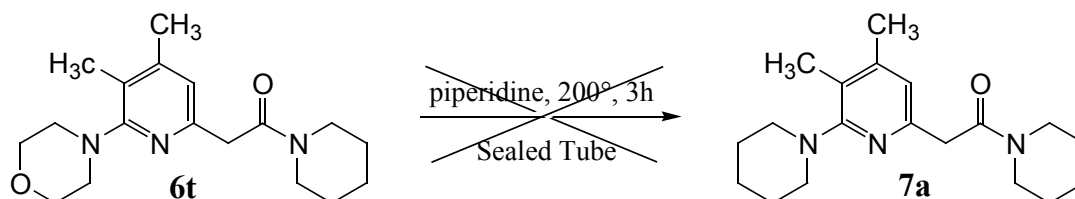


Amidines **4** were mixed with an excess of secondary amine HNR^2_2 in a sealed tube and put in preheated oil bath at 200°C. The transformation required a reaction time within 2-4 hours.

Probably the high temperature of the reaction mixture was responsible in some cases of low yields besides the formation of polymerised material. The best results were achieved from the amidines **4** bearing an aromatic or better an haloaromatic substituent and suggest that the yields of the amide derivatives **6** are depending on easy deprotonation of methylene group bound to aryl substituents. Under these reaction conditions most of the amidines **4** were converted into the expected pyridineacetamides **6**, however amidines bearing a *p*-methoxyphenyl, methyl or methylsulfanylmethyl substituent gave a mixture of two amide derivatives **6** and **7**.

Confirmation of the structures was obtained from both ^1H and ^{13}C NMR of the purified materials obtained in a ratio of about 2:1, respectively. It can be reasonably assumed that amides **7** arise from a transamidation reaction of the corresponding amidines or of their intermediate compounds. Amine exchange reaction has already been studied¹⁷ on formamidines. Considering that the key synthetic step in the formation of pyridine nucleus was the final cyclization of the C- α amidinic carbanion intermediate, the difficult formation of ethyl, methylsulfanylethyl or even *p*-methoxyphenyl carbanions could explain the low yield of the desired amides **6** and the concomitant formation of the amides **7**. In order to verify that the amides **7** do not arise from nucleophilic attack on C- α of the pyridine nucleus¹⁸, the amide **6** 5-methyl substituted was treated with a large amount of piperidine and heated in a sealed tube for 4 hours, under the same previously adopted conditions. ^1H NMR analysis of the crude reaction mixture showed only the amide **6** peaks and confirmed transamidation hypothesis. (Scheme 8)

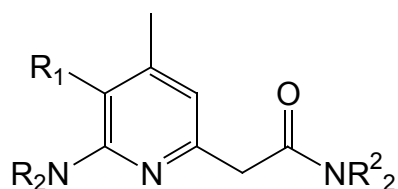
Scheme 8



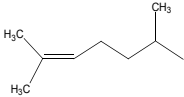
Results of reactions between amidines **4** and a secondary amine are collected in Table 1.

17 Furth, P. S.; Reitmann, M. S.; Cook, A. F. *Tetrahedron Lett.*, **1997**, 38, 5403-5406

18 Vorbrüggen, H. *Adv. Heterocycl. Chem.*, **1990**, 49, 142.

Table 1

R^1	NR_2	NR^2_2	Time (h)	6(%) [*]	7(%) [*]
C_6H_5	morpholine	piperidine	4	70	
C_6H_5	morpholine	N-methylpiperazine	3	72	
C_6H_5	morpholine	morpholine	2.5	85	
C_6H_5	morpholine	diethylamine	2	65	
C_6H_5	morpholine	N-benzylpiperazine	2	65	
C_6H_5	prolinomethylester	morpholine	2	35	
$pCH_3-C_6H_4$	morpholine	piperidine	4	67	
$pOCH_3-C_6H_4$	morpholine	piperidine	7	46	15
$pCl-C_6H_4$	morpholine	piperidine	2,5	70	
$pCl-C_6H_4$	morpholine	N-methylpiperazine	2,5	73	
$pBr-C_6H_4$	morpholine	piperidine	2,5	60	
$pBr-C_6H_4$	morpholine	N-methylpiperazine	2,5	65	
$pBr-C_6H_4$	morpholine	morpholine	2,5	75	
$pBr-C_6H_4$	morpholine	N-carbethoxypiperaz.	4	53	
$pBr-C_6H_4$	N-methylpiperazine	N-methylpiperazine	2	66	
$pF-C_6H_4$	morpholine	piperidine	2,5	65	
$pF-C_6H_4$	morpholine	N-methylpiperazine	2,5	70	
2,4 diCl- C_6H_4	morpholine	N-methylpiperazine	4		65
CH_3	morpholine	piperidine	4	40	20
CH_3	morpholine	N-methylpiperazine	3	57	26
CH_3SCH_2	morpholine	N-methylpiperazine	2	42	23

R^1	NR_2	NR^2_2	Time (h)	6(%) [*]	7(%) [*]
	morpholine	N-methylpiperazine	2	35	Not isolated

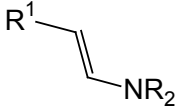
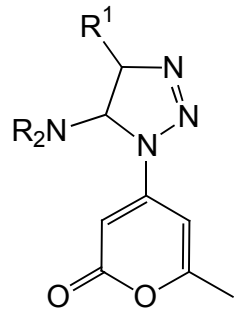
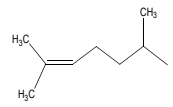
(*yield calculated on isolated product)

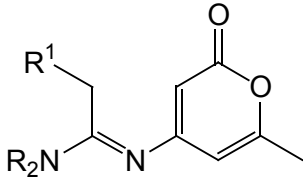
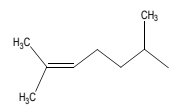
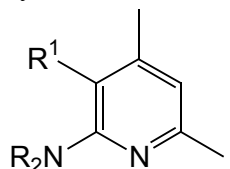
Concluding, these results demonstrated the double reactivity of the amidines functionalized at iminic nitrogen with pyran-2-one nucleus and the synthetic potentiality of the substrate. In this case the amidines became part of a wide chapter of the synthetic methodology to obtain functionalized pyridines.

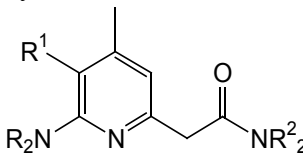
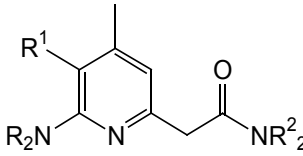
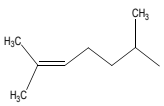
3. Experimental

A list of products described in this experimental section is represented in Table 2

Table 2

	<i>Class</i>	<i>N</i> ^o	<i>R</i> ¹	<i>NR</i> ₂	<i>HNR</i> ² ₂
	<i>Enamines 2</i>	2a	Ph	morpholine	
		2b	<i>p</i> -CH ₃ Ph	morpholine	
		2c	<i>p</i> -ClPh	morpholine	
		2d	<i>p</i> -BrPh	morpholine	
		2e	<i>p</i> -BrPh	N-methylpip.	
		2f	<i>p</i> -FPh	morpholine	
		2g	2,4-diClPh	morpholine	
		2h	<i>p</i> -CH ₃ OPh	morpholine	
		2i	Ph	Prolinomethylester	
				r	
	<i>Triazolines 3</i>	3a	Ph	morpholine	
		3b	<i>p</i> -CH ₃ Ph	morpholine	
		3c	<i>p</i> -ClPh	morpholine	
		3d	<i>p</i> -BrPh	morpholine	
		3e	<i>p</i> -BrPh	N-methylpip.	
		3f	<i>p</i> -FPh	morpholine	
		3g	2,4-diClPh	morpholine	
		3h	<i>p</i> -CH ₃ OPh	morpholine	
		3i	Ph	Prolinomethylester	
		3j	CH ₃	r	
		3k	CH ₃ SCH ₂	morpholine	
		3l		morpholine	

<i>Class</i>	<i>N</i> ^o	<i>R</i> ¹	<i>NR</i> ₂	<i>HNR</i> ²
Amidines 4 	4a	Ph	morpholine	
	4b	<i>p</i> -CH ₃ Ph	morpholine	
	4c	<i>p</i> -ClPh	morpholine	
	4d	<i>p</i> -BrPh	morpholine	
	4e	<i>p</i> -BrPh	N-methylpip.	
	4f	<i>p</i> -FPh	morpholine	
	4g	2,4-diClPh	morpholine	
	4h	<i>p</i> -CH ₃ OPh	morpholine	
	4i	Ph	prolinomethylester	
	4j	CH ₃	morpholine	
	4k	CH ₃ SCH ₂	morpholine	
	4l		morpholine	
Pyridines 5 	5a	Ph	morpholine	

<i>Class</i>	<i>N</i> ^o	<i>R</i> ¹	<i>NR</i> ₂	<i>HNR</i> ² ₂
Pyridines 6 	6a	Ph	morpholine	piperidine
	6b	Ph	morpholine	N-methylpip.
	6c	Ph	morpholine	N-benzylpip.
	6d	Ph	morpholine	morpholine
	6e	Ph	morpholine	diethylamine
	6f	Ph	prolinomethylester	morpholine
	6g	<i>p</i> CH ₃ Ph	morpholine	piperidine
	6h	<i>p</i> ClPh	morpholine	piperidine
	6i	<i>p</i> ClPh	morpholine	N-methylpip.
	6j	<i>p</i> BrPh	morpholine	piperidine
	6k	<i>p</i> BrPh	morpholine	N-methylpip.
	6l	<i>p</i> BrPh	morpholine	N-carboxyethylpip.
	6m	<i>p</i> BrPh	morpholine	morpholine
	6n	<i>p</i> BrPh	morpholine	diethylamine
	6o	<i>p</i> BrPh	N-methylpip.	N-methylpip.
	6p	<i>p</i> F-Ph	morpholine	piperidine
	6q	<i>p</i> F-Ph	morpholine	N-methylpip.
	6r	2,4-diClPh	morpholine	N-methylpip.
	6s	<i>p</i> CH ₃ O-Ph	morpholine	piperidine
	6t	CH ₃	morpholine	piperidine
Pyridines 7 	7a	CH ₃	piperidine	piperidine
	7b	CH ₃	N-methylpip.	N-methylpip.
	7c	CH ₃ SCH ₂	N-methylpip.	N-methylpip.
	7d	<i>p</i> CH ₃ O-Ph	piperidine	piperidine
	6v	CH ₃ SCH ₂	morpholine	N-methylpip.
	6w		morpholine	N-methylpip.

Melting points were determined using a Buchi 510 (capillary) or an Electrothermal 9100 apparatus and are uncorrected. IR spectra were measured using a JASCO IR Report 100 instrument. ¹H and ¹³C-NMR spectra (tetramethylsilane as internal standard) were recorded with EM Varian Gemini 200, Bruker AC 200 and Bruker

Avance 300 Spectrometers. J-Values are given in Hz for solutions in CDCl₃. Column chromatography was performed on Kieselgel 60 (Merck) 0.063-0.200 mm with eluents and ratios indicated in Experimental.

Materials. 2,4-Dichlorophenylacetaldehyde, azide **1**¹⁹ and enamines **2a**, **b**, **d**^{20a}, **2c**^{20b}, **2f**, **2h**^{20c} and **2i**^{20d} have already been described. 4,5-dihydrotriazoles **3a-d**, **3f**, **3h**, **3j** and amidines **4a-d**, **3f**, **3h**, **3j** are known compounds⁶.

When referring to derivatives **2i**, **3i**, **4i**, and **6f** stereochemistry will not be indicated as it's typical of the commercial aminoacid pyrrolidine-2*S*-carboxylic acid methyl ester and the stereocenter is not involved in the reaction. For compounds **3l**, and **6w** the stereochemistry is that of the commercial racemic 2,6-dimethyl-hept-5-enal.

Quantum mechanical computations has been performed using programs GAMESS²¹ version 20 June 2002 (R2) and PCGAMESS²² version 6.2. Geometries has been completely optimized at RHF level using the 6-31G**²³ basis set; minima where confirmed by vibrational analysis and no imaginary frequencies were observed; linear dependence threshold (QMTTOL) was set at 1x10⁻⁷, HONDO/Rys integrals were used for all integrals (INTTYP=HONDO) and DIIS converger was used instead that SOSCF. Geometries has been optimized using GAMESS on a HP64000 machine running HP-UX at CILEA.²⁴

Electrostatic potential calculations has been performed on a Linux-PC using PCGAMESS, while plots of electrostatic potential mapped on isodensity surfaced have been realized with the program GOPEMOL²⁵.

(E) 1-[2-(4-bromophenyl)-ethenyl]-4-methyl-piperazine 2e

The procedure followed is identical to that described for (E) 4-[2-(2,4-

19 M. Cervera, M. Moreno-Mañas and R. Pleixats, *Tetrahedron*, **1990**, 46, 7885.

20 a) N. L. J. M. Broekhof, F. L. Jonkers and A. van der Gen, *Tetrahedron Lett.*, **1979**, 2433.

b) K. Stamos, *Tetrahedron Lett.*, **1982**, 23, 459.

c) G. Crispi, P. Giacconi, E. Rossi and R. Stradi, *Synthesis*, **1982**, 787.

d) M. Costa, G. P. Chiusoli, R. Gaetti, B. Gabriele, G. Salerno, *Russ. Chem. Bl.*, **1998**, 47(5), 936-940.

21 GAMESS version 20 June 2002 (R2) from Iowa State University, M.W.Schmidt, K.K.Baldrige, J.A.Boatz, S.T.Elbert, M.S.Gordon, J.H.Jensen, S.Koseki, N.Matsunaga, K.A.Nguyen, S.J.Su, T.L.Windus, together with M.Dupuis, J.A.Montgomery, *J.Comput.Chem.*, **1993**, 14, 1347-1363.

22 Alex A. Granovsky, [www http://classic.chem.msu.su/gran/gamess/index.html](http://classic.chem.msu.su/gran/gamess/index.html)

23 M. J. Frisch, J. A. Pople and J. S. Binkley, *J. Chem. Phys.*, **1984**, 80, 3265, and ref. cited therein.

24 Centro Interuniversitario Lombardo per l'elaborazione Avanzata, Via R. Sanzio, 4 20090 Segrate, Mi.

25 a) L. Laaksonen, *J. Mol. Graph.*, **1992**, 10, 33-34.

b) D.L. Bergman, L. Laaksonen and A. Laaksonen, *J. Mol. Graph. Model.*, **1997**, 15, 301-306.

Dichlorophenyl)-ethenyl]-morpholine. Yellow pale oil, 90% yield.

^1H NMR δ 2.35(3H, s, CH₃), 2.47-2.52 (4H, m, CH₂NCH₂ linked to CO), 3.08-3.13 (4H, m, CH₂NCH₂), 5.33 (1H, d, J=13.9 Hz, vinylic H), 6.66 (1H, d, J=13.9 Hz, vinylic H), 7.06-7.32 (4H, 2 x d, AB system, J=8.8Hz, ArH).

(E) 4-[2-(2,4-Dichlorophenyl)-ethenyl]-morpholine 2g

2,4-Dichlorophenylacetaldehyde (5.9 g, 30 mmol) and morpholine (2.7 ml, 30mmol) were dissolved in anhydrous toluene (60 ml) and heated at reflux with azeotropic removal of water. The reaction progress was checked by IR spectroscopy until aldehyde absorption disappeared. The toluene solution was dried with Na₂SO₄, filtered and the solvent removed under reduced pressure. After IR and ^1H NMR analysis and without further purification, the pale yellow oily residue (7 g, 90%) was reacted with azide. IR (liquid film) ν_{max} 1633 cm⁻¹; ^1H NMR δ 3.05-3.15 (4H, m, CH₂NCH₂), 3.72-3.80 (4H, m, CH₂OCH₂), 5.63 (1H, d, J=13.9 Hz, vinylic H), 6.60 (1H, d, J=13.9 Hz, vinylic H), 7.07-7.34 (3H, m, ArH). Anal. Calcd. for C₁₂H₁₃Cl₂NO: C, 55.83; H, 5.08; N, 5.43; found: C, 55.64; H, 4.96; N, 5.31.

4-[4-(4-Bromophenyl)-5-(4-methyl-piperazin-1-yl)—4,5-dihydro-[1,2,3]-triazol-1-yl]-6-methyl--pyran-2-one 3e

Azide 1 (3.0 g, 20 mmol) was dissolved in benzene (20 ml) and an equimolar amount of enamine 2, dissolved in benzene (20 ml), was added dropwise. The mixture was stirred overnight at room temperature. (TLC cyclohexane/EtOAc, 1:9) The white precipitate was filtered off and recrystallized from benzene to give pure **3e** as white crystals (5.97 g, 73%); mp 92°C (decomp.); IR (Nujol) ν_{max} 1717 (C=O) cm⁻¹; ^1H NMR δ 2.32 (3H, s, N-CH₃), 2.33 (3H, s, CH₃); 2.48 (8H, m, (CH₂NCH₂)₂); 4.62 (1H, d, J=3.3 Hz, H-5); 5.57 (1H, d, J=3.3 Hz, H-4); 5.73 (1H, s, H-3 pyranone); 6.78 (1H, s, H-5 pyranone); 6.88 and 7.53 (4H, 2 x d, AB system, J=8.4 Hz, ArH).

4-[4-(2,4-Dichlorophenyl)-4,5-dihydro-5-morpholino-1H-1,2,3-triazol-1-yl]-6-methyl-2H-pyran-2-one 3g

Azide 1 (3.0 g, 20 mmol) was dissolved in benzene (20 ml) and an equimolar amount of enamine **2g**, dissolved in benzene (20 ml), was added dropwise. The

mixture was stirred overnight at room temperature. (TLC cyclohexane/EtOAc, 1:9) The white precipitate was filtered off and recrystallized from benzene to give pure **3g** as white crystals (5.97 g, 73%); mp 154°C (decomp.); IR (Nujol) ν_{\max} 1716 (C=O) cm^{-1} ; ^1H NMR δ 2.33 (3H, s, CH_3); 2.43-2.52 (4H, m, CH_2NCH_2); 3.65-3.75 (4H, m, CH_2OCH_2); 4.57 (1H, d, $J=3.3$ Hz, H-5); 5.98 (1H, d, $J=3.3$ Hz, H-4); 5.73 (1H, s, H-3 pyranone); 6.77 (1H, s, H-5 pyranone); 6.57 (1H, d, $J=8.4$ Hz, ArH-6'); 7.25 (1H, dd, $J=8.4$ Hz and 2.2 Hz, ArH-5'); 7.52 (1H, d, $J=2.2$ Hz, ArH-3'). Anal. Calcd. for $\text{C}_{18}\text{H}_{18}\text{Cl}_2\text{N}_4\text{O}_3$: C, 52.83; H, 4.43; N, 13.69; found: C, 52.94; H, 4.51; N, 13.42.

1-[3-(6-methyl-2-oxo-2H-pyran-4-yl)-5-phenyl-4,5-dihydro-3H-[1,2,3]triazol-4-yl]-pyrrolidine-2-carboxylic acid methyl ester 3i

Azide **1** (2.31 g, 10 mmol) was dissolved in benzene (20 ml) and an equimolar amount of enamine **2i**, dissolved in benzene (20 ml), was added dropwise. The mixture was stirred overnight at room temperature. (TLC cyclohexane/EtOAc, 3:7) . Solvent was evaporated *in vacuo* to give **3i** as pale yellow oil; at ^1H NMR the product resulted pure at 70%; further purification was not possible due to its lability. ^1H NMR δ 2.27 (3H, s, CH_3); 1.88-2.45 (6H, m, pyrrolidine); 3.66 (3H, s, OCH_3); 3.81-3.89 (1H, m, H on C*); 5.03 (1H, d, $J=2.2$ Hz, H-5); 5.72 (1H, d, $J=2.2$ Hz, H-4); 5.77 (1H, s, H-3 pyranone); 6.79 (1H, s, H-5 pyranone); 7.04-7.25 (5H, m, ArH).

4-(4,5-Dihydro-4-methylsulfanylmethyl-5-morpholino-1H-1,2,3-triazol-1-yl)-6-methyl-2H-pyran-2-one 3k

A benzene solution (20 ml) of morpholine (1.74 g, 20 mmol) was added dropwise to a stirred solution of azide **1** (3g, 20 mmol) and 3-methylsulfanylpropionaldehyde (2.08 g, 20mmol) in benzene (30 ml). The mixture was stirred at r.t. until the starting azide disappeared (about 3h) (TLC cyclohexane/EtOAc, 1: 9). The solution was dried with Na_2SO_4 , filtered and the filtrate evaporated under reduced pressure. The residue was dissolved in CH_2Cl_2 and by adding *i*Pr₂O afforded pure **3k** (4.8 g, 74%) as cream needles; mp 99°C (decomp.); IR (Nujol) ν_{\max} 1727 (C=O) cm^{-1} ; ^1H NMR δ 2.20 (3H, s, CH_3S), 2.29 (3H, s, CH_3), 2.21-2.45 (5H, m, CH_2NCH_2 and 1 H of CH_2S linked to C-4), 2.99 (1H, dd, $J=4.3$ Hz and $J_{\text{gem}}=13.8$ Hz, H of CH_2S linked

to C-4), 3.60-3.70 (4H, m, CH₂OCH₂), 4.65 (1H, d, $J_{\text{trans}}=3.0$ Hz, H-5), 4.75 (1H, ddd, $J_{\text{trans}}=3.0$ Hz, $J=4.3$ Hz and $J=7.3$ Hz, H-4), 5.77 (1H, s, H-3 pyranone), 6.71 (1H, s, H-5 pyranone). Anal. Calcd. for C₁₄H₂₀N₄O₃S: C, 51.84; H, 6.21; N, 17.27; found C, 51.89; H, 6.27; N, 16.98.

4-[4-(1,5-dimethyl-hex-4-enyl)-5-morpholin-4-yl-4,5-dihydro-[1,3,4]triazol-1-yl]-6-methyl-pyran-2-one 3l

Azide **1** (2.0 g, 13 mmol) was dissolved in benzene (40 ml) with equimolar amounts of racemic 2,6-dimethyl-hept-5-enal and morpholine. The mixture was stirred overnight at room temperature (TLC cyclohexane/EtOAc, 3:7) Evaporation of the solvent gave **3l** as a yellow oil (85%); ¹H NMR δ 0.75-0.87 (3H, dd, $J=6.59$ CH₃ on C*); 1.22-1.52 (2H, m, CH₂); 1.63 (3H, s, CH₃), 1.71 (3H, s, CH₃), 1.97-2.24 (2H, m, CH₂), 2.30 (3H, s, CH₃); 2.29-2.36 (4H, m, CH₂NCH₂); 3.63-3.68 (4H, m, CH₂OCH₂); 4.39 (1H, m, H-5); 4.52 (1H, m, H-4); 5.09 (1H, m, vinyl H); 5.69 (1H, s, H-3 pyranone); 6.74 (1H, s, H-5 pyranone).

4-[2-(4-Bromophenyl)-1-(4-methyl-piperazin-1-yl)-ethylideneamino]-6-methyl-pyran-2-one 4e

Dihydrotriazole **3e** (10 mmol) was dissolved in *n*-propanol (70 ml) and heated under reflux until the starting compound disappeared (2 hours), progress of the reaction being followed by TLC (cyclohexane/ EtOAc 1:9). The solvent was removed in vacuo. The crude residue was taken up with CH₂Cl₂ and insoluble precipitate was filtered off. The filtrate was evaporated under reduced pressure to give a residue, which was crystallized from *n*.PrOH to afford the amidine **4e** (70%) as yellow plates; mp 149°C; IR (Nujol) ν_{max} 1715 (C=O) cm⁻¹; ¹H NMR δ 2.17 (3H, s, CH₃); 2.31 (3H, s, NCH₃); 2.34-2.37 (4H, m, CH₂NCH₂); 3.51 (4H, m, CH₂NCH₂); 3.76 (2H, s, CH₂); 5.24 (1H, s, H-3), 5.64 (1H, s, H-5); 7.01 and 7.48 (4H, 2 x d, AB system, $J=8.4$ Hz, ArH); ¹³C NMR δ 19.9 (CH₃ pyrone), 33.8 (CH₂), 44.9 (CH₂NCH₂), 45.9 (N-CH₃), 54.6 (CH₂NCH₂), 95.8 (pyrone C-5), 104.6 (pyrone C-3), 120.99 (Ar C-Br), 129.4 (Ar CH), 132.2 (Ar CH), 134.2 (Ar C-CH₂), 155.7 (pyrone C-6), 161.41 (pyrone C-4), 164.6 (amidinic C), 164.9 (CO).

4-[2-(2,4-Dichlorophenyl)-1-morpholino-ethylideneamino]-6-methyl-2H-pyran-

2-one 4g

Dihydrotriazole **3g** (4.1 g, 10 mmol) was dissolved in *n*-propanol (70 ml) and heated under reflux until the starting compound disappeared (2 hours), progress of the reaction being followed by TLC (cyclohexane/ EtOAc 4:6). The solvent was removed in vacuo. The crude residue was taken up with CH₂Cl₂ and insoluble precipitate was filtered off. The filtrate was evaporated under reduced pressure to give a residue, which was crystallized from *n*-PrOH to afford the amidine **4g** (2.67 g, 70%) as orange plates; mp 137°C; IR (Nujol) ν_{\max} 1715 (C=O) cm⁻¹; ¹H NMR δ 2.18 (3H, s, CH₃); 3.41-3.65 (8H, m, morpholine); 3.78 (2H, s, CH₂); 5.23 (1H, s, H-3), 5.63 (1H, s, H-5); 7.10 (1H, d, J=8.4 Hz, ArH-6'), 7.29 (1H, dd, J=8.4 Hz and J=1.8 Hz, ArH-5'), 7.44 (1H, d, J=1.8 Hz, ArH-3'). Anal. Calcd. for C₁₈H₁₈Cl₂N₂O₃: C, 56.71; H, 4.76; N, 7.35. Found: C, 56.68; H, 4.74; N, 7.41.

1-[1-(6-methyl-2-oxo-2H-pyran-4-ylimino)-2-phenyl-ethyl]-pyrrolidine-2-carboxylic acid methyl ester 4i

Dihydrotriazole **3** (7 mmol) was dissolved in *n*-propanol (50 ml) and heated under reflux until the starting compound disappeared (2 hours), progress of the reaction being followed by TLC (cyclohexane/ EtOAc 3:7). The solvent was removed in vacuo. The crude residue was taken up with CH₂Cl₂ and insoluble precipitate was filtered off. The filtrate was evaporated under reduced pressure to give a yellow oil that was purified by chromatography on silica gel (cyclohexane/ EtOAc 3:7) to yield 1.1 g (43%) of pure **4i** as a pale yellow oil; IR (Nujol) ν_{\max} 1715 (C=O) cm⁻¹; ¹H NMR δ 1.88-2.19 (4H, m, pyrrolidine); 2.13 (3H, s, CH₃); 3.38-3.41 (2H, m, CH₂); 3.76 (3H, s, OCH₃); 3.79 (2H, s, CH₂Ph); 4.52-4.56 (1H, m, H on C*); 5.28 (1H, s, H-3), 5.56 (1H, s, H-5); 7.20-7.38 (5H, m, ArH); ¹³C NMR δ 19.9 (CH₃ pyrone); 24.8 and 29.4 (2 x CH₂ pyrrolidine); 35.4 (CH₂Ph); 47.6 (CH₂N); 52.2 (OCH₃); 60.3 (*CH); 96.4 (pyrone C-5); 105.1 (pyrone C-3); 127.0 (Ar CH); 128.0 (Ar CH); 129.1 (Ar CH); 134.6 (Ar C); 155.1 (pyrone C-6), 161.4 (pyrone C-4), 164.5 (amidinic C), 165.2 (CO pyrone); 173.2 (COO).

6-Methyl-4-(3-methylsulfanyl-1-morpholino-propylideneamino)-2H-pyran-2-one 4k

A solution of dihydrotriazole **3** (3.2 g, 10 mmol) was refluxed in toluene (60 ml),

progress of the reaction being followed by TLC (cyclohexane/EtOAc, 1:9). After disappearance of the starting material (3 hours) the solvent was removed in vacuo and the oily residue crystallized by adding of Et₂O to give **4** (2.46 g, 83%) as cream needles; mp 111°C; IR (Nujol) ν_{max} 1690 (C=O) cm⁻¹; ¹H NMR δ 2.08 (3H, s, CH₃); 2.22 (3H, s, SCH₃), 2.56-2.70 (4H, m, 2 x CH₂), 3.45-3.53 (4H, m, CH₂NCH₂); 3.70-3.78 (4H, m, CH₂OCH₂); 5.28 (1H, s, H-3), 5.67 (1H, s, H-5). Anal Calc. for C₁₄H₂₀N₂O₃S: C, 56.74; H, 6.80; N, 9.45; found: C, 56.65; H, 6.73; N, 9.30.

4-(4,8-dimethyl-1-morpholin-4-yl-non-7-enylideneamino)-6-methyl-pyran-2-one 4l

Dihydrotriazole **3** (13 mmol) was dissolved in *n*.propanol (70 ml) and heated under reflux until the starting compound disappeared (2 hours), progress of the reaction being followed by TLC (cyclohexane/ EtOAc 3:7). The solvent was removed in vacuo. The crude residue was taken up with CH₂Cl₂ and insoluble precipitate was filtered off. The filtrate was evaporated under reduced pressure to give **4e** as a yellow oil (65%); ¹H NMR δ 0.87 (3H, d, J=6.59 CH₃ on C*); 1.23-1.31 (2H, m, CH₂); 1.60 (3H, s, CH₃); 1.70 (3H, s, CH₃); 1.95-2.06 (2H, m, CH₂); 2.21 (3H, s, CH₃); 2.27-2.37 (2H, m, CH₂); 3.47-3.52 (4H, m, CH₂NCH₂); 3.70-3.74 (4H, m, CH₂OCH₂); 5.03 (1H, m, vinyl H); 5.20 (1H, s, H-3 pyranone); 5.60 (1H, s, H-5 pyranone).

Reaction of the amidine 4a with piperidine at reflux. Synthesis of 4-(4,6-dimethyl-3-phenyl-pyridin-2-yl)-morpholine 5a and 2-(4-methyl-6-morpholino-5-phenyl-pyridin-2-yl)-1-piperidin-1-yl-ethanone 6a

Amidine **4a** (R¹=Ph, HNR₂=morpholine, 1.56 g, 5 mmol) was suspended in piperidine (15 ml). The reaction mixture was refluxed until disappearance (TLC monitoring) of the starting compound (17 hours). The amine excess was removed *in vacuo* and the crude residue chromatographed on a silica gel column, eluent EtOAc/cyclohexane (4:6). Two fractions were collected: a first minor fraction containing the pyridine derivative **5a** and a second fraction containing the pyridine amide **6a**:

5a: white crystals from *i*Pr₂O, 0.39 g, yield 29%, mp 87°C; ¹H NMR δ 2.05 (3H, s, *p*-CH₃); 2.44 (3H, s, *o*-CH₃); 2.92-3.02 (4H, m, CH₂NCH₂); 3.43-3.50 (4H, m,

CH₂OCH₂); 6.70 (1H, s, H-3); 7.2-7.44 (5H, m, ArH); ¹³C NMR δ 20.8 (*p*-CH₃); 24.5 (*o*-CH₃); 50.1 (CH₂NCH₂); 67.4 (CH₂OCH₂); 119.1 (*m*-CH); 127.3, 128.8, 130.6, (ArCH); 125.0, 138.8, 147.2 (ArC_{qu}); 155.2 (C bound to *o*-CH₃); 160.0 (C bound to morpholino group). Anal. Calcd. for C₁₇H₂₀N₂O: C, 76.09; H, 7.51; N, 10.44; found: C, 76.01; H, 7.62; N, 10.33.

6a: cream crystals from petroleum ether, 1.14 g, yield 60%, mp 112°C; IR (Nujol) ν_{\max} 1630 (C=O) cm⁻¹; ¹H NMR δ 1.45-1.70 (6H, m, CH₂CH₂CH₂); 2.06 (3H, s, *p*-CH₃); 2.90-3.00 (4H, m, CH₂NCH₂); 3.42-3.50 (4H, m, CH₂OCH₂); 3.54-3.69 (4H, m, O=C-N(CH₂)₂); 3.80 (2H, s, CH₂); 6.87 (1H, s, H-3); 7.29-7.47 (5H, m, ArH); ¹³C NMR δ 20.6 (*p*-CH₃); 24.6, 25.6, 26.5 (CH₂CH₂CH₂); 43.0, 43.6 (O=C-N(CH₂)₂); 47.7 (CH₂-C=O); 49.7 (CH₂NCH₂); 66.9 (CH₂OCH₂), 118.9 (C-3); 127.1, 128.5, 130.1 (ArCH); 125.6, 138.0, 147.4 (ArC_{qu}), 152.2 (C-2); 159.6 (C-6); 169.0 (C=O). Anal. Calcd. for C₂₃H₂₉N₃O₂: C, 72.79; H, 7.70; N, 11.07; found: C, 72.67; H, 7.63; N, 11.09.

General procedure for the preparation of amide derivatives 6 and 7

Amidines **4** (5 mmol) mixed with a large amount of the appropriate amine (100 mmol) in a sealed tube were put in a preheated oil bath at 200°C and heated for at least 2 hours. Afterwards, the progress of the reaction was monitored by TLC every 30 minutes, until disappearance of the starting amidine **4**.

The amine excess was removed *in vacuo* and the residue was chromatographed on silica gel affording compound **6** and in some cases minor amounts of compound **7** (eluent see later) The yields of isolated and purified products **6** and **7** are listed in Table 1.

2-(4-Methyl-6-morpholino-5-phenyl-pyridin-2-yl)-1-piperidin-1-yl-ethanone 6a (EtOAc/cyclohexane, 4:6). Analytical data are shown above.

2-(4-Methyl-6-morpholino-5-phenyl-pyridin-2-yl)-1-(4-methyl-piperazin-1-yl)-ethanone 6b

(MeOH/EtOAc, 7:3); cream plates from *i*Pr₂O; mp 110°C; IR (Nujol) ν_{\max} 1620 (C=O) cm⁻¹; ¹H NMR δ 2.05 (3H, s, *p*-CH₃); 2.33 (3H, s, H₃C-N); 2.35-2.47 (4H, m, H₃C-N(CH₂)₂); 2.87-2.96 (4H, m, CH₂NCH₂); 3.38-3.48 (4H, m, CH₂OCH₂); 3.67-

3.82 (4H, m, O=CN(CH₂)₂); 3.80 (2H, s, CH₂); 6.85 (1H, s, H-3); 7.20-7.42 (5H, m, ArH). ¹³C NMR δ 20.9 (*p*-CH₃); 42.0 and 43.8 (H₃C-N(CH₂)₂); 46.3 (H₃C-N); 46.6 (CH₂-C=O); 50.1 (CH₂NCH₂); 55.0 and 55.6 (O=C-N(CH₂)₂); 67.2 (CH₂OCH₂); 119.3 (C-3); 127.5, 128.9, 130.4 (ArCH); 126.2, 138.3, 147.9 (ArC_{qu}); 152.3 (C-2); 160.1 (C-6); 169.5 (C=O). Anal. Calcd. for C₂₃H₃₀N₄O₂: C, 70.02; H, 7.66; N, 14.20; found: C, 69.87; H, 7.54; N, 13.99.

2-(4-Methyl-6-morpholino-5-phenyl-pyridin-2-yl)-1-(4-methyl-N-benzyl-piperazin-1-yl)-ethanone 6c

(MeOH/EtOAc, 7:3); cream plates from *i*Pr₂O; mp 141°C; IR (Nujol) ν_{max} 1636 (C=O) cm⁻¹; ¹H NMR δ 2.07 (s, 3H, CH₃); 2.44 (m, 4H, CH₂N(benzyl)CH₂); 2.95 (m, 4H, CH₂NCH₂); 3.47 (m, 4H, CH₂OCH₂); 3.54 (s, 2H, CH₂Ph); 3.72 (m, 4H, CH₂N(CO)CH₂); 3.81 (s, 2H, CH₂CO); 6.83 (s, 1H, H-*meta*); 7.38 (m, 10H, ArH); ¹³C NMR δ 20.6 (CH₃-*para*); 41.9 and 43.5 (H₃C-N(CH₂)₂); 46.6 (CH₂-C=O); 49.7 (CH₂NCH₂); 52.8 and 53.3 (O=C-N(CH₂)₂); 63.0 (CH₂-Ph); 66.9 (CH₂OCH₂); 118.9 (CH-*meta*); 127.1, 127.4, 128.4, 128.5, 129.23, 130.1 (arom. CH); 125.7, 137.7, 138.0 and 147.5 (arom C_{qu}); 152.0 (C-2, N=C-CH₂); 159.7 (C-6 linked to Morph.); 169.1 (C=O).

2-(4-Methyl-6-morpholino-5-phenyl-pyridin-2-yl)-1-morpholin-4-yl-ethanone 6d

(EtOAc); orange plates from *i*Pr₂O; mp 134°C; IR (Nujol) ν_{max} 1634 (C=O) cm⁻¹; ¹H NMR δ 2.06 (3H, s, *p*-CH₃); 2.90-2.98 (4H, m, CH₂NCH₂); 3.42-3.50 (4H, m, CH₂OCH₂); 3.60-3.77 (8H, m, O=CN(CH₂)₂ and CH₂OCH₂); 3.80 (2H, s, CH₂); 6.87 (1H, s, H-3); 7.26-7.45 (5H, m, ArH). ¹³C NMR δ 20.6 (*p*-CH₃); 42.3 and 43.3 (O=C-N(CH₂)₂); 47.0 (CH₂-C=O); 49.7 (CH₂NCH₂); 66.9 (2 x CH₂OCH₂); 119.0 (C-3); 127.2, 128.5, 130.0 (ArCH); 125.9, 137.8, 147.6 (ArC_{qu}); 151.7 (C-2); 159.7 (C-6); 169.4 (C=O). Anal. Calcd. for C₂₂H₂₇N₃O₃: C, 69.27; H, 7.13; N, 11.02; found: C, 69.02; H, 7.16; N, 10.81.

N,N-Diethyl-2-(4-methyl-6-morpholino-5-phenyl-pyridin-2-yl)-acetamide 6e

(EtOAc/cyclohexane, 7:3); chestnut plates from *i*Pr₂O; mp 77°C; IR (Nujol) ν_{max} 1631 (C=O) cm⁻¹; ¹H NMR δ 1.13-1.25 (6H, m, 2 x CH₃CH₂); 2.08 (3H, s, *p*-CH₃);

2.93-3.01 (4H, m, CH₂NCH₂); 3.43-3.50 (4H, m, CH₂OCH₂); 3.52-3.63 (4H, m, 2 x CH₂CH₃); 3.79 (2H, s, CH₂C=O); 6.88 (s, 1H, H-3); 7.27-7.43 (5H, m, ArH); ¹³C NMR δ 13.1 (CH₃); 14.4 (CH₃); 20.5 (p-CH₃); 40.3 (CH₂); 42.6 (CH₂); 43.2 (CH₂C=O); 49.7 (CH₂NCH₂); 66.9 (CH₂OCH₂); 119.0 (C-3); 127.0, 128.5, 130.1 (ArCH); 125.6, 138.1, 147.3 (ArCqu); 152.5 (C-2); 159.6 (C-6); 169.9 (C=O). Anal. Calcd. for C₂₂H₂₉N₃O₂: C, 71.89; H, 7.96; N, 11.44; found: C, 71.75; H, 7.83; N, 11.29.

1-[4-methyl-6-(2-morpholin-4-yl-2-oxo-ethyl)-3-phenyl-pyridin-2-yl]-pyrrolidine-2-carboxylic acid methyl ester 6f

(EtOAc/cyclohexane, 7:3); pale yellow oil; ¹H NMR δ 1.67-1.83 (4H, m, 2 x CH₂ proline); 2.06 (3H, s, p-CH₃); 2.9 (2H, m, CH₂-N); 3.55-3.68 (8H, m, O=CN(CH₂)₂ and CH₂OCH₂); 3.72 (3H, s, OCH₃); 3.79 (2H, s, CH₂); 4.80 (1H, m, H on C*); 6.57 (1H, s, H-3); 7.21-7.37 (5H, m, ArH).

2-(4-Methyl-6-morpholino-5-p-tolyl-pyridin-2-yl)-1-piperidin-1-yl-ethanone 6g

(EtOAc/cyclohexane, 7:3); cream needles from *i*Pr₂O; mp 90°C; IR (Nujol) ν_{max} 1644 (C=O) cm⁻¹; ¹H NMR δ 1.42-1.65 (6H, m, CH₂CH₂CH₂); 2.05 (3H, s, p-CH₃); 2.39 (3H, s, CH₃-tolyl); 2.84-2.98 (4H, m, CH₂NCH₂); 3.43-3.50 (4H, m, CH₂OCH₂); 3.56-3.68 (4H, m, O=CN(CH₂)₂); 3.79 (2H, s, CH₂); 6.85 (1H, s, H-3); 7.11-7.24 (4H, m, ArH); ¹³C NMR δ 20.6 (p-CH₃); 21.3 (CH₃-tolyl); 24.6, 25.6, 26.5 (CH₂CH₂CH₂); 43.0 and 43.7 (O=C-N(CH₂)₂); 47.6 (CH₂-C=O); 49.6 (CH₂NCH₂); 66.9 (CH₂OCH₂); 118.8 (C-3); 129.2, 129.9, (ArCH); 125.5, 134.9, 136.6, 147.4 (ArCqu); 152.0 (C-2); 159.6 (C-6); 168.9 (C=O). Anal. Calcd. for C₂₄H₃₁N₃O₂: C, 73.25; H, 7.94; N, 10.68; found: C, 73.17; H, 7.85; N, 10.89.

2-[5-(4-Chlorophenyl)-4-methyl-6-morpholino-pyridin-2-yl]-1-piperidin-1-yl-ethanone 6h

(EtOAc/cyclohexane, 6:4); cream plates from *i*Pr₂O; mp 86°C; IR (Nujol) ν_{max} 1620 (C=O) cm⁻¹; ¹H NMR δ 1.38-1.70 (6H, m, CH₂CH₂CH₂); 2.04 (3H, s, p-CH₃); 2.90-3.00 (4H, m, CH₂NCH₂); 3.43-3.54 (4H, m, CH₂OCH₂); 3.53-3.68 (4H, m, O=C-N(CH₂)₂); 3.79 (2H, s, CH₂); 6.87 (1H, s, H-3); 7.23 and 7.40 (4H, 2 x d, AB system, J=8.5 Hz, ArH); ¹³C NMR δ 20.9 (p-CH₃); 25.0, 26.0, 26.9 (CH₂CH₂CH₂);

43.4 and 43.9 (O=C-N(CH₂)₂); 48.0 (CH₂-C=O); 50.2 (CH₂NCH₂); 67.2 (CH₂OCH₂); 119.5 (C-3); 129.2, 131.9 (ArCH); 124.9, 133.3, 136.9, 147.7 (ArCqu); 153.1 (C-2); 160.0 (C-6); 169.1 (C=O). Anal Calcd. for C₂₃H₂₈ClN₃O₂: C, 66.74, H, 6.82, N, 10.15; found: C, 66.63; H, 6.77; N, 10.21.

2-[5-(4-Chlorophenyl)-4-methyl-6-morpholino-pyridin-2-yl]-1-(4-methyl-piperazin-1-yl)-ethanone 6i

(MeOH/EtOAc, 7:3); cream plates from *i*Pr₂O; mp 115°C; IR (Nujol) ν_{\max} 1630 (C=O) cm⁻¹; ¹H NMR δ 2.06 (3H, s, *p*-CH₃); 2.31 (3H, s, CH₃-N); 2.30-2.50 (4H, m, (CH₂)₂NCH₃); 2.93-3.00 (4H, m, CH₂NCH₂); 3.45-3.57 (4H, m, CH₂OCH₂); 3.65-3.80 (4H, m, O=C-N(CH₂)₂); 3.81 (2H, s, CH₂); 6.88 (1H, s, H-3); 7.25 and 7.41 (4H, 2 x d, AB system, J=8.4 Hz, ArH); ¹³C NMR δ 20.4 (*p*-CH₃); 41.8 and 43.3 (H₃C-N(CH₂)₂); 46.1 (H₃C-N); 46.5 (CH₂-C=O); 49.8 (CH₂NCH₂); 54.7 and 55.3 (O=CN(CH₂)₂); 66.8 (CH₂OCH₂); 119.2 (C-3); 128.8, 131.5 (ArCH); 124.6, 133.0, 136.4, 147.5 (ArCqu); 152.4 (C-2); 159.6 (C-6); 169.0 (C=O). Anal. Calcd. for C₂₃H₂₉ClN₄O₂: C, 66.46; H, 6.83; N, 13.08; found: C, 66.39; H, 6.81; N, 13.09.

2-[5-(4-Bromophenyl)-4-methyl-6-morpholino-pyridin-2-yl]-1-piperidin-1-yl-ethanone 6j

(EtOAc/cyclohexane, 7:3); orange plates from *i*Pr₂O; mp 93°C; IR (Nujol) ν_{\max} 1633 (C=O) cm⁻¹; ¹H NMR (200 MHz, δ) 1.40-1.78 (6H, m, CH₂CH₂CH₂), 2.06 (3H, s, *p*-CH₃), 2.92-3.00 (4H, m, CH₂NCH₂), 3.48-3.56 (4H, m, CH₂OCH₂); 3.58-3.71 (4H, m, O=C-N(CH₂)₂); 3.81 (2H, s, CH₂); 6.89 (1H, s, H-3) 7.20 and 7.56 (4H, 2 x d, AB system, J=8.4 Hz, ArH); ¹³C NMR δ 20.5 (*p*-CH₃); 24.6, 25.6, 26.6 (CH₂CH₂CH₂); 43.0 and 43.6 (O=C-N(CH₂)₂); 47.6 (CH₂-C=O); 49.8 (CH₂NCH₂); 66.9 (CH₂OCH₂); 119.2 (C-3); 121.5 (C-5); 131.7 and 131.8 (ArCH) 124.5 and 137 (2 ArCqu) 147.3 (C-4); 152.8 (C-2); 159.5 (C-6); 168.8 (C=O). Anal. Calcd. for C₂₃H₂₈BrN₃O₂: C, 60.26; H, 6.16; N, 9.17; found: C, 59.94; H, 6.15; N, 8.98.

2-[5-(4-Bromophenyl)-4-methyl-6-morpholino-pyridin-2-yl]-1-(4-methyl-piperazin-1-yl)-ethanone 6k

(MeOH/EtOAc, 7:3); ochre plates from *i*Pr₂O; mp 112°C; IR (Nujol) ν_{\max} 1650 (C=O) cm⁻¹; ¹H NMR δ 2.06 (3H, s, 3H, *p*-CH₃); 2.32 (3H, s, N-CH₃); 2.36-2.44

(4H, m, (CH₂)₂NCH₃); 2.92-2.97 (4H, m, CH₂NCH₂); 3.47-3.52 (4H, m, CH₂OCH₂); 3.68-3.79 (4H, m, O=C-N(CH₂)₂); 3.81 (2H, s, CH₂); 6.88 (1H, s, H-3); 7.19 and 7.57 (4H, 2 x d, AB system, J=8.1 Hz, ArH); ¹³C NMR δ 20.5 (*p*-CH₃); 41.8 and 43.3 (H₃C-N(CH₂)₂); 46.1 (H₃C-N); 46.5 (CH₂-C=O); 49.8 (CH₂NCH₂); 54.7 and 55.3 (O=C-N(CH₂)₂); 66.8 (CH₂OCH₂); 119.2 (C-3); 131.8 (ArCH); 121.1, 124.6, 136.9, 147.4 (ArCqu); 152.4 (C-2); 159.6 (C-6); 169.0 (C=O). Anal. Calcd. for C₂₃H₂₉BrN₄O₂: C, 58.35, H, 6.17, N, 11.83; found: C, 58.50; H, 6.17; N, 11.71

4-{2-[5-(4-Bromophenyl)-4-methyl-6-morpholino-pyridin-2-yl]-acetyl}-piperazine-1-carboxylic acid ethyl ester 6l

(EtOAc/cyclohexane, 9:1); white crystals from *i*Pr₂O; mp 142°C; IR (Nujol) ν_{\max} 1632 (C=O), 1680 (N-C=OO) cm⁻¹; ¹H NMR δ 1.29 (3H, t, J=7 Hz, CH₃-CH₂); 2.07 (3H, s, *p*-CH₃), 2.92-2.97 (4H, m, CH₂NCH₂); 3.40-3.60 (8H, m, CH₂OCH₂ and (CH₂)₂NCOOEt); 3.64-3.77 (4H, m, O=C-N(CH₂)₂); 3.83 (2H, s, CH₂); 4.17 (2H, dd, J=7 Hz, CH₂-CH₃); 6.89 (1H, s, H-3); 7.19 and 7.58 (4H, 2 x d, AB system, J=8.4 Hz, ArH); ¹³C NMR δ 14.7 (CH₃-CH₂); 20.5 (*p*-CH₃); 41.7 (C₂H₅OCO-N(CH₂)₂); 43.5 and 43.9 (O=C-N(CH₂)₂); 46.3 (CH₂-C=O); 49.8 (CH₂NCH₂); 61.8 (CH₂OC=O); 66.8 (CH₂OCH₂); 119.2 (C-3); 132.0 and 132.1 (ArCH); 121.2, 124.8, 136.7, 147.6 (ArCqu); 152.1 (C-2); 155.8 (COOC₂H₅); 160.0 (C-6); 169.2 (C=O). Anal. Calcd. for C₂₅H₃₁BrN₄O₄: C, 56.59; H, 5.89; N, 10.57; found: C, 56.36; H, 5.72; N, 10.34.

2-[5-(4-Bromophenyl)-4-methyl-6-morpholino-pyridin-2-yl]-1-morpholin-4-yl-ethanone 6m

(EtOAc/cyclohexane, 6:4); white plates from *i*Pr₂O; mp 131°C; IR (Nujol) ν_{\max} 1650 (C=O) cm⁻¹; ¹H NMR δ 2.07 (s, 3H, CH₃ on C-4); 2.95 (m 4H, CH₂NCH₂); 3.50 (m, 4H, CH₂OCH₂); 3.64-3.77 (m, 8H, O=C-N(CH₂)₂ and CH₂OCH₂); 3.81 (s, 2H, CH₂); 6.90 (s, 1H, H-meta); 7.20 and 7.58 (2xd, 4H, J=8.4, ArylH); ¹³C NMR δ 20.5 (CH₃ para) 42.3 and 43.2 (O=C-N(CH₂)₂); 47.0 (CH₂-C=O); 49.8 (CH₂NCH₂ morph.); 66.8 (CH₂OCH₂), 66.9 (CH₂OCH₂); 119.3 (C-3); 131.8 (Ar CH); 121.2, 124.8 (Ar Cqu); 157.564 (C-2); 152.245 (C-6 linked to Morph.); 169.201 (C=O).

2-[5-(4-Bromophenyl)-4-methyl-6-morpholin-4-yl-pyridin-2-yl]-*N,N*-diethyl-4-

acetamide 6n

(MeOH/EtOAc, 1:1); pale yellow-orange oil; ^1H NMR δ 1.13-1.27 (m, 6H, 2 x $\text{CH}_3\text{-CH}_2$); 2.06 (s, 3H, CH_3); 2.94-2.98 (m 4H, CH_2NCH_2 morph); 3.39-3.62 (m, 8H, CH_2NCH_2 diethyl and CH_2OCH_2); 3.77 (s, 2H, CH_2); 6.89 (s, 1H, H-meta); 7.20 and 7.57 (2xd, 4H, $J=8.4$, ArylH).

2-[5-(4-Bromophenyl)-4-methyl-6-piperazino-pyridin-2-yl]-1-(4-methyl-piperazin-1-yl)-ethanone 6o

(MeOH/EtOAc, 1:1); ochre plates from *i*Pr₂O; mp 118°C; IR (Nujol) ν_{max} 1635 (C=O) cm^{-1} ; ^1H NMR δ 2.05 (s, 3H, CH_3 in para), 2.26 (s, 3H, N- CH_3 pip. in 6) 2.30 (s, 3H, N- CH_3 amidic piperazine); 2.24-2.29 (m, 4H, $(\text{CH}_2)_2\text{NCH}_3$ in 6); 2.33-2.415 (m, 4H, $(\text{CH}_2)_2\text{NCH}_3$ amidic); 3.00-3.05 (m, 4H, $(\text{CH}_2)_2\text{N}$ in 6); 3.66-3.77 (m, 4H, $\text{O=C-N}(\text{CH}_2)_2$); 3.80 (s, 2H, CH_2); 6.86 (s, 1H, H-meta); 7.18 and 7.56 (2xd, 4H, $J=8.4$, ArylH); ^{13}C NMR δ 20.6 (CH_3 on C-4 para); 41.8 and 43.4 ($\text{H}_3\text{C-N}(\text{CH}_2)_2$); 45.6 (CH_3 linked to C-6) 46.1 ($\text{H}_3\text{C-N-}$ on amidic piperazine); 46.5 ($\text{CH}_2\text{-C=O}$); 49.1 (CH_2NCH_2); 54.7 and 55.3 ($\text{O=C-N}(\text{CH}_2)_2$); 55.0 (CH_2NCH_2); 118.9 (C-3-meta); 131.7-131.9 (Ar CH); 121.0, 124.4, 137.1, 147.2 (Ar Cqu); 152.3 (C-2); 159.7 (C-6); 169.1 (C=O).

2-[5-(4-Fluorophenyl)-4-methyl-6-morpholino-pyridin-2-yl]-1-piperidin-1-yl-ethanone 6p

(EtOAc/cyclohexane, 7:3); pale yellow oil; IR (liquid film) ν_{max} 1640 (C=O) cm^{-1} ; ^1H NMR δ 1.42-1.63 (6H, m, $\text{CH}_2\text{CH}_2\text{CH}_2$); 2.04 (3H, s, *p*- CH_3); 2.95-2.99 (4H, m, CH_2NCH_2); 3.45-3.51 (4H, m, CH_2OCH_2); 3.54-3.67 (4H, m, $\text{O=C-N}(\text{CH}_2)_2$); 3.79 (2H, s, CH_2); 6.87 (1H, s, H-3); 7.10 and 7.29 (4H, 2 x d, AB system, $J=8.8$ Hz, ArH); ^{13}C NMR δ 20.4 (*p*- CH_3); 24.5, 25.6, 26.5 ($\text{CH}_2\text{CH}_2\text{CH}_2$); 42.9 and 43.5 ($\text{O=C-N}(\text{CH}_2)_2$); 47.6 ($\text{CH}_2\text{-C=O}$); 49.7 (CH_2NCH_2); 66.8 (CH_2OCH_2); 115.3 and 115.7 (ArCH. *ortho* to F, $J=21.5$ Hz); 119.0 (C-3); 124.7 (C-5); 131.6 and 131.8 (ArCH *meta* to F, $J=7.7$ Hz); 133.7 and 133.8 (ArCqu *para* to F, $J=3$ Hz); 147.4 (C-4); 152.5 (C-2); 159.7 (C-6); 159.3 and 164.2 (C linked to F, $J_{\text{CF}}=247.0$ Hz); 168.8 (C=O). Anal. Calcd. for $\text{C}_{23}\text{H}_{28}\text{FN}_3\text{O}_2$: C, 69.48; H, 7.10; N, 10.58; found: C, 69.39; H, 7.03; N, 10.46.

2-[5-(4-Fluorophenyl)-4-methyl-6-morpholino-pyridin-2-yl]-1-(4-methyl-piperazin-1-yl)-ethanone 6q

(MeOH/EtOAc, 7:3); cream plates from *i*Pr₂O; mp 50°C; IR (Nujol) ν_{\max} 1632 (C=O) cm⁻¹; ¹H NMR δ 2.04 (3H, s, *p*-CH₃), 2.27 (3H, s, CH₃-N); 2.30-2.43 (4H, m, (CH₂)₂NCH₃); 2.85-2.97 (4H, m, CH₂NCH₂); 3.35-3.47 (4H, m, CH₂OCH₂); 3.60-3.75 (4H, m, O=C-N(CH₂)₂); 3.78 (2H, s, CH₂); 6.87 (1H, s, H-3); 7.10 and 7.29 (4H, 2 x d, AB system J=8.8 Hz, ArH). ¹³C NMR δ 20.4 (*p*-CH₃); 41.8 and 43.3 (H₃C-N(CH₂)₂); 46.1 (H₃C-N); 46.4 (CH₂-C=O); 49.8 (CH₂NCH₂); 54.7 and 55.3 (O=C-N (CH₂)₂); 66.8 (CH₂OCH₂); 115.3 and 115.8 (ArCH. *ortho* to F, J=21.5); 119.1 (C-3); 124.8 (C-5); 131.6 and 131.8 (ArCH *meta* to F J=7.8); 133.7 and 133.8 (ArCqu *para* to F, J=2.9 Hz); 147.5 (C-4); 152.2 (C-2); 159.80 (C-6); 159.4 and 164.3 (C linked to F, J_{CF}=247.0); 169.1 (C=O). Anal. Calcd. for C₂₃H₂₉FN₄O₂: C, 66.95; H, 7.09; N, 13.59; found: C, 66.75; H, 6.99; N, 13.51.

2-[5-(2,4-Dichlorophenyl)-4-methyl-6-morpholino-pyridin-2-yl]-1-(4-methyl-piperazin-1-yl)-ethanone 6r

(MeOH/EtOAc, 7:3); yellow oil; IR (liquid film) ν_{\max} 1643 (C=O) cm⁻¹; ¹H NMR δ 2.00 (3H, s, *p*-CH₃); 2.30 (3H, s, CH₃-N); 2.32-2.40 (4H, m, (CH₂)₂NCH₃); 2.95-3.00 (4H, m, CH₂NCH₂); 3.47-3.55 (4H, m, CH₂OCH₂); 3.66-3.78 (4H, m, O=C-N (CH₂)₂); 3.83 (2H, s, CH₂); 6.90 (1H, s, H-3); 7.18 (1H, d, J=8.1 Hz, H-6'); 7.34 (1H, dd, J=8.1 Hz and J=2.2 Hz, H-5'), 7.53 (1H, d, J=2.2 Hz, H-3'); ¹³C NMR δ 19.6 (*p*-CH₃); 41.8 and 43.5 (H₃C-N(CH₂)₂); 46.0 (H₃C-N); 46.4 (CH₂-C=O); 49.73 (CH₂NCH₂); 54.7 and 55.2 (O=C-N(CH₂)₂); 66.8 (CH₂OCH₂); 118.9 (C-3); 127.5, 129.7, 132.8 (Ar CH); 122.9, 134.0, 135.1, 135.7, 148.5 (Ar Cqu); 153.3 (C-2); 159.7 (C-6); 169.0 (C=O). Anal. Calcd. for C₂₃H₂₈Cl₂N₄O₂: C, 59.72; H, 6.11; N, 12.12; found: C, 59.57; H, 6.04; N 11.96.

2-[5-(4-Methoxyphenyl)-4-methyl-6-morpholino-pyridin-2-yl]-1-piperidin-1-yl-ethanone 6s

(EtOAc/cyclohexane, 7:3); pale yellow-orange oil; IR (liquid film) ν_{\max} 1625 (C=O) cm⁻¹; ¹H NMR δ 1.40-1.70 (m, 6H, CH₂CH₂CH₂); 2.05 (s, 3H, CH₃-*para*); 2.90-3.00 (m, 4H, CH₂NCH₂); 3.43-3.53 (m, 4H, CH₂OCH₂); 3.50-3.67 (m, 4H, O=C-N(CH₂)₂); 3.78 (s, 2H, CH₂); 3.85 (s, 3H, OCH₃); 6.85 (s, 1H, H-3); 6.94 and 7.20 (2

x d, 4H, aromatic AB system, $J=8.7$, arom H). ^{13}C NMR δ 21.6 (CH_3); 25.0, 26.0, 26.9 ($\text{CH}_2\text{CH}_2\text{CH}_2$); 43.4, 44.0 (CH_2NCH_2); 48.1 ($\text{CH}_2\text{-C=O}$); 50.0 (CH_2NCH_2 linked to C=O); 55.7 (OCH_3); 67.4 (CH_2OCH_2); 114.3, 131.5 (Ar CH); 119.3 (C-3); 125.6, 130.4, 147.9 (Ar C_{qu}); 152.3 (C-2, N=C-CH_2); 158.9 (C_{qu} OCH_3 linked); 160.2 (C-6); 169.4 (C=O).

2-(4,5-Dimethyl-6-morpholino-pyridin-2-yl)-1-piperidin-1-yl-ethanone 6t

(EtOAc/cyclohexane, 7:3); white needles from $i\text{Pr}_2\text{O}$; mp 81°C ; IR (Nujol) ν_{max} 1630 (C=O) cm^{-1} ; ^1H NMR δ 1.30-1.65 (6H, m, $\text{CH}_2\text{CH}_2\text{CH}_2$); 2.17 (3H, s, $m\text{-CH}_3$); 2.23 (3H, s, $p\text{-CH}_3$); 2.98-3.10 (4H, m, CH_2NCH_2); 3.50-3.68 (4H, m, $\text{O=C-N}(\text{CH}_2)_2$); 3.78 (2H, s, CH_2); 3.80-3.87 (4H, m, CH_2OCH_2); 6.87 (1H, s, H-3); ^{13}C NMR δ 14.2 ($m\text{-CH}_3$); 20.2 ($p\text{-CH}_3$); 24.9, 25.9, 26.9 ($\text{CH}_2\text{CH}_2\text{CH}_2$); 43.3 and 44.1 ($\text{O=C-N}(\text{CH}_2)_2$); 47.9 ($\text{CH}_2\text{-C=O}$); 51.1 (CH_2NCH_2); 67.6 (CH_2OCH_2); 120.1 (C-3); 121.7 (C-5); 148.4 (C-4); 151.1 (C-2); 161.4 (C-6); 169.3 (C=O). Anal. Calcd. for $\text{C}_{18}\text{H}_{27}\text{N}_3\text{O}_2$: C, 68.09; H, 8.58; N, 13.24; found: C, 68.36; H, 8.65; N 13.19

2-(4,5-dimethyl-6-piperidino-pyridin-2-yl)-1-piperidin-1-yl-ethanone 7a

white needles from $i\text{Pr}_2\text{O}$; mp 72°C ; IR (Nujol) ν_{max} 1630 (C=O) cm^{-1} ; ^1H NMR δ 1.30-1.80 (12H, m, 2 x $\text{CH}_2\text{CH}_2\text{CH}_2$); 2.15 (3H, s, $m\text{-CH}_3$); 2.19 (3H, s, $p\text{-CH}_3$); 2.92-3.06 (4H, m, CH_2NCH_2); 3.50-3.68 (4H, m, $\text{O=C-N}(\text{CH}_2)_2$); 3.76 (2H, s, CH_2); 6.80 (1H, s, 1H, H-3); ^{13}C NMR δ 14.3 ($m\text{-CH}_3$); 20.3 ($p\text{-CH}_3$); 25.0, 25.1, 26.0, 26.7, 26.8 (CH_2 of piperidines); 43.3, 44.4 ($\text{O=C-N}(\text{CH}_2)_2$); 47.9 ($\text{CH}_2\text{-C=O}$); 52.0 (CH_2NCH_2); 119.3 (C-3); 121.9 (C-5); 148.0 (C-4); 150.8 (C-2); 162.9 (C-6); 169.6 (C=O). Anal. Calcd. for $\text{C}_{19}\text{H}_{29}\text{N}_3\text{O}$: C, 72.33, H, 9.27, N, 13.33; found: C, 72.28; H, 9.19; N, 13.25.

2-(4,5-Dimethyl-6-morpholino-pyridin-2-yl)-1-(4-methyl-piperazin-1-yl)-ethanone 6u

(MeOH/EtOAc, 7:3); pale yellow oil; IR (liquid film) ν_{max} 1644 (C=O) cm^{-1} ; ^1H NMR δ 2.18 (3H, s, $m\text{-CH}_3$); 2.23 (3H, s, $p\text{-CH}_3$); 2.31 (3H, s, $\text{CH}_3\text{-N}$); 2.33-2.43 (4H, m, $(\text{CH}_2)_2\text{NCH}_3$); 3.02-3.10 (4H, m, CH_2NCH_2); 3.62-3.76 (4H, m, $\text{O=C-N}(\text{CH}_2)_2$); 3.77 (2H, s, CH_2); 3.82-3.88 (4H, m, CH_2OCH_2); 6.85 (1H, s, H-3); ^{13}C NMR δ 14.0 ($m\text{-CH}_3$); 20.0 ($p\text{-CH}_3$); 41.7 and 43.5 ($(\text{CH}_2)_2\text{NCH}_3$); 46.1 (N-CH_3);

46.3 (CH₂C=O); 50.8 (CH₂NCH₂); 54.7 and 55.3 (O=C-N(CH₂)₂); 67.2 (CH₂OCH₂); 119.9 (C-3); 121.6 (C-5); 148.3 (C-4); 150.4 (C-2); 161.1 (C-6); 169.3 (C=O). Anal. Calcd. for C₁₈H₂₈N₄O₂: C, 65.02, H, 8.48, N, 16.86; found: C, 64.83; H, 8.42; N 16.68.

2-[4,5-dimethyl-6-(4-methyl-piperazin-1-yl)-pyridin-2-yl]-1-(4-methyl-piperazin-1-yl)-ethanone 7b

pale yellow oil; IR (liquid film) ν_{\max} 1643 (C=O) cm⁻¹; ¹H NMR δ 2.15 (3H, s, *m*-CH₃); 2.21 (3H, s, *p*-CH₃); 2.27 (3H, s, N-CH₃); 2.33-2.38 (4H, m, (CH₂)₂NCH₃); 2.44 (3H, s, N-CH₃); 2.64-2.74 (4H, m, (CH₂)₂NCH₃); 3.12-3.22 (4H, m, CH₂NCH₂); 3.61-3.73 (4H, m, O=C-N-(CH₂)₂); 3.76 (2H, s, CH₂); 6.83 (1H, s, H-3); ¹³C NMR δ 14.1 (*m*-CH₃); 20.0 (*p*-CH₃); 41.7 and 43.6 ((CH₂)₂NCH₃); 46.0 (N-CH₃); 46.2 (N-CH₃); 46.4 (CH₂C=O); 50.0 (CH₂NCH₂); 54.7 and 55.3 (O=C-N(CH₂)₂ and CH₂NCH₂); 119.5 (C-3); 121.5 (C-5); 148.1 (C-4); 150.2 (C-2); 161.1 (C-6); 169.4 (C=O). Anal. Calcd. for C₁₉H₃₁N₅O: C, 66.04, H, 9.05, N, 20.28; found: C, 66.31; H, 9.13; N 20.07.

2-(4-Methyl-5-methylsulfanylmethyl-6-morpholino-pyridin-2-yl)-1-(4-methyl-piperazin-1-yl)-ethanone 6v

(MeOH/EtOAc, 7:3); chestnut plates from *i*Pr₂O; mp 72°C; IR (Nujol) ν_{\max} 1643 (C=O) cm⁻¹; ¹H NMR δ 2.11 (3H, s, CH₃S); 2.25 (3H, s, *p*-CH₃); 2.20-2.34 (4H, m, (CH₂)₂NCH₃); 2.37 (3H, s, N-CH₃); 3.08-3.14 (4H, m, CH₂NCH₂); 3.40-3.72 (4H, m, O=C-N(CH₂)₂); 3.75 (2H, s, CH₂S); 3.77 (2H, s, CH₂CO); 3.80-3.86 (4H, m, CH₂OCH₂); 6.87 (1H, s, H-3); ¹³C NMR δ 16.3 (CH₃S); 19.2 (*p*-CH₃); 31.3 (CH₂S); 41.8 and 43.5 ((CH₂)₂NCH₃); 46.0 (NCH₃); 46.3 (CH₂C=O); 51.8 (CH₂NCH₂); 54.7 and 55.2 (O=C-N(CH₂)₂); 67.3 (CH₂OCH₂); 121.3 (C-3); 123.0 (C-5); 149.5 (C-4); 152.2 (C-2); 161.9 (C-6); 168.9 (C=O). Anal. Calcd. for C₁₉H₃₀N₄O₂S: C, 60.28; H, 7.99; N, 14.81; found: C, 60.35; H, 8.13; N, 14.76.

2-[4-Methyl-6-(4-methyl-piperazin-1-yl)-5-methylsulfanylmethyl-pyridin-2-yl]-1-(4-methyl-piperazin-1-yl)-ethanone 7c

yellow oil; IR (liquid film) ν_{\max} 1644 (C=O) cm⁻¹; ¹H NMR δ 2.13 (3H, s, CH₃S); 2.27 (3H, s, *p*-CH₃); 2.30-2.42 (4H, m, (CH₂)₂NCH₃); 2.39 (3H, s, N-CH₃); 2.41

(3H, s, N-CH₃); 2.58-2.67 (4H, m, (CH₂)₂NCH₃); 3.18-3.24 (4H, m, CH₂NCH₂); 3.58-3.72 (4H, m, O=C-N(CH₂)₂); 3.77 (2H, s, CH₂S); 3.78 (2H, s, CH₂CO); 6.89 (1H, s, H-3); ¹³C NMR δ 16.3 (CH₃S); 19.3 (*p*-CH₃); 31.3 (CH₂S); 41.8 and 43.6 (CH₂)₂NCH₃); 46.1 (N-CH₃); 46.3 (N-CH₃); 46.4 (CH₂C=O); 51.3 (CH₂NCH₂); 54.7 and 55.0 (O=C-N (CH₂)₂); 55.2 and 55.5 ((CH₂)₂NCH₃); 121.0 (C-3); 122.9 (C-5); 149.3 (C-4); 152.0 (C-2); 161.9 (C-6); 169.1 (C=O). Anal. Calcd. for C₂₀H₃₃N₅OS: C, 61.34; H, 8.50; N, 17.90; found: C, 61.39; H, 8.65; N, 17.81.

2-[3'-(4-Methoxyphenyl)-4'-methyl-3,4,5,6-tetrahydro-2*H*-[1,2']bipyridin-yl-6'-yl]-1-piperidin-1-yl-ethanone 7d

(EtOAc/cyclohexane, 7:3); pale yellow-orange oil; IR (liquid film) ν_{\max} 1620 (C=O) cm⁻¹; ¹H NMR δ 1.25-1.62 (m, 12H, 2 x CH₂CH₂CH₂); 2.03 (s, 3H, CH₃-*para*); 2.89-2.94 (m, 4H, CH₂NCH₂); 3.56-3.67 (m, 4H, O=C-N(CH₂)₂); 3.78 (s, 2H, CH₂); 3.85 (s, 3H, OCH₃); 6.79 (s, 1H, H-3); 6.91 and 7.21 (2 x d, 4H, aromatic AB system, *J*=8.7, arom H). ¹³C NMR δ 21.1 (CH₃); 25.1, 26.1, 26.3, 26.9 (2 x CH₂CH₂CH₂); 43.4, 44.3 (CH₂NCH₂); 48.1 (CH₂-C=O); 50.9 (CH₂NCH₂ linked to C=O); 55.7 (OCH₃); 114.1, 131.6 (Ar CH); 118.5 (C-3); 125.8, 131.1, 147.5 (Ar C_{qu}); 152.1 (C-2, N=C-CH₂); 158.7 (C_{qu} OCH₃ linked); 161.6 (C-6); 169.6 (C=O).

2-[5-(1,5-dimethyl-hex-4-enyl)-4-methyl-6-morpholin-4-yl-pyridin-2-yl]-1-(4-methyl-piperazin-1-yl)-ethanone 6w

(EtOAc/cyclohexane, 7:3); pale yellow oil; ¹H NMR δ 1.31 (d, 3H, *J*=7.0, CH₃ on CH); 2.26 (s, 3H, CH₃-*para*); 2.22-2.36 (4H, m, (CH₂)₂NCH₃); 2.33 (s, 3H, CH₃ vinyl); 2.41 (s, 3H, CH₃ vinyl); 2.37 (s, 3H, N-CH₃); 3.02-3.09 (m, 4H, CH₂NCH₂); 3.40-3.62 (m, 4H, O=C-N(CH₂)₂); 3.64-3.73 (m, 4H, CH₂OCH₂); 3.75 (s, 2H, CH₂CO); 5.11 (m, 1H, CH vinyl); 6.88 (s, 1H, H-3);

2CH₂ fall between 1.3 and 2.2 ; H on C* should fall between 2 and 4 based on enamine spectra.

Chapter 2

Pharmacology

1. Background

Since several years our group collaborate with the research group of Prof. Alberto Corsini at “Dipartimento di Scienze Farmacologiche” providing novel organic small molecules for a blind screening project. Aim of this study is to isolate new molecules potentially active for pathologies derived from abnormal cellular proliferation, as atherosclerosis and cancer. The inhibitory activity of the considered organic molecules is evaluated as their ability to inhibit rat's aorta smooth muscular cells proliferation. Migration and proliferation of smooth muscle cells in the arterial wall are early prominent features of atherogenesis and represent major mechanisms involved in vascular occlusion in both atherosclerosis and restenosis after angioplasty²⁶.

A preliminary screening showed certain activity for some of our early synthesized 2-pyridinacetamides, inhibiting SMC proliferation with IC₅₀'s between 50 and 100 μ M, values not enthralling but enough to induce us to deeper explore an eventual role of those novel amides in interfering with the cellular activities. Our next task was then to identify a potential target, thus we performed an exhaustive bibliography search using the SciFinder database. Most molecules containing in their structures the 2-pyridinacetamidic nucleus resulted to be tyrosin kinase receptors inhibitors²⁷. Indeed, an arterial injury leads to extensive platelet activation, adhesion, followed by platelet aggregation and secretion²⁸. Platelet secretion results in the local release of intracellular granuli constituents, including platelet-derived growth factor PDGF, as well as epidermal growth factor EGF²⁹; these factors have been identified as potent endogenous smooth muscle cell mitogens^{26b}. PDGF-BB is also one of the most potent chemoattractive agents^{26b}. Furthermore, the epidermal growth factor receptor (EGFRK) is a rational target for antitumor strategies. EGFRK signaling causes increased proliferation, decreased apoptosis, and enhanced tumor cell

26a) J.H. Ip et al., *J. Am. Coll. Cardiol.*, **1990**, *15*, 1667-1687.

b) R. Ross, *Nature*, **1993**, *362*, 801-809.

c) J.M. Isner et al., *Trends Cardiovasc. Med.*, **1994**, *4*, 213-221.

27W.E. Barth and M.J. Luzzio, Pfizer, PCT C07D 401/14, 7 June 2001

28a) J.H. Ip et al., *J. Am. Coll. Cardiol.*, **1990**, *15*, 1667-1687.

b) R. Ross, *Nature*, **1993**, *362*, 801-809.

c) H. Le Breton et al., *J. Am. Coll. Cardiol.*, **1996**, *28*, 1643-1651.

29a) Y. Oka and D.N. Orth, *J. Clin. Invest.*, **1983**, *72*, 249-259.

b) R.K. Assoian et al., *Nature*, **1984**, *309*, 804-806.

c) R. Ross, *Nature*, **1993**, *362*, 801-809.

motility and neo-angiogenesis.

2. Receptor Tyrosine Kinases

Receptors tyrosine kinases (RTK) are trans membrane glycoproteins activated by the binding of peptidic ligands, transducing the extracellular signal to the cytoplasm by phosphorylating tyrosine residues on the receptors themselves (autophosphorylation) and on downstream signaling proteins, thus leading to cell proliferation, differentiation, migration or metabolic changes³⁰. The RTK family includes receptor for insulin and growth factors like epidermal growth factor, fibroblast growth factor, platelet-derived growth factor, vascular endothelial growth factor and nerve growth factor. The specific reaction catalyzed by phosphorylated RTK is the transfer of the γ phosphate from ATP to the hydroxyl group of a tyrosine in a protein substrate. Due to their role in cellular proliferation RTKs are actually one of the most important target for new anti-proliferative therapies. Several groups all over the world are involved in structural and functional classification of Tyrosine Kinase receptors (RTK), as in the design and synthesis of selective inhibitors³¹. Crystal structures of the tyrosine kinase domains from several RTKs have been reported³², the first of which was cyclic AMP-dependent protein kinase (PKA)³³. One of the best characterized catalytic domain is that of insulin receptor³⁴, represented in Figure 1. The overall architecture of the tyrosine kinase domain consist in an amino-terminal lobe comprising a five-stranded β sheet and one α helix, and a larger carboxy-terminal lobe that is mainly α -helical. ATP binds in the cleft between the two lobes, and the tyrosine-containing peptide substrate binds to the carboxy-terminal lobe. Several residues are highly conserved in all protein kinases, including several glycines in the nucleotide-binding loop, a lysine in β -strand 3, a glutamic acid in α -helix C, an aspartic acid and asparagine in the catalytic loop, and a DFG motif in the beginning of the activation loop¹³. RTKs could assume two conformations, an inactive form or an active form. In the non-signaling state, most RTKs possess low basal kinase activity that increase substantially upon growth factor binding (activation). This results from receptor

30 J. Schlessinger and A. Ullrich, **1992**, 9, 383-391.

31 a) L. Sun et al., *Bioorganic & Medicinal Chemistry Letters*, **2002**, 12, 2153-2157.

b) W. A. Denny et al., *J. Med. Chem.*, **2000**, 42, 2373-2382.

32 Taylor SS, Radzio-Andzelm E. 1994. *Structure* 2:345-55

33 Knighton DR, Zheng J, Ten Eyck LF, Ashford VA, Xuong N, et al. 1991. *Science* 253:407-14

34 S.R. Hubbard, *EMBO J.*, **1997**, 16, 5572-81.

oligomerization and subsequent transphosphorylation of tyrosine residues within a

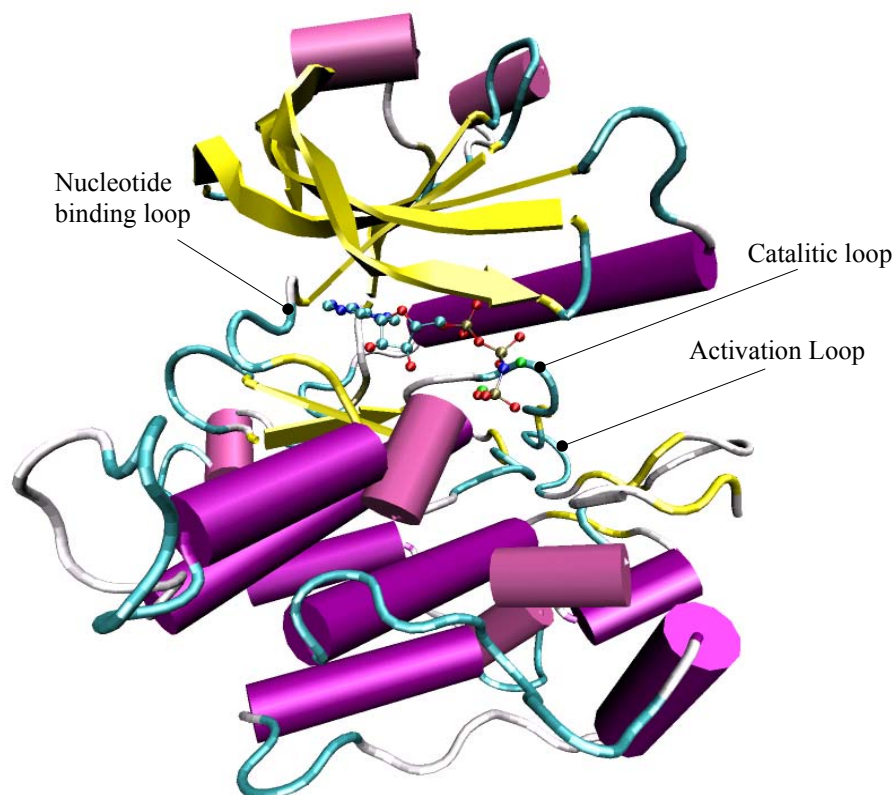


Figure1: cartoon diagram of the tyrosine kinase domain of the insulin receptor. The alpha helices are shown in purple, beta strands in yellow.

partner kinase domain: initial phosphotyrosine modification of the activation loop generates optimal catalytic activity and subsequent rapid phosphorylation at substrate docking sites elsewhere on the receptor intracellular domain. In the RTKs for which crystal structures of both unphosphorylated and phosphorylated versions of the kinase domain are available it's evident that phosphorylation in the activation loop causes a large structural reorganization that relieves steric and chemical restraints on the catalytic active site³⁵. An exception to this are RTKs of the EGFRK family that do not require this initial phosphorylation of kinase domain residues for full catalytic competency and such unique feature could partially explain why EGFRK family members are frequently involved in abnormal cellular proliferation. Due to unexpected results in anti proliferation activity of some of the 2-pyridineacetamides reported in this dissertation, we will consider more closely

³⁵ R. Hubbard and J. H. Till, *Annu. Rev. Biochem.*, **2000**, *69*, 373-98.

some TKR strongly implicated in angiogenesis associated with solid tumors, the platelet derived growth factor receptor (PDGFRK), the vascular endothelial growth factor receptor (VEGFRK) and the epidermal growth factor receptor (EGFRK).

Figure 2

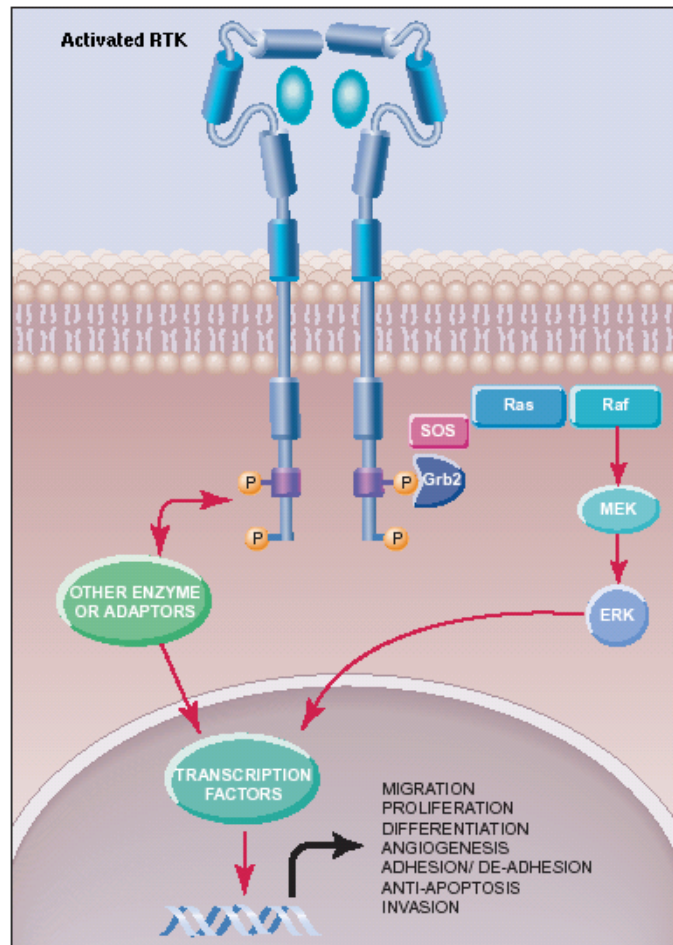


Figure 2: receptors tyrosin kinase signal transduction paths

Figure 2 shows the main paths, common for the considered RTKs, for signal transduction: the interaction with specific ligands promotes receptor oligomerization then autophosphorylation of tyrosine residues thus generating docking sites for mediatory molecules responsible of transferring the message to the nucleus.

The platelet-derived growth factor (PDGF) plays a vital role as a regulator of cell growth³⁶. Binding of PDGF to its trans membrane receptor leads to activation of its

36 a) L. Claesson-Welsh, *Cytokines*, **1993**, 5, 31-43.

b) W. Meyer-Ingold, W. Eichner, *Cell. Biol. Int.*, **1995**, 19, 389-398.

intrinsic tyrosine kinase and autophosphorylation of the intracellular part of the receptor. The autophosphorylated tyrosine residues mediate interactions with downstream signal transduction molecules and thereby initiate different signaling pathways, leading to activation of the GTP-binding protein Ras³⁷ involving the adaptor molecule GRB2. It has also been reported that ligand stimulation of the PDGFRK beta leads to autophosphorylation of tyrosine residues, which is known to mediate interactions with several SH2 domain-containing signaling molecules, such as Shc³⁸, mediating cellular activity.

Vascular endothelial growth factor (VEGF) is a dimeric glycoprotein which induces angiogenesis through binding to VEGF-receptor-2 tyrosine kinase (VEGFRK) or KDR (kinase insert domain-containing receptor) on the surface of endothelial cells. According to sequence homology studies, VEGFRK is composed of an extracellular ligand-binding region, a short membrane-spanning sequence, and an intracellular region containing a putative tyrosine kinase domain³⁹. On the basis of studies with similar receptors of this type, VEGFRK is hypothesized to undergo dimerization upon binding to VEGF, resulting in its activation. Upon activation, the receptor is thought to initiate a cascade of phosphorylation which eventually leads to vascularization⁴⁰. Therefore, VEGFRK is recognized as the target for the development of therapeutic drugs against angiogenesis. The crystal structure of VEGFRK has been resolved⁴¹, providing a useful tool for drug discovery and design.

EGFRK, also called HER and ErbB, belongs to the ErbB family of trans membrane tyrosine kinase growth factor receptors. In addition to EGFRK, this family includes ErbB2 (Neu, HER2), ErbB3 (HER3), and ErbB4 (HER4). Activities of EGFRK are mediated by several signal transduction pathways. The best characterized of these is the Ras/Raf/ERK pathway. On ligand binding and receptor activation, tyrosine residues in the C-terminal region of EGFRK become phosphorylated and bind various adaptor and signaling molecules. In the Ras/Raf/ERK pathway, the binding of Grb2 recruits son-of-sevenless (SOS) to the membrane, which in turn activates Ras and Raf. Activation of ERK leads to gene transcription resulting principally in

37 A.K. Arvidsson et al., *Mol. Cell. Biol.*, **1994**, 14, 6715-6726.

38 K. Yokote et al., *J. Biol. Chem.*, **1994**, 269, 15337-43

39 K. A. Thomas, *J. Biol. Chem.*, **1996**, 271, 603-606.

40 A. Ullrich and J. Schlessinger, *Cell*, **1990**, 61, 203-212.

41 Michele A McTigue et. al., *Structure*, **1999**, 7, 319-330.

cell growth and proliferation (as well as other activities depending on the cell's tissue of origin and differentiation). The binding of ligands by EGFRK can activate other signaling pathways, such as the PI3K/PKB, PLC- γ /PKC, and MEKK/JNK pathways, leading to various other cell activities.

Recent attention has focused on the epidermal growth factor receptor (EGFRK) system because of the observation that deregulation of this receptor system is a significant factor in the genesis or progression of several human cancers, including those of the brain, lung, breast, ovary, pancreas, and prostate.

Figure 3

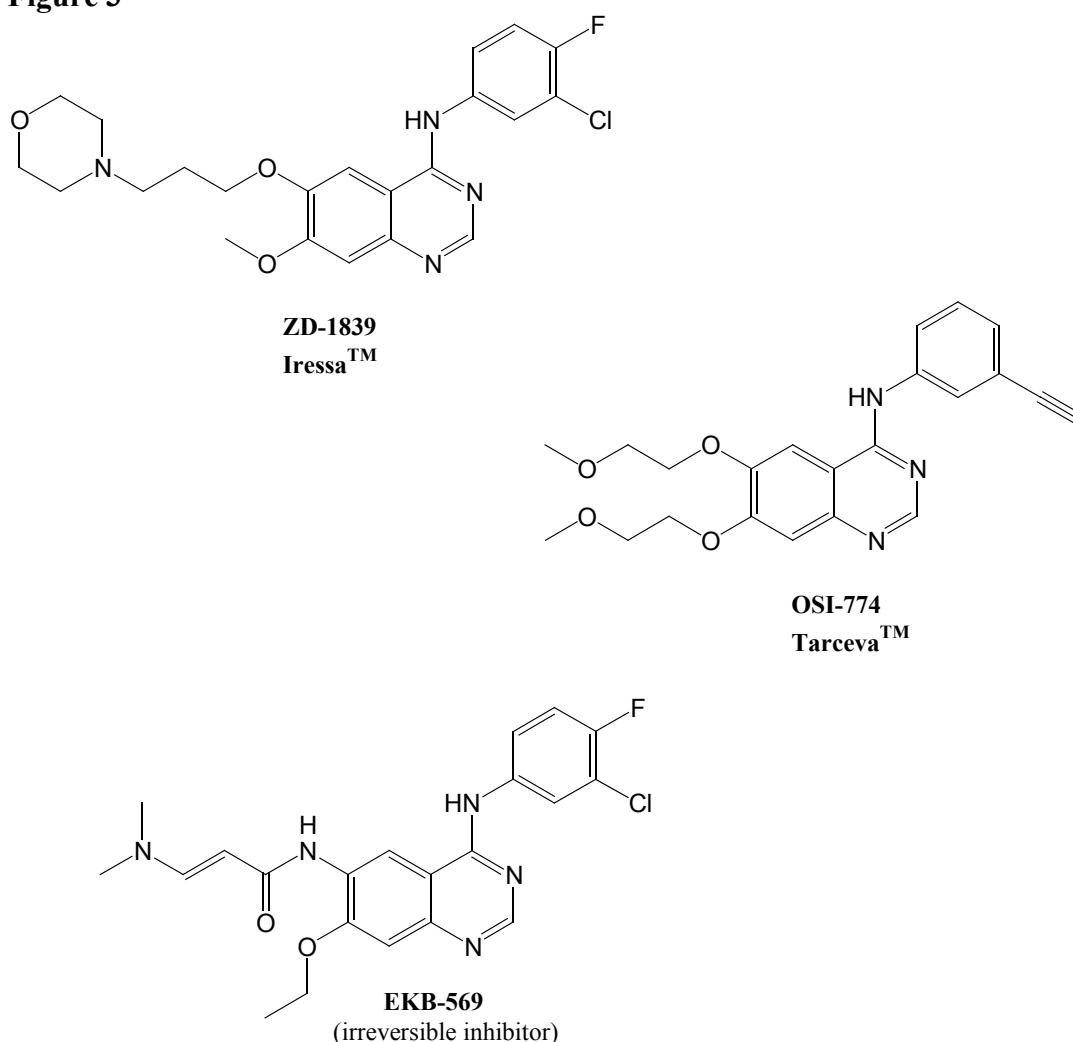


Figure 3: EGFRK inhibitors currently in clinical trials

Few inhibitors of EGFRK are currently in clinical trial; promising drugs are

anilinoquinazoline derivatives such OSI-774 (Tarceva)⁴² and ZD-1839 (Iressa)⁴³, both currently in Phase III clinical trial, and EKB-569. OSI-774 (Tarceva), developed by OSI Pharmaceuticals/Genentech, like ZD-1839, is a highly specific, orally active, and reversible inhibitor of EGFRK tyrosine kinase⁴⁴. In clinical trials, OSI-774 has shown anti tumor activity when given alone against non-small cell lung carcinoma, ovarian cancer, and head and neck cancer. OSI-774 is now being tested in phase III trials against non-small cell lung cancer and pancreatic cancer. EKB-569 is instead an irreversible inhibitor of EGFRK, that might have the benefit of eliminating all EGFRK kinase activity, which then can only be regenerated by new synthesis of EGFRK by the cell. However, the advantage of this over reversible inhibitors needs to be evaluated; actually EKB-569 is in Phase I clinical trial. As shown in Figure 4, the peculiar aspect of irreversible inhibitors⁴⁵ is the presence of a Michael acceptor functional group at the C-6 or C-7 position, that form a covalent linkage with the sulfhydryl group of the Cys 773 of EGFRK.

42 A. J. Barker et al., *Bioorg. Med. Chem. Lett.*, **2001**, *11*, 1911.

43 M. Hidalgo et al., *J. Clin. Oncol.*, **2001**, *19*, 3267.

44 M. Ranson et al., *J. Clin. Oncol.*, **2002**, *20*, 2240-2250.

45 H. Tsou et al., *J. Med. Chem.*, **2001**, *44*, 2719-2734.

Figure 4

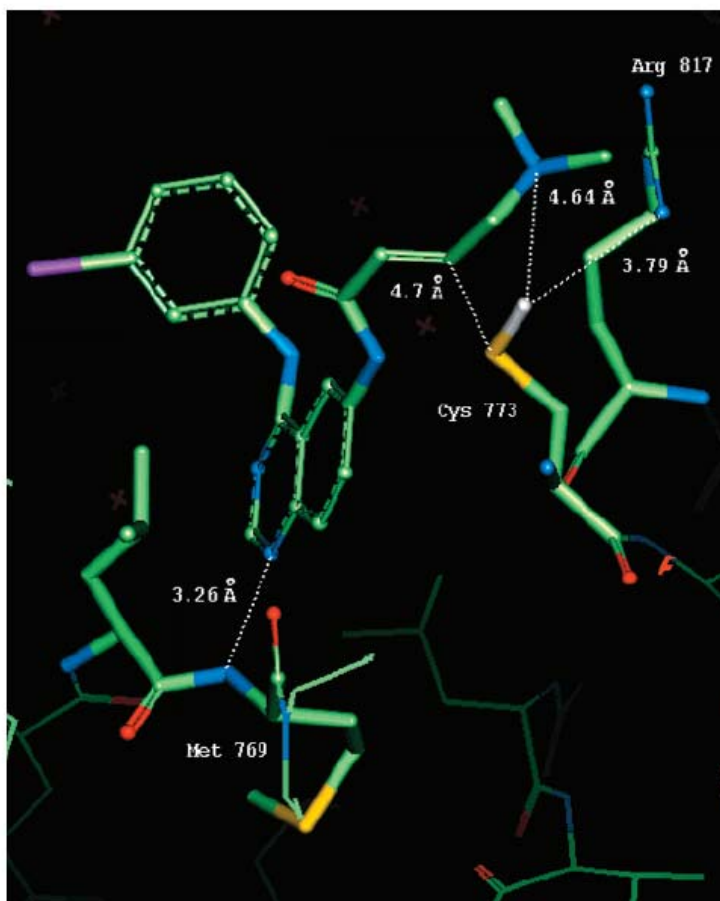


Figure 4: proposed binding mode for EKB-569 derivative; distances between Cys773 and the Michael acceptor group suggest the possibility of a covalent linkage.

As we can understand from what stated above targeting TK receptor in abnormal cellular proliferation diseases is shown to be a promising therapy, but the relative lack in selective inhibitors joint with recent advances made by biochemists in describing the structures of catalytic domains and pathways involved in signal transduction set the basis for a real need for identifying new structures with tyrosin kinase receptors inhibitory activity.

3. Pharmacological Results

We discuss now the ability of amido derivatives of 2-pyridinacetic acid **6** described in **Chapter 1** to inhibit rat's aorta smooth muscular cells proliferation.

Effect of 2-pyridinacetamides **6** on SMC proliferation

Smooth muscle cells were cultured according to Ross²⁶ from intimal medial layers of aorta of male Sprague Dawley rats (200 250 g). Cells were grown in monolayers at 37°C in a humidified atmosphere of 5% CO₂ in MEM supplemented with 10% (v:v) fetal calf serum, 100 U/ml penicillin, 0.1 mg/ml streptomycin, 20 mM buffer tricine and 1% v:v non-essential amino acid solution⁴⁶. The medium was changed every third day. Cells were used between the fourth and tenth passage. Smooth muscle cells were identified for growth behaviour, morphology and using monoclonal antibody specific for α -actin, the actin isoform typical of smooth muscle cells. The cells grew out of explants after 12-16 days, piled up after confluency and contained numerous myofilaments and dense bodies, as observed by transmission electron microscopy.

Myocytes were seeded at a density of 2×10^5 per 35 mm dish, and incubated with MEM supplemented with 10% fetal calf serum⁴⁷. 24 h later, the medium was changed to one containing 0.4% fetal calf serum to stop cell growth and the cultures incubated for 72 h. At this time (time 0), the medium was replaced with one containing 10% fetal calf serum in the presence or absence of known concentrations of the tested compounds and the incubations were continued for further 72 h at 37°C. At time 0, just before the addition of the substances to be tested, three petri dishes were used for cell counting. Cell proliferation was evaluated by cell count after trypsinization of the monolayers using a Coulter Counter model ZM. Smooth muscle cell doubling time was computed according to Elmore and Swift⁴⁸.

Results obtained by tests on 2-pyridinacetamides **6** are collected in table 1. Such data show that many of the evaluated 2-pyridinacetamides **6** are able to inhibit SMC proliferation with IC₅₀ ranging from 100 μ M to 3.5 μ M when the mythogenicstimula is given by FCS. Inside tested molecules, those resulted more active are amides **6** where $R^1 = p\text{-Br-C}_6\text{H}_4$ and $\text{NR}_2 = \text{N-methylpiperazine}$ or morpholine, showing

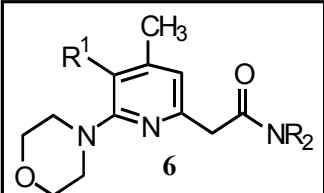
46 A. Corsini et al, *Atherosclerosis*, **1993**, 101, 117-125.

47 A. Corsini et al, *Arterioscler. Thromb. Vasc. Biol.*, **1995**, 15, 420-428.

48 E. Elmore and M. Swift, *J. Cell Physiol.*, **1976**, 87, 229-234.

respectively IC₅₀ values of 5 and 3.5 μM.

Table 1

<div data-bbox="264 407 586 842">  <p>Antiproliferative Activity, here reported in terms of IC₅₀, has been evaluated on rat's aorta muscular smooth cells stimulated with FCS 10%</p> </div>	Comp	R ¹	NR ₂	IC ₅₀ (μM)
	6a	C ₆ H ₅	piperidine	NE
	6b	C ₆ H ₅	N-methylpiperazine	>100
	6d	C ₆ H ₅	morpholine	46.65
	6e	C ₆ H ₅	diethylamine	23.22
	6s	<i>p</i> CH ₃ O-C ₆ H ₄	piperidine	22.5
	6g	<i>p</i> CH ₃ -C ₆ H ₄	piperidine	NE
	6h	<i>p</i> Cl-C ₆ H ₄	piperidine	35.93
	6i	<i>p</i> Cl-C ₆ H ₄	N-methylpiperazine	16
	6j	<i>p</i> Br-C ₆ H ₄	piperidine	16
	6k	<i>p</i> Br-C ₆ H ₄	N-methylpiperazine	5
	6l	<i>p</i> Br-C ₆ H ₄	N-carbethoxypiperazine	43
	6m	<i>p</i> Br-C ₆ H ₄	morpholine	3.5
	6p	<i>p</i> F-C ₆ H ₄	piperidine	NE
	6q	<i>p</i> F-C ₆ H ₄	N-methylpiperazine	>50
	6r	2,4 diCl-C ₆ H ₄	N-methylpiperazine	13
	6t	CH ₃	piperidine	NE
	6u	CH ₃	N-methylpiperazine	NE
	6v	CH ₃ SCH ₂	N-methylpiperazine	NE

Effect of 2-pyridinacetamides 6 on doubling time of SMC

Doubling time, the time that cells need to duplicate, is another important parameter for evaluating the antiproliferative effect, because it's known that this value increases in a concentration dependent manner with either more potent and less potent compounds. Doubling time is calculated with the following formula:

$$(\log 2) \times (\text{time range in hours}) / \log(\text{final n}^\circ \text{ of cells}) - \log(\text{initial n}^\circ \text{ of cells})$$

Experiments conducted on rat's SMC show that all active 2-pyridinacetamides are able to increase the doubling time in a concentration dependent manner .

Experiments with PDGF and EGF as mitogenic stimulus

In order to assess if the activity of valuated 2-pyridinacetamides was somehow selective on tyrosine kinase receptors PDGFRK and/or EGFRK a new set of experiments where done. It's known that SCF mitogenic stimulus is not selective for any particular target, and for this reason following experiments where done using PDGF-BB or EGF as mitogenic stimulus. Rat's aorta SMC used for this study express both receptors for the considered growht factors and for this reason are reliable for our screening.

Synchronization of smooth muscle cells to the G₀/G₁ interphase of the cell cycle was accomplished by incubating logarithmically growing cultures (3x10⁵ myocytes/petri dish) for 5 days in a medium containing 0.4% fetal calf serum. Quiescent cells were then incubated for 20 h in a fresh medium containing 10% fetal calf serum in the presence or absence of testing compounds. When PDGF-BB was investigated, quiescence medium was replaced at the fourth day with one containing 1% plasma-derived bovine serum. After 24 h, mitogenic stimuli were added directly to the medium in the presence or absence of testing compounds. A medium containing 0.1% bovine serum albumin was utilized when EGF was employed as mitogenic stimulus. After 20 h, DNA synthew 3 x sis was estimated by nuclear incorporation of [³H]thymidine, incubated with the cells (2 µCi/ml medium) for 2 h according to Corsini et al.⁴⁹ and radioactivity was measured with Aquasol scintillation cocktail.

At the moment such experiments were conducted only on pyridinacetamides where R¹= *p*-BrPhenyl and NR₂ = piperidine or morpholine, but soon will be extended to

49 A. Corsini et al., *J. Cardiovasc. Pharmacol.*, **1996**, 28, 687-694.

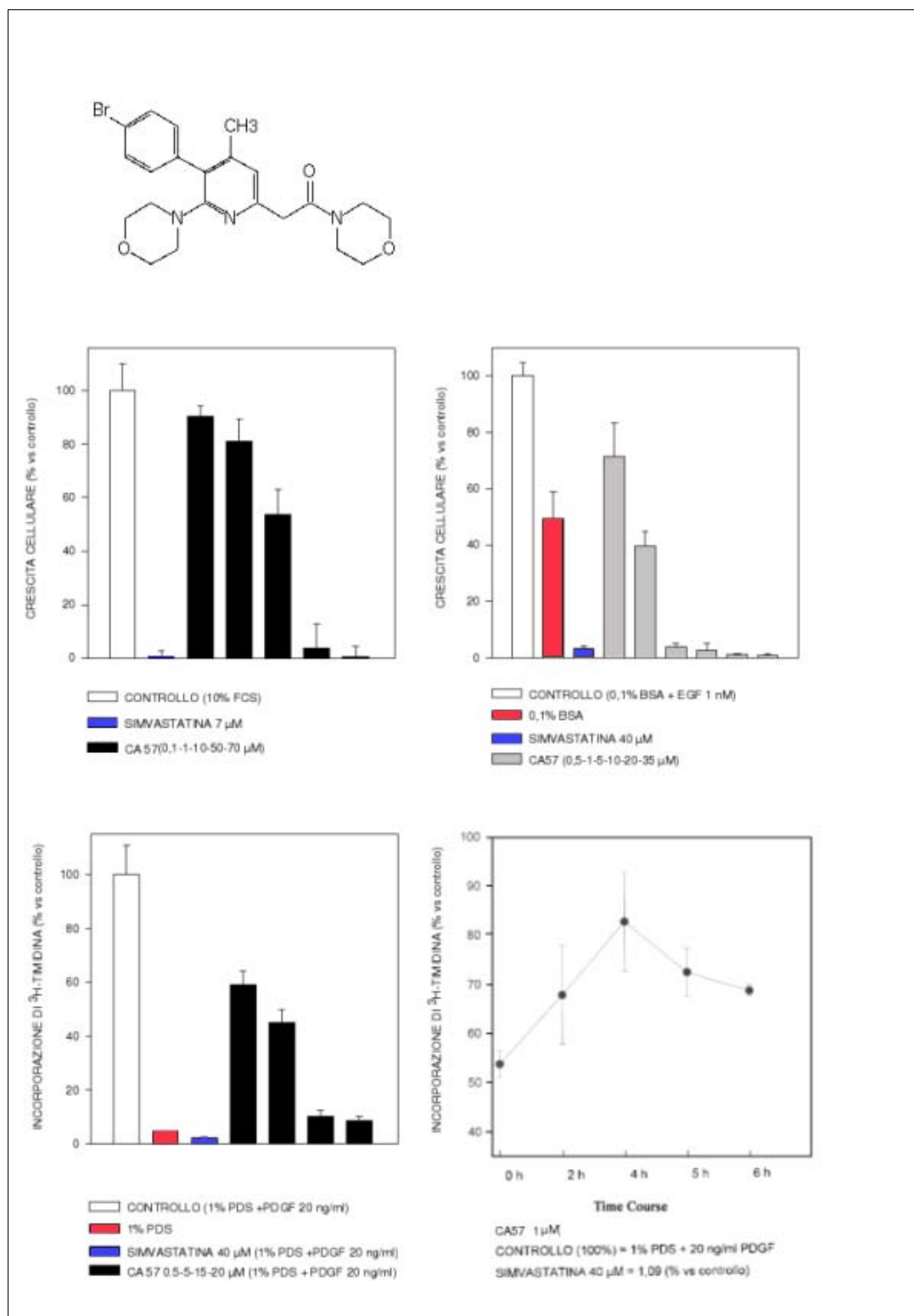
the whole series. Results (IC_{50} μ M) are summarized in Table 2.

Table 2

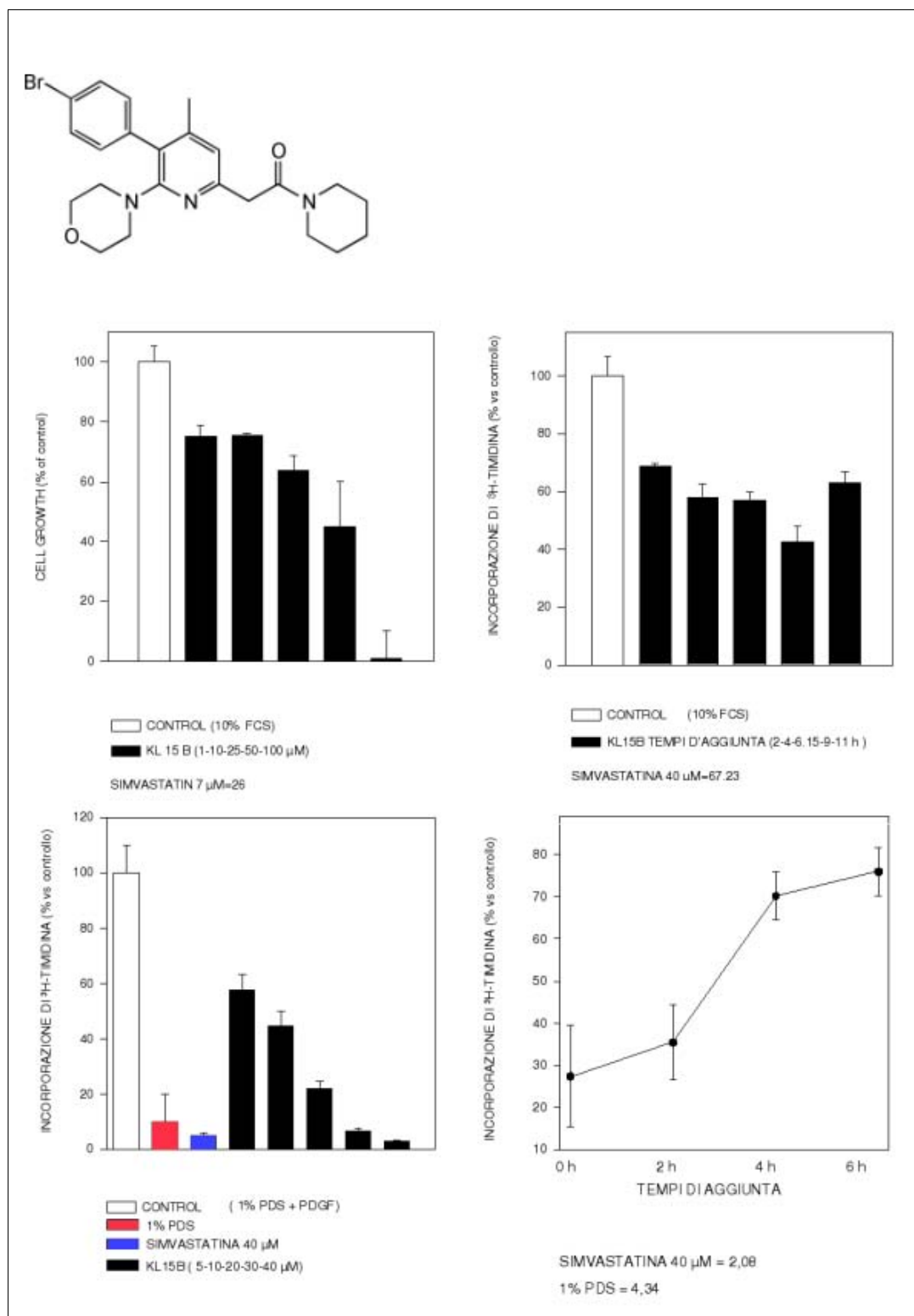
R¹	NR₂	FCS	PDGF	EGF
<i>p</i> Br-C ₆ H ₄	piperidine	16	7.18	1.5
<i>p</i> Br-C ₆ H ₄	morpholine	3.5	1.8	0.7

As we can notice from data reported in Table 2 the tested compounds are 2 folds more potent on cell lines stimulated to proliferation with PDGF-BB and about 10 folds more potent when EGF is used, compared to the results obtained on cells stimulated with FCS. This results could confirm that examined 2-pyridinacetamides act with a mechanism through receptors Tyrosine Kinase, and seems selective toward EGFRK.

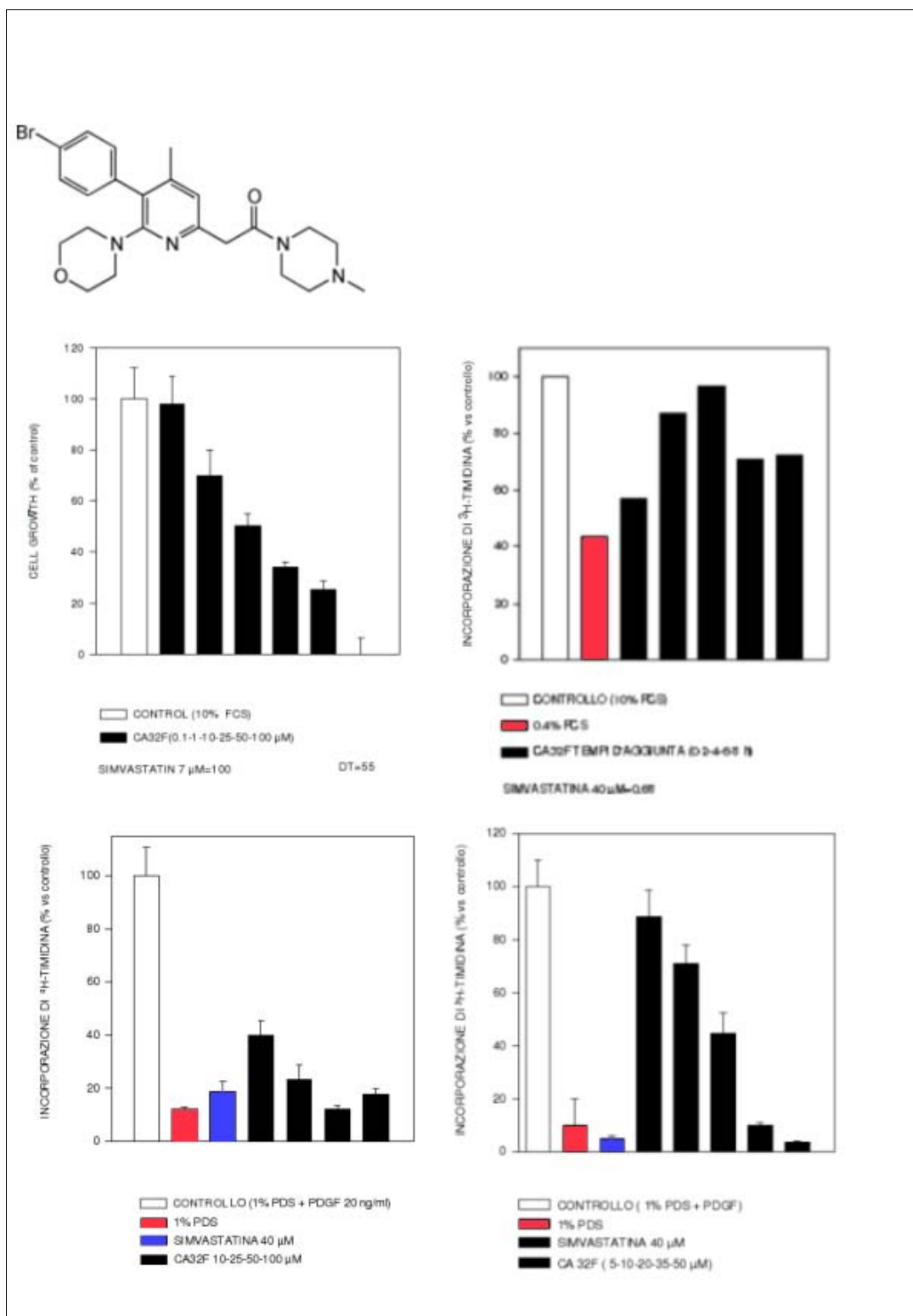
Graph 1: *Pharmacological results for compound 6m*



Graph 2: *Pharmacological results for compound 6j*



Graph 3: *Pharmacological results for compound 6k*



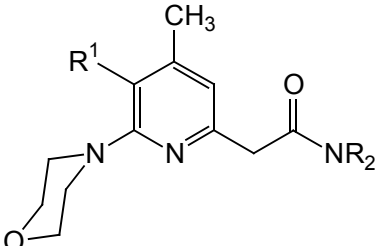
Chapter 3

Medicinal Chemistry

1. Structure Activity Relationships

The first series of pyridineacetamides submitted to pharmacological screening was formed by compounds **6a**, **6b**, **6s**, **6g** and **6h** represented in Table 1

Table 1



N°	R ¹	NR ₂	IC ₅₀
6a	C ₆ H ₅	piperidine	NE
6b	C ₆ H ₅	N-methylpiperazine	101
6s	<i>p</i> CH ₃ O-C ₆ H ₄	piperidine	22
6g	<i>p</i> CH ₃ -C ₆ H ₄	piperidine	NE
6h	<i>p</i> Cl-C ₆ H ₄	piperidine	36

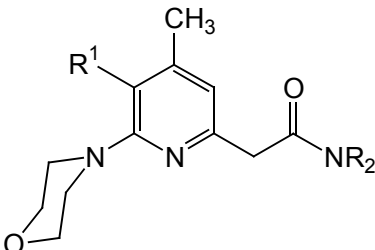
Compound **6b** resulted a modes inhibitor of rat's SMC, while the piperidinic amide **6a** was totally inactive. However certain substituents at the para position of the phenyl ring at C-5, namely the methoxy group or chlorine atom, are able to confer to piperidinic amides **6s** and **6h** a certain antiproliferative activity, with IC₅₀ respectively of 22 and 36 μM; compound **6g** *p*-tolyl substituted was inactive.

Analyzing those results we retained obvious that the nucleus 2-pyridinacetamido could represent a potential pharmacophore moiety if opportunely substituted, and that R¹ and NR₂ were critical for activity. However, at the moment we discovered such potentiality we had no idea about the potential mechanism of action.

We decided than to use classical QSAR techniques in order to help us choosing the right substitutions for improving compound **6** pharmacological properties.

Our first task was to valuate the need of an aromatic substituent at the C-5 position, synthesizing a series of amides preneting an aliphatic or ethero aliphatic chain at C-5, namely compounds **6t-w** reported below.

Table 2



N°	R ¹	NR ₂	IC ₅₀
6t	CH ₃	piperidine	NE
6u	CH ₃	N-methylpiperazine	NE
6v	CH ₃ SCH ₂	N-methylpiperazine	NE
6w	H ₃ C-CH=CH-CH(CH ₃)-CH ₃	N-methylpiperazine	NE

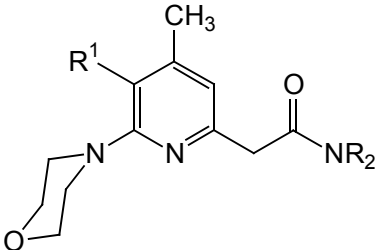
No 5-aliphatic substituted pyridine was found to inhibit SMC proliferation, giving

us a confirmation that the aromatic substituent at C-5 is essential for activity.

We decided than to investigate the influence of the substitution on the phenyl ring, keeping constant the NR₂ moiety.

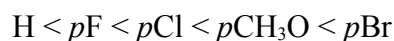
The *para*-methyl substituent didn't play any role in pharmacological activity, however *p*-methoxy and *p*-chlorine did. Because of the positive effect that halogens play on the synthetic route to achive final amides and commercial avaylability of aldehyde precursors our choice was to evaluate the effect of fluorine and bromine atoms. Results, compared to those obatained for **6h**, are summarized in Table 3.

Table 3

	N°	R ¹	NR ₂	IC ₅₀
	6j	4-BrPh	piperidine	16
	6p	4-F-Ph	piperidine	NE
	6r	4-Cl-Ph	piperidine	36

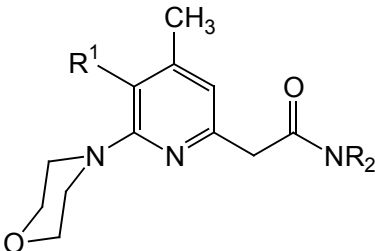
Pharmacological results evidenced increasing activity proportionally to the steric hindrance and lipophily of the halogen, in fact fluorine does not contribute to pharmacological activity, while bromine halves IC₅₀ values.

Summarizing R¹ should be a substituted arylic group, and the substituent on the phenyl ring influences the potency in the order:



Our efforts were than concentrated on investigating the role of the NR₂ moiety.

Preliminary results showed that compound **6a** (R¹ = Ph, NR₂ = piperidine) was totally inactive, while compound **6b** (R¹ = Ph, NR₂ = N-methylpiperazine) gave a modest activity. In order to better evaluate the effect of the amido substituent without further influence we kept as reference compound the pyridine where R¹ = Ph. Synthesized products and pharmacological results are collected in Table 4.

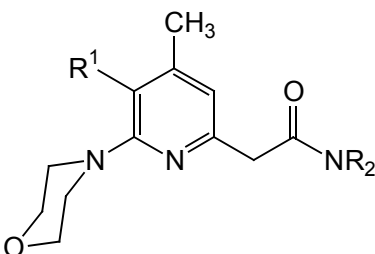
Table 4


N°	R ¹	NR ₂	IC ₅₀
6a	Ph	piperidine	NE
6b	Ph	N-methylpiperazine	101
6d	Ph	morpholine	47
6e	Ph	diethylamine	23

Values reported in Table 4 underline the importance of the amido substituent for antiproliferative activity, as it's contribution to the potency increases in the order:

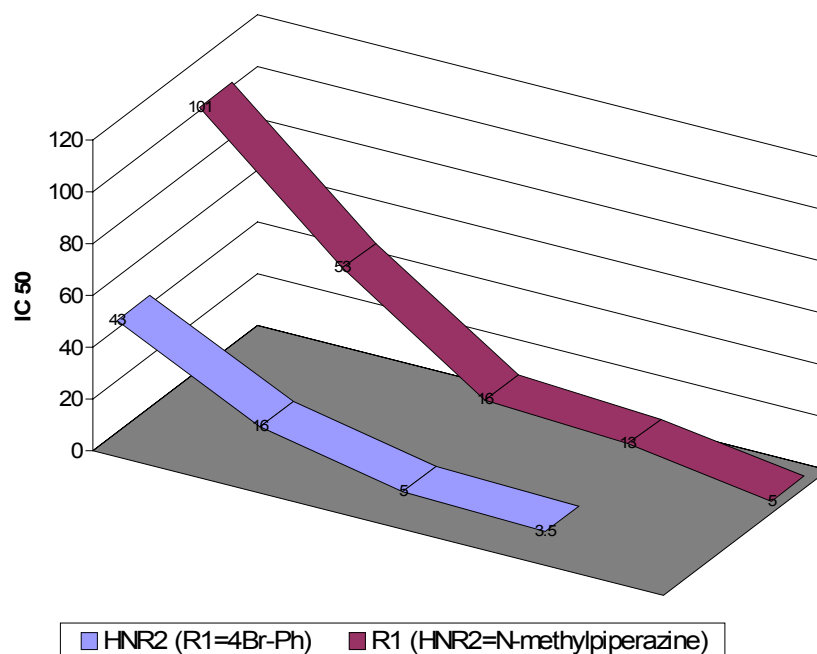


To confirm those results we repeated this study by varying NR₂ on compounds bearing R¹ = *p*BrPh, wich resulted the aryl substituent apporting the greater contribution to pharmacological potency, and by varying R¹ on compounds bearing N-methylpiperazine as amidic substitution. Further evaluations involved a 2,4 dichlorophenil group as R¹ and N-carbethoxypiperazine as amine. Results are summarized in Table 4 and Graph 1.

Table 4


N°	R ¹	NR ₂	IC ₅₀
6j	<i>p</i> Br Ph	piperidine	16
6k	<i>p</i> Br Ph	N-methylpiperazine	5
6l	<i>p</i> Br Ph	N-carbethoxypiperazine	43
6m	<i>p</i> Br Ph	morpholine	3.5
6b	Ph	N-methylpiperazine	101
6i	<i>p</i> Cl Ph	N-methylpiperazine	16
6q	<i>p</i> F-Ph	N-methylpiperazine	55
6r	2,4diClPh	N-methylpiperazine	13

Graph 1



Results presented here show that compounds **6** are able to express an evident structure/activity relationship when evaluated as inhibitors of rat's aorta SMC proliferation. The *p*-Bromophenyl substitution at C-5 seems to supply the greatest contribution to pharmacological activity, and the same does morpholine when choose as NR₂. A further halosubstitution at the *ortho* position of the phenyl ring seems to supply a positive contribution as it's shown for compound **6r**, but at the moment this effect has been evaluated only for the dichloro derivative. Diethylamine seems to increase notably the potency of the derivative as demonstrated by results on compound **6e**.

In the next subchapter will be threatened an exhaustive *in silico* study in order to describe the potential action mechanism of our 2-pyridinacetamides **6**.

2. Docking of 2-pyridinacetamides to RTK's

In order to confirm our observations upon the mechanism of action of 2-pyridinacetamides previously synthesized and to hypothesize a potential binding mode we performed docking experiments on different receptors tyrosine kinase, using the program AutoDock3⁵⁰, a docking software suitable for deep analysis of single ligand docking; in fact reported techniques for automated docking fall into two broad categories: matching methods and docking simulation methods. Matching methods create a model of the active site, typically including sites of hydrogen bonding and sites that are sterically accessible, and then attempt to dock a given inhibitor structure into the model as a rigid body by matching its geometry to that of the active site. The most successful example of this approach is DOCK⁵¹ which is efficient enough to screen entire chemical databases rapidly for lead compounds. The second class of docking techniques model the docking of a ligand to a target in greater detail: the ligand begins randomly outside the protein, and explores translations, orientations, and conformations until an ideal site is found. These techniques are typically slower than the matching techniques, but they allow flexibility within the ligand to be modeled and can utilize more detailed molecular mechanics to calculate the energy of the ligand in the context of the putative active site. They allow computational chemists to investigate modifications of lead molecules suggested by the chemical intuition and expertise of organic synthetic chemists. AutoDock3 is an example of the latter, more physically detailed, flexible docking technique.

Molecular docking is a difficult optimization problem, requiring efficient sampling across the entire range of positional, orientational, and conformational possibilities. Genetic algorithms (GA) fulfill the role of global search particularly well and are increasingly being applied to both drug design and docking.

Genetic algorithms⁵² use ideas based on the language of natural genetics and biological evolution. In the case of molecular docking, the particular arrangement of a ligand and a protein can be defined by a set of values describing the translation,

50 G.M. Morris et al., *J. Comp. Chem.*, **1998**, *19*, 1639-1662.

51 a)I. D. Kuntz et al., *J. Mol. Biol.*, **1982**, *161*, 269.

b)B. K. Shoichet et al., *Prot. Eng.*, **1993**, *6*, 723.

52 J. H. Holland, *Adaptation in Natural and Artificial Systems*, University of Michigan Press, Ann Arbor, MI, **1975**.

orientation, and conformation of the ligand with respect to the protein: these are the ligand's state variables and, in the GA, each state variable corresponds to a gene. The ligand's state corresponds to the genotype, whereas its atomic coordinates correspond to the phenotype. In molecular docking, the fitness is the total interaction energy of the ligand with the protein, and is evaluated using the energy function. Random pairs of individuals are mated using a process of crossover, in which new individuals inherit genes from either parent. In addition, some offspring undergo random mutation, in which one gene changes by a random amount. Selection of the offspring of the current generation occurs based on the individual's fitness: thus, solutions better suited to their environment reproduce, whereas poorer suited ones die. A variety of approaches have been adopted to improve the efficiency of the genetic algorithm. Classical genetic algorithms represent the genome as a fixed-length bit string, and employ binary crossover and binary mutation to generate new individuals in the population. Unfortunately, in many problems, such binary operators can generate values that are often outside the domain of interest, leading to gross inefficiencies in the search. The use of real encodings helps to limit the genetic algorithm to reasonable domains. Alternative genetic algorithms employ more complicated representations and more sophisticated operators besides crossover and mutation. Some of these retain the binary representation, but must employ decoders and repair algorithms to avoid building illegal individuals from the chromosome, and these are frequently computationally intensive. However, the search performance of the genetic algorithm can be improved by introducing a local search method.

AutoDock3 can then use a genetic algorithm GA for global searching, a local search LS method to perform energy minimization, or a combination of both. The local search method is based on that of Solis and Wets⁵³, which has the advantage that it does not require gradient information about the local energy landscape, thus facilitating torsional space search. In addition, the local search method is adaptive, in that it adjusts the step size depending upon the recent history of energies: a user-defined number of consecutive failures, or increases in energy, cause the step size to be doubled; conversely, a user-defined number of consecutive successes, or decreases in energy, cause the step size to be halved. The hybrid of the GA method with the

⁵³ F. J. Solis and R. J.B. Wets, *Math. Oper. Res.*, **1981**, 6, 19.

adaptive LS method together form the so-called Lamarckian genetic algorithm LGA, which has enhanced performance relative to simulated annealing and GA alone. Thus, the addition of these new GA-based docking methods allows problems with more degrees of freedom to be tackled. Furthermore, it is now possible to use the same force field as is used in docking to perform energy minimization of ligands.

Another useful implementation of AutoDock3 is the empirical free energy function used for scoring. The study of molecular structure underpins much of computational molecular biology. There are several established methods for performing molecular mechanics and molecular dynamics, notably AMBER⁵⁴, CHARMM⁵⁵ and GROMOS⁵⁶. Many of these traditional force fields model the interaction energy of a molecular system with terms for dispersion/repulsion, hydrogen bonding, electrostatics and deviation from ideal bond lengths and bond angles. These methods are excellent for studying molecular processes over time, for optimizing bound conformations, and for performing free energy perturbation calculations between molecules with a single atom change, but they often require considerable investments of computer time and, unfortunately, these approaches tend to perform less well in ranking the binding free energies of compounds that differ by more than a few atoms. What is needed is an empirical relationship between molecular structure and binding free energy. The first thoroughly established linear free energy relationship was observed by Hammett in 1933, and reported in 1937⁵⁷. It was used to relate structure and reactivity of small organic molecules on a quantitative basis. Hammett was able to derive substituent constants and reaction constants that could then be used to calculate rate constants and equilibrium constants for a specific reaction of a specific compound. Hammett's work was the forerunner of modern-day quantitative structure-activity relationships (QSAR), pioneered by Hansch and coworkers in the 1960s. Here it is assumed that the sum of the steric, electronic, and hydrophobic effects of substituents in a compound

54 W. D. Cornell, P. Cieplak, C. I. Bayly, I. R. Gould, K. M. Merz Jr., D. M. Ferguson, D. C. Spellmeyer, T. Fox, J. W. Caldwell, and P. A. Kollman, *J. Am. Chem. Soc.*, **1995**, *117*, 5179.

55 B. R. Brooks, R. E. Bruccoleri, B. D. Olafson, D. J. States, S. Swaminathan, and M. Karplus, *J. Comput. Chem.*, **1983**, *4*, 187

56 H. J. C. Berendsen, J. P. M. Postma, W. F. van Gunsteren, A. . diNola, and J. R. Haak, *J. Chem. Phys.*, **1984**, *81*, 3684.

57 L. P. Hammett, *J. Am. Chem. Soc.*, **1937**, *59*, 96.

determines its biological activity⁵⁸. Current structure-based scoring functions seek to remedy some of the deficiencies of traditional force fields by developing empirical free energy functions that reproduce observed binding constants. Most of these approaches use an expanded master equation to model the free energy of binding, adding entropic terms to the molecular mechanics equations:

$$\Delta G = \Delta G_{\text{vdw}} + \Delta G_{\text{hbond}} + \Delta G_{\text{elec}} + \Delta G_{\text{conform}} + \Delta G_{\text{tor}} + \Delta G_{\text{sol}}$$

where the first four terms are the typical molecular mechanics terms for dispersion/repulsion, hydrogen bonding, electrostatics, and deviations from covalent geometry, respectively; ΔG_{tor} models the restriction of internal rotors and global rotation and translation and ΔG_{sol} models desolvation upon binding and the hydrophobic effect solvent. Entropy changes at solute/solvent interfaces. This latter term is the most challenging. Most softwares use variants of the method of Wesson and Eisenberg⁵⁹, calculating a desolvation energy based on the surface area buried upon complex formation, with the area of each buried atom being weighted by an atomic solvation parameter. AutoDock3 has implemented a similar approach using the thermodynamic cycle of Wesson and Eisenberg. The form of this free energy function is:

$$\begin{aligned} \Delta G = & \Delta G_{\text{vdW}} \sum_{i,j} \left(\frac{A_{ij}}{r_{ij}^{12}} - \frac{B_{ij}}{r_{ij}^6} \right) \\ & + \Delta G_{\text{hbond}} \sum_{i,j} E(t) \left(\frac{C_{ij}}{r_{ij}^{12}} - \frac{D_{ij}}{r_{ij}^{10}} + E_{\text{hbond}} \right) \\ & + \Delta G_{\text{elec}} \sum_{i,j} \frac{q_i q_j}{\epsilon(r_{ij}) r_{ij}} \\ & + \Delta G_{\text{tor}} N_{\text{tor}} \\ & + \Delta G_{\text{sol}} \sum_{i_C, j} S_i V_j e^{(-r_{ij}^2 / 2 \sigma^2)} \end{aligned}$$

where the five ΔG terms on the right-hand side are coefficients empirically determined using linear regression analysis from a set of protein/ligand complexes with known binding constants. The summations are performed over all pairs of

58 C. Hansch, A. R. Steward, J. Iwasa, and E. W. Deutsch, *Mol. Pharmacol.*, **1965**, 1, 205.

59 L. Wesson and D. Eisenberg, *Prot. Sci.*, **1992**, 1, 227.

ligand atoms, i , and protein atoms, j , in addition to all pairs of atoms in the ligand that are separated by three or more bonds. The in vacuo contributions include three interaction energy terms: a Lennard-Jones 12-6 dispersion/repulsion term; a directional 12-10 hydrogen bonding term, where $E(t)$ is a directional weight based on the angle, t , between the probe and the target atom; and a screened Coulombic electrostatic potential. A measure of the unfavorable entropy of ligand binding due to the restriction of conformational degrees of freedom is added to the in vacuo function. This term is proportional to the number of sp³ bonds in the ligand, N_{tor} .

E_{hbond} is the estimated average energy of hydrogen bonding of water with a polar atom, and the summation in the solvation term is performed over all pairs consisting of only carbon atoms in the ligand, i , and atoms of all types, j , in the protein. Note that the internal or intramolecular interaction energy of the ligand is not included in the calculation of binding free energy; during docking, however, internal energy is included in the total docked energy, because changes in ligand conformation can affect the outcome of the docking, so this must be taken into consideration. The assumption made is that the internal energy of the ligand in solution and in the complex are the same. The energies used and reported by AutoDock3 should be distinguished: there are docked energies, which include the intermolecular and intramolecular interaction energies, and which are used during dockings; and predicted free energies, which include the intermolecular energy and the torsional free energy. Such scoring function is then claimed to be able to correctly predict inhibitors k_i with enough accuracy to discriminate between millimolar, micromolar and nanomolar inhibitors.

Target structures, when available, were downloaded from the Protein Data Bank (PDB)⁶⁰. PDGFRK crystallographic structure has not been resolved yet, then it has been constructed by homology modelling using PDB files 1AGW (FGFRK) and 1VR2 (VEGFR2K) as templates for the catalytic domain. The program Modeller6v2⁶¹ was used for homology modelling with alignments generated with T-COFFEE⁶² as it's thoroughly described in the experimental section.

Human EGFRK, PDGFRK, VEGFR2K and FGFR1K, have been considered in this

60 H.M. Berman, J. Westbrook, Z. Feng, G. Gilliland, T.N. Bhat, H. Weissig, I.N. Shindyalov, P.E. Bourne: The Protein Data Bank, *Nucleic Acids Research*, **2000**, 235-242.

61 A. Šali and T.L. Blundell, *J. Mol. Biol.*, **1993**, 234, 779-815.

62 C. Notredame, D. Higgins, J. Heringa, *Journal of Molecular Biology*, **2000**, 302, 205-217.

docking study. The protocol used has been validated by reproducing the binding mode of the cocrystallized inhibitor if present in the PDB file, or otherwise by reproducing dockings present in literature⁶³. Ligands has been constructed using the commercial program LINMOPAC from Fujitsu. Geometries has been optimized using the semiempirical theory with the Austin Model 1⁶⁴ (AM1) to a gradient of 0.01 with the commercial program MOPAC2002. Partial charges has been derived from electrostatic potential calculated *ab-initio* at the HF/6-31G* level of theory²³ using the program GAMESS²¹, according to the Merz-Kollman procedure⁶⁵, this because one key criterion for molecular simulations is the accurate description of the electrostatic potential around the solute, achieved by the so-called potential derived atomic charges obtained from a least-squares fit to the quantum mechanically determined molecular electrostatic potential, discretized on a grid of points, and targeted at the faithful reproduction of the latter quantity. Such is generally the case for polar systems, in which the local multipoles borne by each atomic site can be represented satisfactorily by a simple set of atom-centered point charges. The approximation that the electrostatics of the system formed by the solute and the solvent could be reduced to a sum of pairwise Coulomb interactions neglects, however, the polarization of the neighboring solvent molecules by the solute, and, in turn, the polarization of the solute by its surroundings. Employing the most accurate geometry and *ab initio* wave function, the one guaranteeing a correct reproduction of the molecular multipole moments of the solute in the gas phase, one clearly cannot hope to describe satisfactorily such intermolecular induction effects. To circumvent this difficulty, Kollman et al. suggest that electrostatic potential derived charges computed at the restricted Hartree Fock (RHF) level of approximation, using the split-valence 6-31G* basis set, could allow polarization effects to be included in molecular mechanical simulations in an average manner. This heuristic method is based on the observation that dipole moments evaluated at this level of theory generally overestimate the corresponding experimental quantities by 10-15%, thereby increasing artificially the polarity of the solute and compensating for the missing induction term in the force field.

63 Brian D. Palmer et al., *J. Med. Chem.*, **1999**, 42, 2373-2382

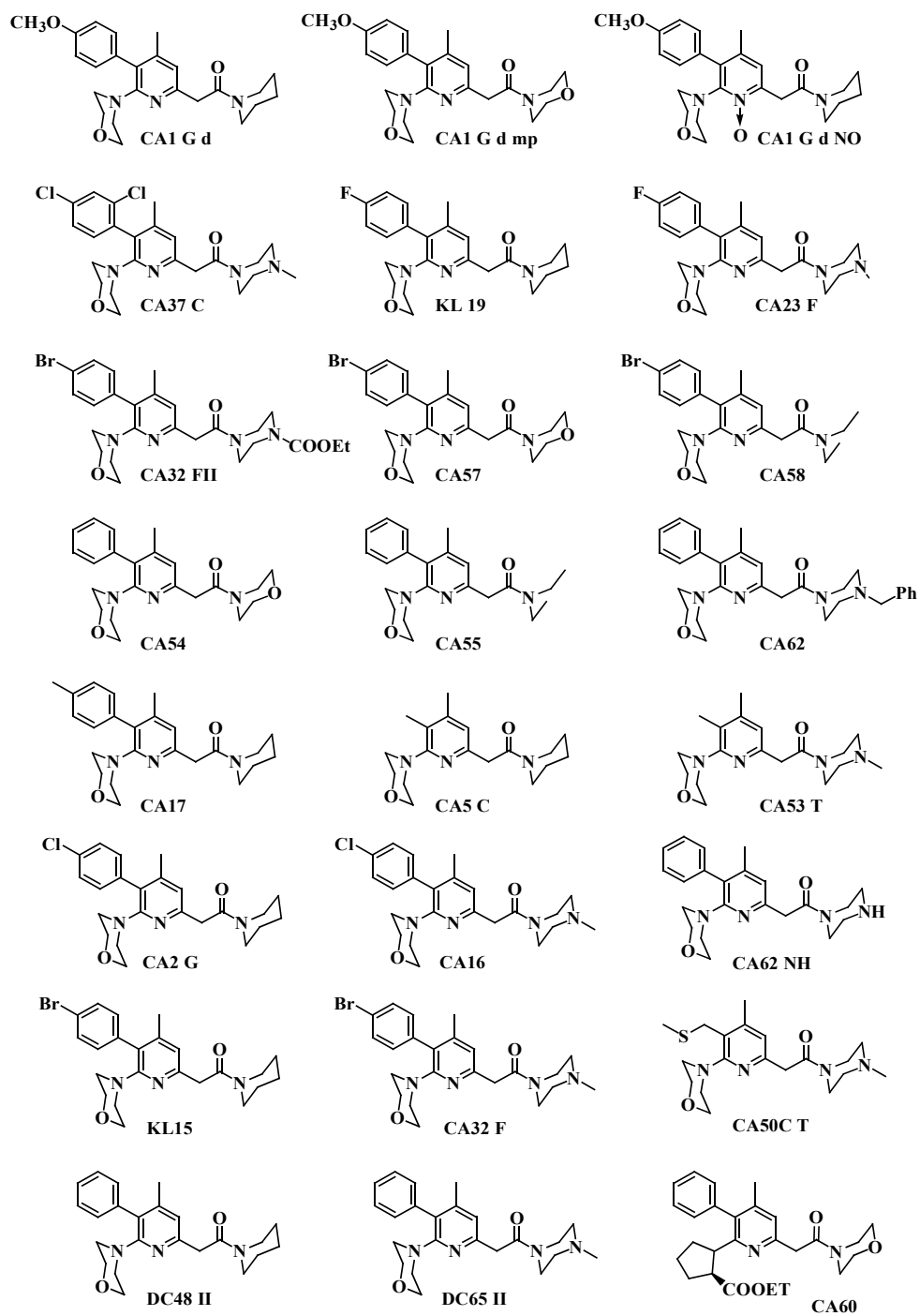
64M.J.S. Dewar, E.G. Zoebisch, E.F. Healy and J.J.P. Stewart, *J. Am. Chem. Soc.*, **1985**, 107, 3902

65 a)Besler, B. H.; Merz Jr., K. M.; Kollman, P. A. *J Comput Chem*, **1990**, 11, 431.

b)Merz, K. M. *J Comput Chem* , **1992**, 13, 749.

2-Pyridinacetamides included in this docking study are represented in Figure 1 below.

Figure 1: 2-Pyridinacetamides considered for docking to receptors tyrosine kinase



Docking of 2-Pyridineacetamides to EGFRK

Cristal structures of EGFRK alone or complexed with it's inhibitor Tarceva® (Erlotinib)⁶⁶ have been recently resolved and made available on the Protein Data Bank, respectively as 1M14 and 1M17. The EGFRK kinase domain adopts the bilobate-fold characteristic of all previously reported protein kinase domains. The NH₂-terminal lobe (N-lobe) is formed from mostly β -strands and one α -helix (α C), whereas the larger COOH terminal lobe (C-lobe) is mostly α -helical. The two lobes are separated by a cleft similar to those in which ATP, ATP analogues, and ATP-competitive inhibitors have been found to bind. Important elements of the catalytic machinery bordering the cleft on the N-lobe include the glycine-rich nucleotide phosphate- binding loop (Gly695-Gly700), whereas the C-lobe contributes the DFG motif (Asp831-Gly833), the presumptive catalytic (general base) Asp813, the catalytic loop (Arg812-Asn818), and the A-loop (Asp831-Val852). The NH₂-terminal lobe of EGFRK adopts a tertiary structure similar to previously observed structures of RTKs (r.m.s. deviations for superpositioning C- α atoms with the kinase domain from the fibroblast growth factor receptor is about 1.2 Å), although a few features distinguish the N-lobe of EGFRK from other kinase domains. The NH₂-terminal nine amino acids are influenced by several intermolecular contacts including H-bonds involving main chain atoms of residues Asn676 and Leu680, although intramolecular H-bonds between Asn676 and both Tyr740 and Ser744 also contribute. At Glu685, the polypeptide chain assumes a trace more similar to those of the lymphocyte tyrosine kinase (LCK, PDB code 3lck), the insulin receptor kinase-phosphorylated form (p-IRK, PDB code 1ir3), and the unphosphorylated form of the FGF receptor kinase (FGFRK, PDB code 1fgk). However, EGFRK lacks the tryptophan- glutamate (WE) motif found in these related kinases, and has Arg681-Ile682 instead. In the WE-containing kinases, hydrophobic interactions of the tryptophan and an H-bond between the glutamate and a threonine or serine and the neighboring β -strand tie the NH₂-terminal region to the N-lobe. In EGFRK Arg681 projects into solvent, but Ile682 contacts Leu782 and Ile756 on the neighboring β -strand and thereby affords a similar effect. Among the canonical features characterizing the N-lobes of active forms of kinases is a salt bridge between two highly conserved side chains that interact with the α - and β -phosphates

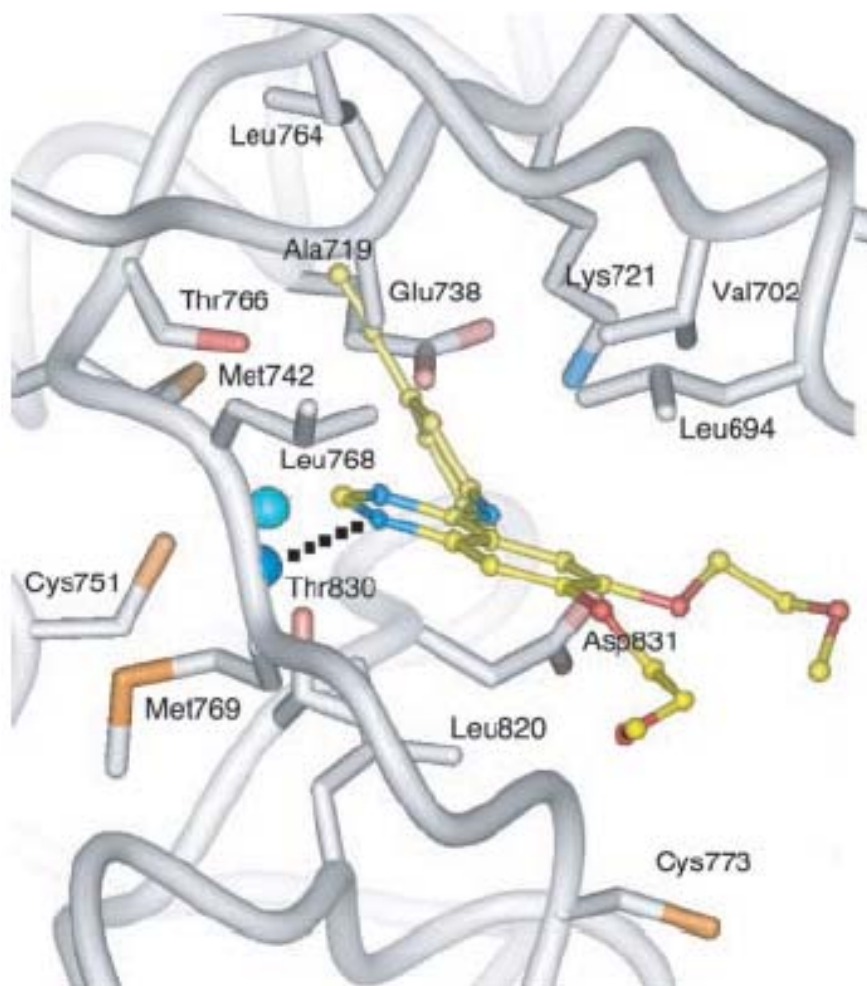
66 J. Stamos, M. X. Sliwkowski, and C. Eigenbrot, *JBC*, **2002**, 277, 46265-46272.

when ATP or a close homologue is present. Such salt bridge inhibitor-bound forms of EGFRK, between Lys721 and Glu738 is present in both ligated and unligated structure, suggesting that EGFRK does not require large rearrangements within the N-lobe for catalytic competence. The COOH-terminal domain of EGFRK contains the usual organization of α -helices present in other kinase domain structures. Superpositioning of the C-lobes of kinase domains from both LCK and p-IRK yield a r.m.s. deviation of 1.1 Å. However, as with the N-lobe, a few key features differ from previously elucidated RTK structures. In most protein kinases, the activation loop assumes its catalytically competent conformation only if it first becomes phosphorylated on a Tyr or Thr. For these kinases, the unphosphorylated activation loop is positioned many Angstroms from the active conformation and may include a direct inhibitory element. For instance, the unphosphorylated A-loop in FGFRK is incompatible with substrate binding, and the unphosphorylated insulin receptor kinase A-loop blocks ATP binding as well as the substrate tyrosine site. The A-loop in ligated and unligated EGFRK differs significantly from other unphosphorylated A-loop structures and adopts an active conformation similar to the phosphorylated A-loop of p-IRK. The well conserved sequence of the EGFRK catalytic-loop (HRDLAARN), also present in p-IRK and FGFRK, shares structural conservation with these RTKs as well with a r.m.s. deviation of most atoms of only 0.1 Å. The nearby conserved DFG sequence, important for ATP coordination, adopts the p-IRK-like arrangement well with a r.m.s. deviation of most atoms of only 0.1 Å. The principle difference between the p-IRK and EGFRK structures in this region is in the nucleotide phosphate-binding loop.

Figure 2 shows interactions between Tarceva and EGFRK. 4-anilinoquinazolines such as Tarceva cause inhibition through binding to the site occupied by ATP during phosphotransfer. Tarceva lies with the N-1- and C-8-containing edge of the quinazoline directed toward the peptide segment connecting N- and C-lobes, with the ether linkages projecting past the connecting segment into solvent and the anilino substituent on the opposite end sequestered in a hydrophobic pocket. The N-1 of the quinazoline accepts an H-bond from the Met769 amide nitrogen. The other quinazoline nitrogen atom (N-3) is not within H-bonding distance of the Thr766 side chain (4.1 Å), but a water molecule bridges this gap. Such a water molecule contacts the side chain of Cys751. The less robust nature of this water-mediated H-

bond between Tarceva and EGFRK parallels the relatively small effect on inhibitor affinity seen for substitution with carbon for N-3 among compounds characterized by Rewcastle et al⁶⁷.

Figure 2: *interactions between Tarceva and EGFRK active site*



The interplanar angle of aromatic ring systems in Tarceva is 42°. This directs the acetylene moiety into a pocket that many kinase domains share when the amino acid side chain at position 766 is small (threonine in EGFRK). Thr766, Lys721, and Leu764 are 4 Å from the acetylene moiety on the anilino ring (Thr766 and Leu764 are 3.4 Å).

Our first task was then to validate our docking protocol by reproducing accurately the binding mode of the inhibitor cocrystallized with EGFRK as reported above.

Current docking procedure is to remove all non-protein atoms from the PDB file, thus including water molecules, but a recent study⁶⁸ conducted at the ETH by Prof.

67 G. W. Rewcastle et al., *J. Med. Chem.*, **1995**, 38, 3482-3487.

68 P. Pospisil, T. Kuoni, L. Scapozza and G. Folkers., *J. Receptor & Signal Transduction Res.*,

Folkers and Scapozza revealed the importance that water molecules could play in molecular docking. Has been reported above that a water molecule bridges the gap between Tarceva's N-3 and the Thr766 side chain. Furthermore such water is present either in the ligated and unligated structure of EGFRK with superposable coordinates, suggesting that this water molecule could be a structural and not only crystallization water. For those reasons we set up two docking experiments, one following the standard procedure (removal of all water from the PDB file) and one keeping the water molecule H-linked to Thr766 (water number 10 in the PDB file). Figures 3 and 4 show resulted “top 5” docked structures of Tarceva in the EGFRK active site. It's evident from Figure 3 that the ligand docks in a really disordered way, each structure assuming different orientations and not allowing the obtainment of a significative cluster of conformations to describe the binding mode. Moreover only one structure assume an orientation close to that described by crystallography.

Figure 3: Docking of Tarceva to the EGFRK active site without considering water

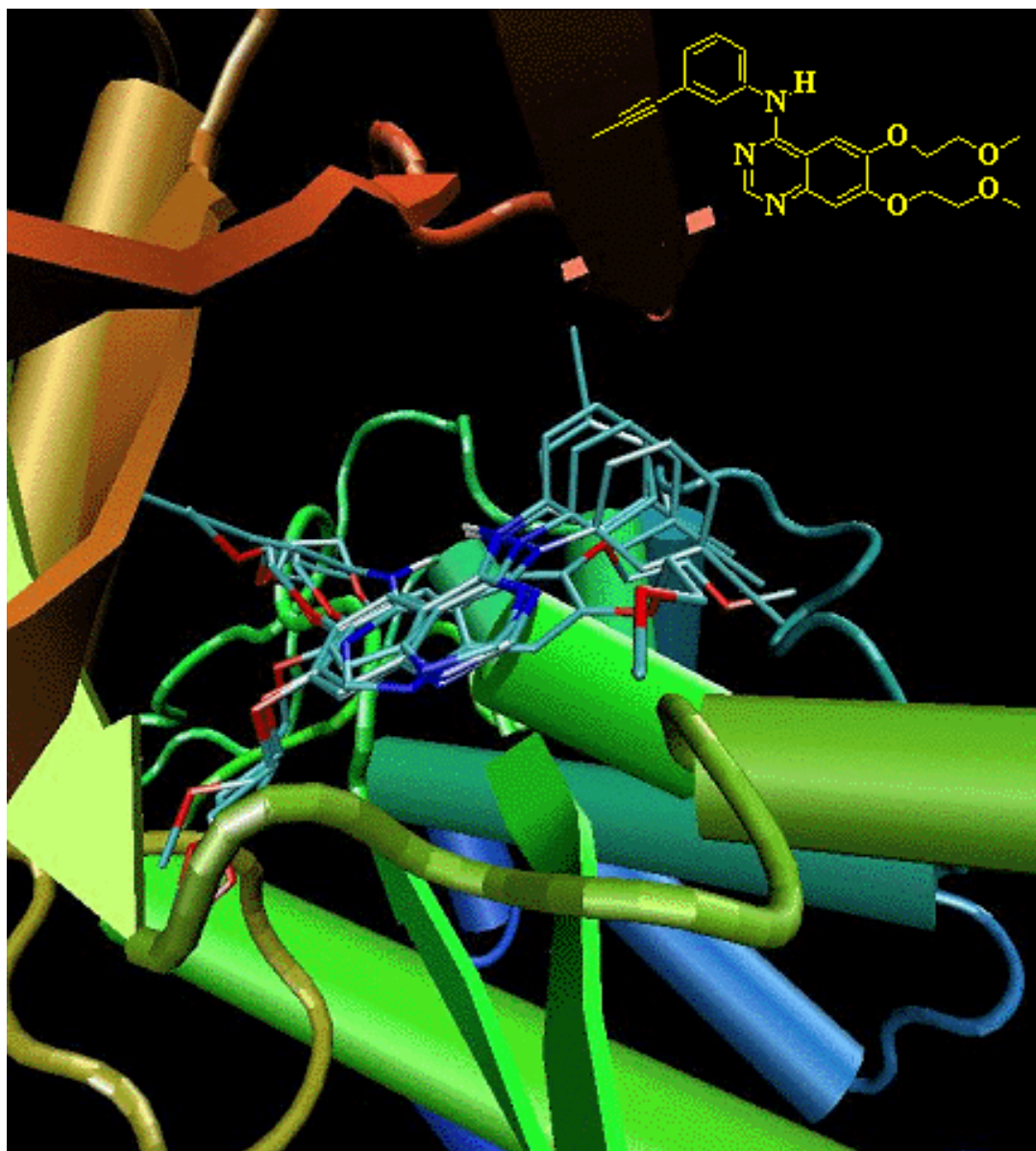
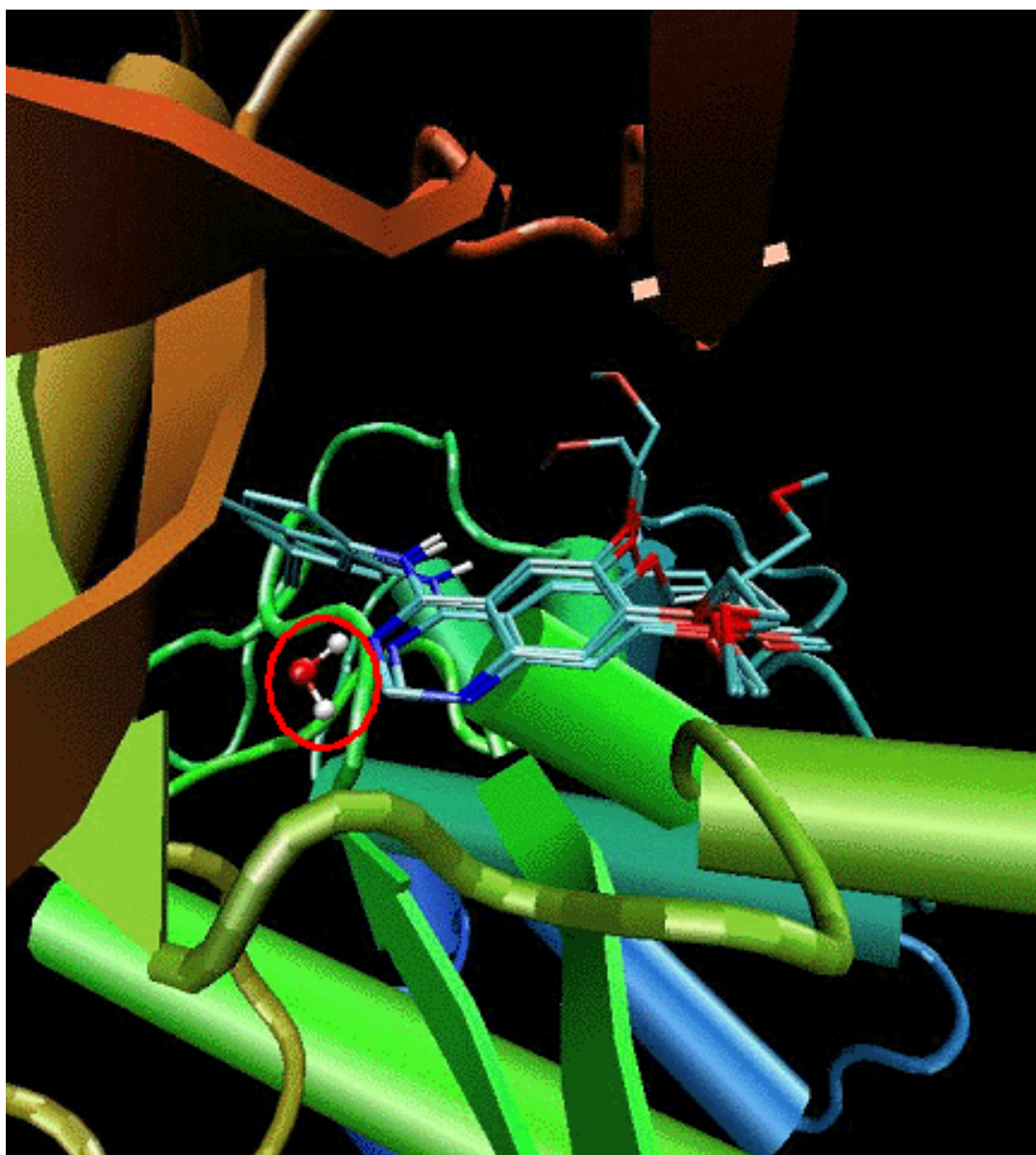


Figure 4 shows “top 5” results obtained by a docking run considering water 10 as a part of the active site during calculations of grids of potential necessary for AutoDock3 calculation and water parameters are taken from the well tested Amber force field. Results from this run are enthusiastic, as all of the 50 conformations obtained from the calculation are within a rmsd of 0.5 with the reference crystallographic compound. The major differences occur at the sidechains, extremely flexible and probably allowed to move; this observation could be confirmed by the absence of description of any role of those in the receptor binding, and they probably constitute the aptophore moiety of the drug.

Figure 4: *Docking of Tarceva to the EGFRK active site considering water 10*



Those results confirm the validity of the docking protocol used, as it has been possible to highly reproduce the binding mode of Tarceva as described by crystallographic resolution.

In order to assess if the presence or absence of water 10 could affect also docking of 2-pyridinacetamides we performed a docking run on the compound **CA1Gd** considering or not water 10 as a part of the active sites. “Top 5” structures resulted from both calculations are represented in Figures 5 and 6, and the importance of the presence of water bridge between Thr766 and inhibitor results even more evident.

The distance observed between pyridin's N and water's H is of about 3 Å, probably a distance too high to hypothesize a real H-bond, but enough to stabilize the orientation of compound **CA1Gd** inside the binding pocket. Subsequent calculations have then been made considering water 10 as constitutive of the active site.

Figure 5: Docking of CA1Gd to the EGFRK active site without considering water

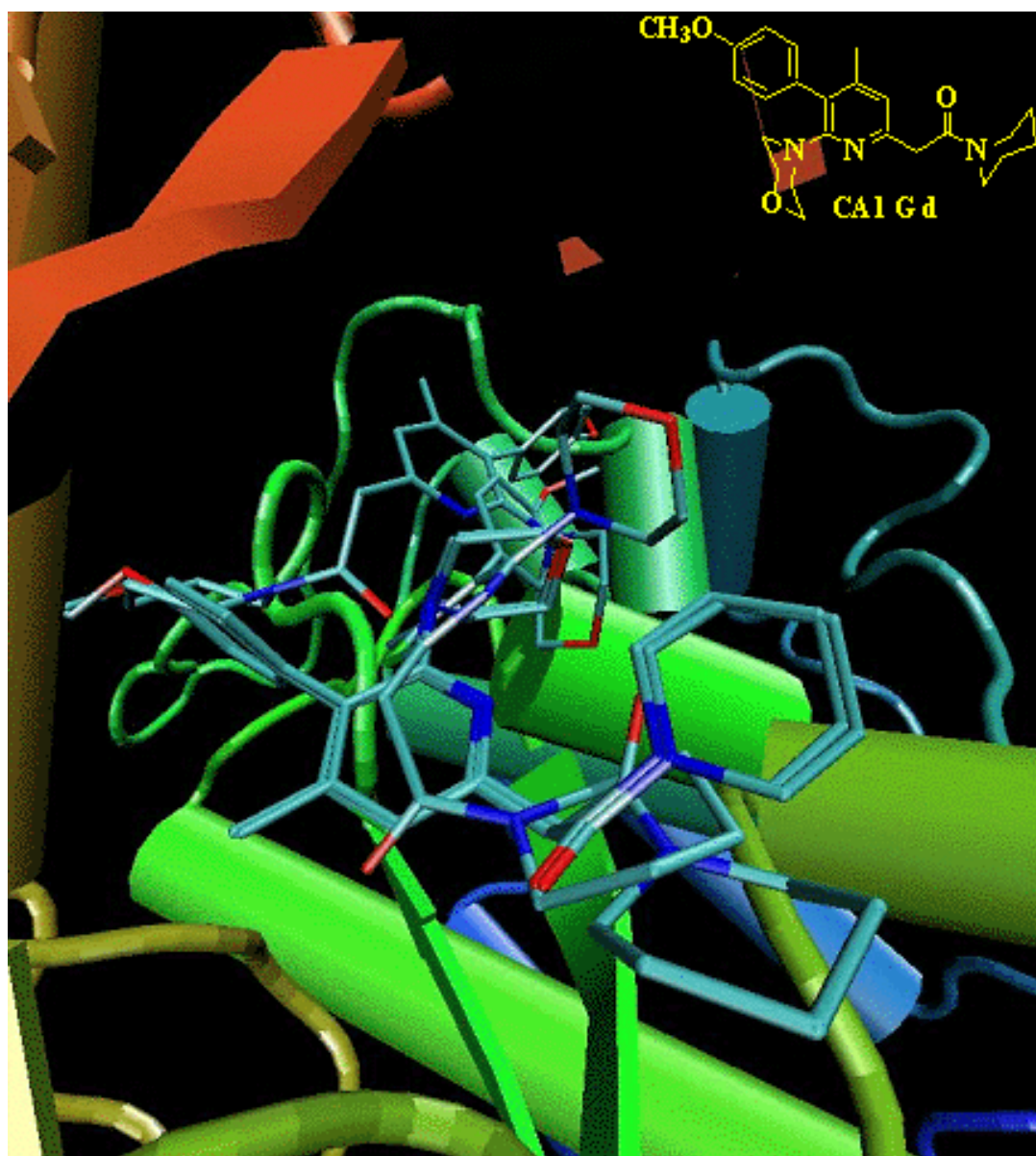
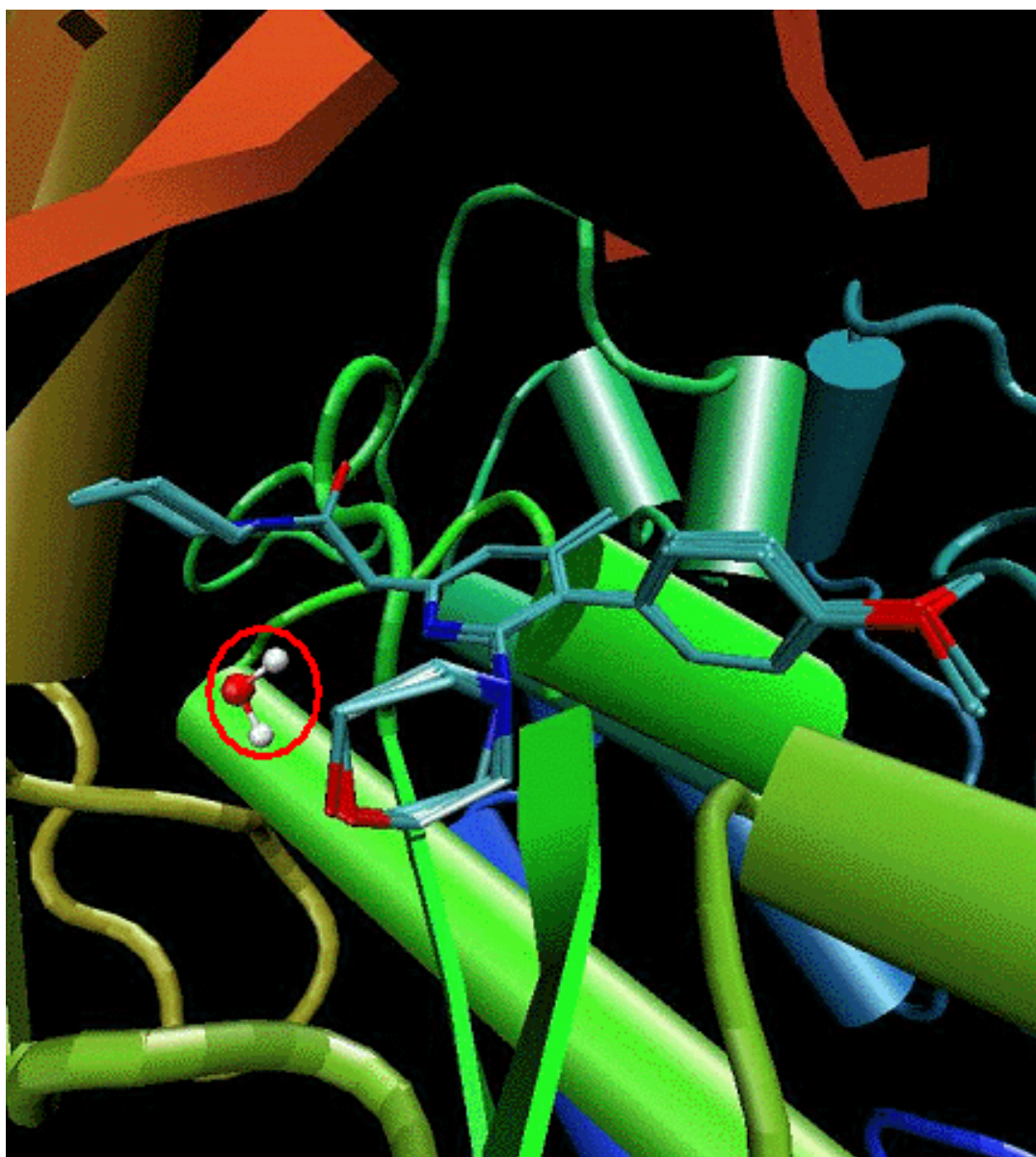


Figure 6: Docking of CA1Gd to the EGFRK active site considering water 10

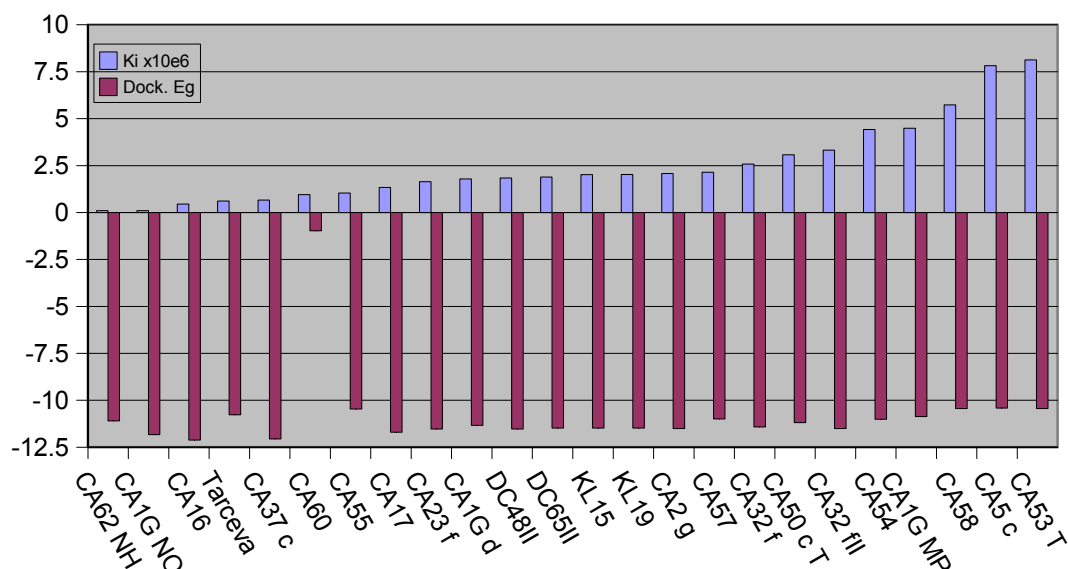


All 2-pyridineacetamides reported in figure 1 has been docked to EGFRK and results are summarized in Table 1 and represented graphically in Graph1

Table 1: *Docking of 2-Pyridinacetamides to the EGFRK active site:
energy results and scoring*

	Ki x10e6	Dock. Eg	Mol/cluster	Cluster Rank
CA62 NH	0.1	-11.09	33	1
CA1G NO	0.11	-11.82	26	1
CA16	0.45	-12.12	12	2
Tarceva	0.61	-10.77	8	1
CA37 c	0.66	-12.06	18	2
CA60	0.96	-0.97	7	2
CA55	1.04	-10.46	16	1
CA17	1.34	-11.7	29	1
CA23 f	1.64	-11.53	20	2
CA1G d	1.79	-11.33	18	1
DC48II	1.84	-11.53	38	1
DC65II	1.89	-11.48	20	1
KL15	2.02	-11.48	25	1
KL19	2.03	-11.48	22	1
CA2G	2.08	-11.5	31	1
CA57	2.15	-10.99	18	2
CA32 FII	2.58	-11.42	21	1
CA50 c T	3.08	-11.19	7	1
CA32 FII	3.32	-11.5	7	9
CA54	4.42	-11.01	29	1
CA1G MP	4.49	-10.86	14	1
CA58	5.73	-10.44	8	1
CA5 c	7.82	-10.41	41	1
CA53 T	8.13	-10.44	32	1

Graph1: Docking of 2-Pyridinacetamides to the EGFRK active site:
energy results and scoring



Graph1 represents predicted K_i (blue) compared with resulted docked energy (red). In order to assign correct scoring to docked compounds it's necessary to consider always more than one scoring function; for example in graph 1 compound CA60 shows a really low K_i , but high docked energy suggest really unfavorable steric clashes for the resulted complex. For greater accuracy it's also important to consider the maximum number of conformations per cluster (wich shows how well is reproduced a paticular conformation inside the docking run) and the energy ranking of the most representative cluster. Anyway a visual inspection of results is a must fo a correct interpretation; in fact, docking of Tarceva seems to result a poor cluster of conformations, but this is due to the high flexibility of side chains and considering the quinazoline pharmacophoric nucleus it's correctly docked for more than 40 conformations, compared with cristallographic results.

It's interesting to notice how well tested 2-pyridineacetamides fit in the EGFRK active site: most of them show clusters of more than 20 orientations, ranked as first or second in energy. Scoring is also interesting: in the top 10 results are reported the reference compound Tarceva (ERL), CA16, CA37c, CA55, CA23 F, CA1G D, all resulted active at the pharmacological tests on SMC proliferation; CA62 NH, CA1G

NO and CA60 has never been tested and CA17 resulted completely inactive. Unfortunately the compound resulted more potent in cellular assays it's ranked only 16th, however we have to consider that docking assays are a model for reproducing binding assays on purified enzyme, being the cellular model more complicated, since must be considered also the ability of tested compounds to reach the target enzyme (membrane permeation, interaction with other binding sites, enzymatic degradation etc.). However, generally predicted results are in good agreement with pharmacological results.

It should be noticed that conformations resulted from docking of 2-pyridineacetamides and ranked as reported in Table 1, present all the same orientation inside the active site of EGFRK, and this could be considered as another proof of the accuracy of those successful run. In fact it has been possible to describe a common binding mode for all compounds.

Figure 7 depicts compound CA1G d docked in EGFRK's active site cavity, while Figure 8 describe the proposed binding mode for CA1Gd, but we generally observed the same interactions for all 2-pyridineacetamides included in this docking.

Figure 7: *Compound CA1Gd docked inside EGFRK's active site cavity*

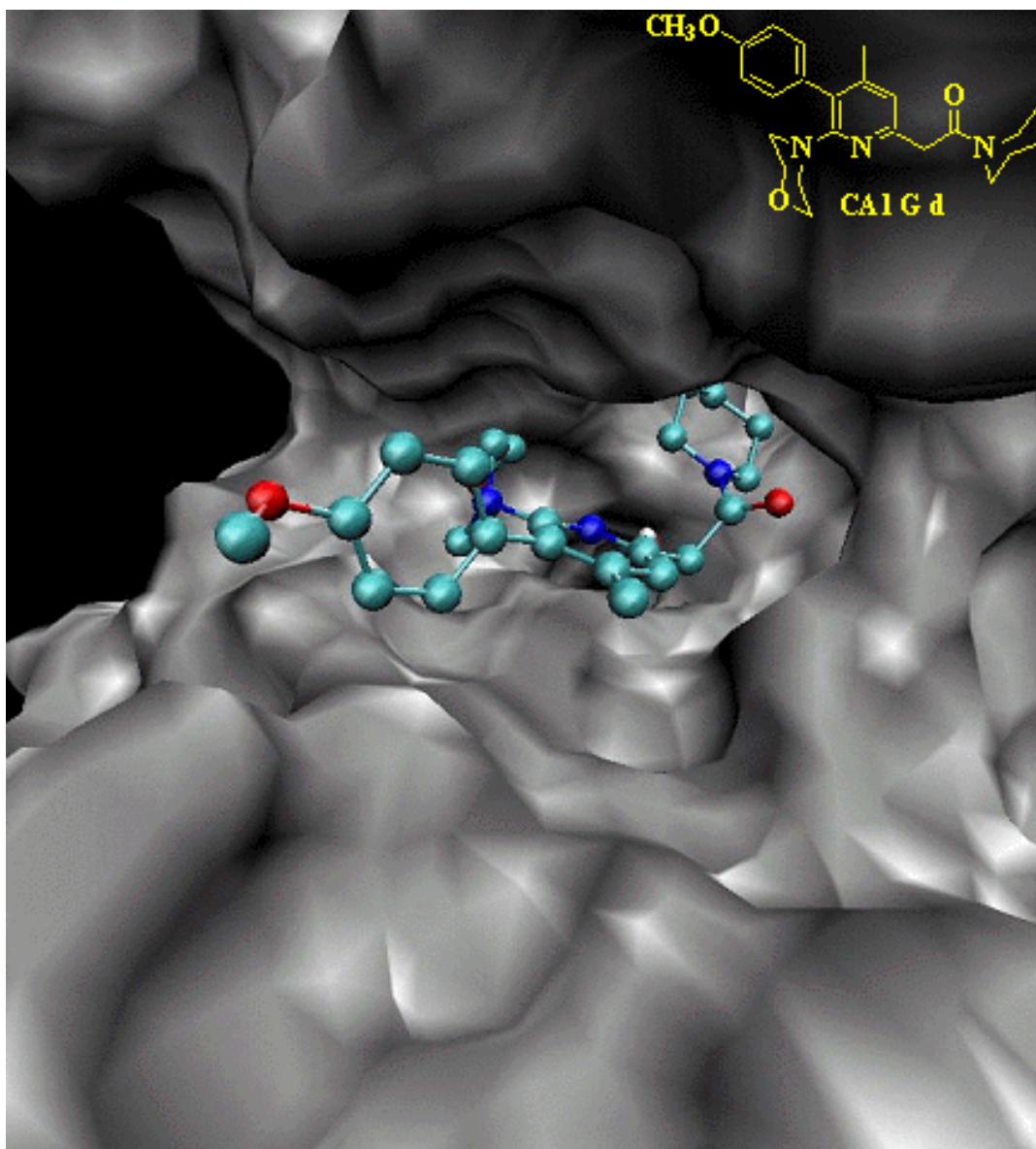
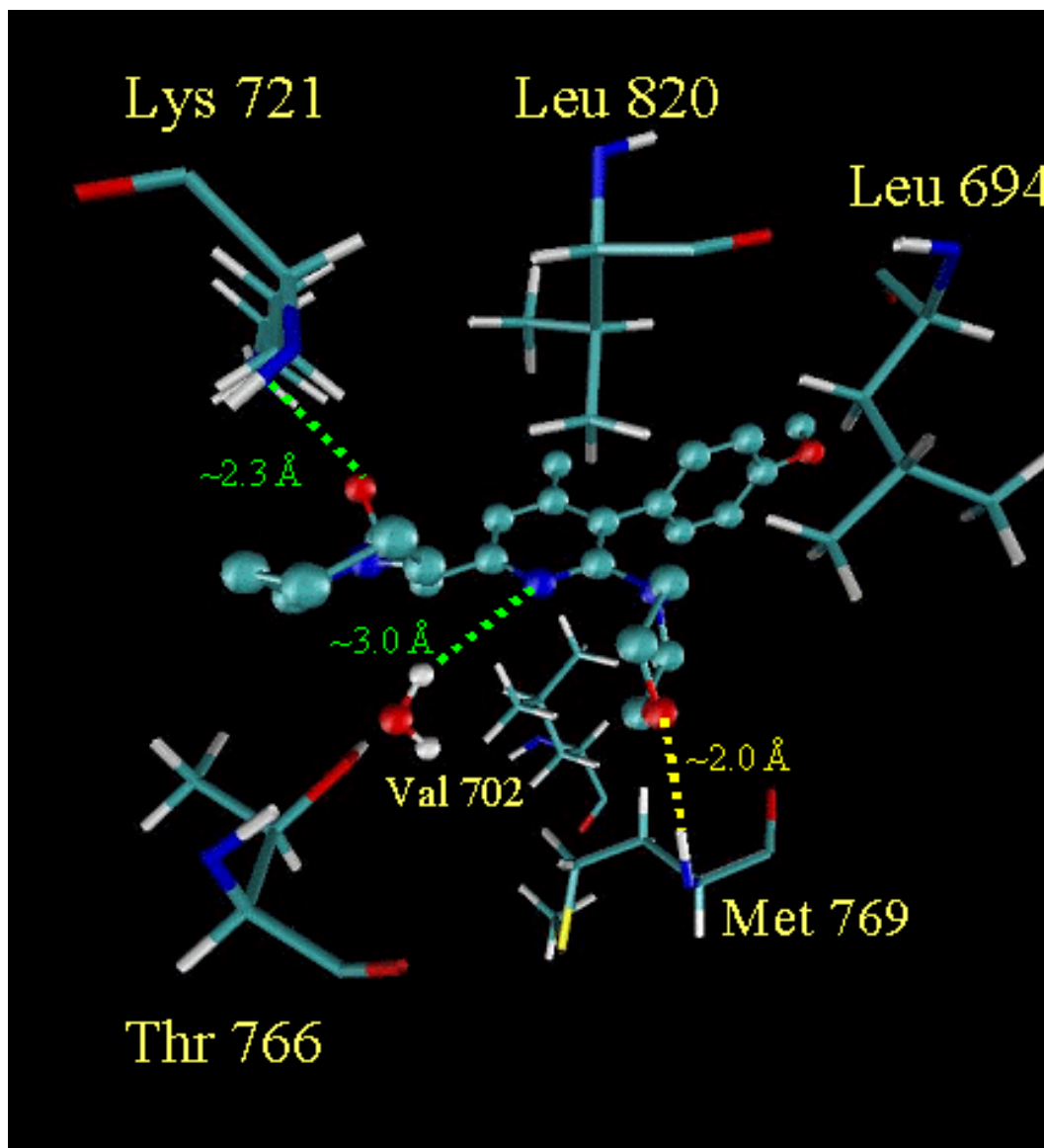


Figure 8: *Proposed binding mode for 2-Pyridinacetamides to EGFRK. Compound CA1Gd is shown as example*



As shown in figure 8, main interaction observed are:

- H-bond between Met769 and morpholine-6 oxygen
- H-bond between Lys721 and amidic C=O
- H-bond bridged by water between Thr766 and pyridine's N
- Hydrophobic interactions between Leu820 and Val702 with pyridine nucleus
- Hydrophobic interactions between Leu694 and the aromatic substituent at C-5.

The proposed binding mode is in agreement with the reported binding mode for literature compounds described in Chapter 2 and 3, as it involves or the same aminoacids or aminoacids close to them, well inside the active site. This hypothesized binding mode is also reasonable considering the absence of pharmacological activity on SMC proliferation assays for all 2-pyridineacetamides lacking of the aromatic substituent at C-5 position.

A potential improvement to the docking of 2-pyridineacetamides in the active site of EGFRK could be done by an opportune substitution at the pyridine nitrogen with a polar chain, in order to displace water and bind threonine OH. This could yield a great gain in docking energy due to a further H-bond and to the entropic contribution caused by the expulsion of water from the active site. However such substitution could be done only by generating a salt (i. e. by a nucleophilic addition to an epoxyde of the pyridin nitrogen) that would encounter much more difficulties in permeating cellular membranes and thus in reaching tyrosin kinase receptors.

Docking of 2-Pyridineacetamides to PDGFRK

Docking of compounds reported in Figure 1 to PDGF receptor kinase required particular attention, as a model of the structure has to be constructed due to the lack of crystal structures. Homology modelling is the most reliable technique for generating protein models for docking purposes, allowing the prediction of the 3D structure of a given protein sequence (target) based primarily on its alignment to one or more proteins of known structure (templates). The prediction process consists of fold assignment, target-template alignment, model building, and model evaluation. The number of protein sequences that can be modeled and the accuracy of the predictions are increasing steadily because of the growth in the number of known protein structures and because of the improvements in the modeling software. It is currently possible to model with useful accuracy significant parts of approximately one half of all known protein sequences⁶⁹.

Despite progress in ab initio protein structure prediction⁷⁰, comparative modeling remains the only method that can reliably predict the 3D structure of a protein with an accuracy comparable to a low-resolution experimentally determined structure⁷¹.

The starting point in comparative modeling is to identify all protein structures related to the target sequence, and then select those structures that will be used as templates.

There are three main classes of protein comparison methods that are useful in fold identification:

1. The **first** class includes the methods that compare the target sequence with each of the database sequences independently, using pairwise sequence-sequence comparison⁷². Frequently used programs in this class include FASTA⁷³ and BLAST⁷⁴.
2. The **second** set of methods relies on multiple sequence comparisons to improve the sensitivity of the search⁷⁵. A widely used program in this class is PSI-

69 U. Pieper et al., *Nucleic Acids Res.*, **2002**, 30, 255-259

70 a) D. Baker, *Nature*, **2000**, 405, 39-42

b) R. Bonneau and D. Baker, *Annu. Rev. Biophys. Biomol. Struct.*, **2001**, 30, 173-189

71 M. A. Marti-Renom et al., *Annu. Rev. Biophys. Biomol. Struct.*, **2000**, 29, 291-325

72 A. Apostolico and R. Giancarlo, *J. Comput. Biol.*, **1998**, 5, 173-196

73 a) W. R. Pearson and D. J. Lipman, *Proc Natl Acad Sci USA*, **1988**, 85, 2444-2448

b) W. R. Pearson, *Protein Sci.*, **1995**, 4, 1145-1160

74 S. F. Altschul et al., *J. Mol. Biol.*, **1990**, 215, 403-410

75 L. Rychlewski et al., *Fold Des.*, **1998**, 3, 229-238 and ref. cited therein

BLAST, which iteratively expands the set of homologs of the target sequence. For a given sequence, an initial set of homologs from a sequence database is collected, a weighted multiple alignment is made from the query sequence and its homologs, a position specific scoring matrix is constructed from the alignment, and the matrix is used to search the database for additional homologs. These steps are repeated until no additional homologs are found. In comparison to BLAST, PSI-BLAST finds homologs of known structure for approximately twice as many sequences⁷⁶.

3. The **third** class of methods is the so-called threading or 3D template matching methods⁷⁷. These methods rely on pairwise comparison of a protein sequence and a protein of known structure. Whether or not a given target sequence adopts any one of the many known 3D folds is predicted by an optimization of the alignment with respect to a structure dependent scoring function, independently for each sequence-structure pair. That is, the target sequence is threaded through a library of 3D folds.

This latter method is included in the program Modeller6V2 inside the SEQ_SEARCH routine. These methods are especially useful when there are no sequences clearly related to the modeling target, and thus the search cannot benefit from the increased sensitivity of the sequence profile methods. A useful fold assignment approach is to accept an uncertain assignment provided by any of the methods, build an all-atom comparative model of the target sequence based on this match, and make the final decision about whether or not the match is real by evaluating the resulting comparative model⁷⁸.

Once a list of all related protein structures was obtained, it is necessary to select those templates that are appropriate for the given modeling problem. Usually, a higher overall sequence similarity between the target and the template sequence yields a better model. The quality of the experimental template structure is another important factor in template selection. The resolution and the R-factor of a

76 a) J. Park et al., *J. Mol. Biol.*, **1998**, 284, 1201-1210

b) M. J. Sternberg et al., *Curr. Opin. Struct. Biol.*, **1999**, 9, 368-373

77 a) J. U. Bowie et al., *Science*, **1991**, 253, 164-170

b) D. T. Jones et al., *Nature*, **1992**, 358, 86-89

c) A. Godzik et al., *J. Mol. Biol.*, **1992**, 227, 227-238

78 a) R. Sanchez and A. Sali, *Curr. Opin. Struct. Biol.*, **1997**, 7, 206-214

b) B. Guenther et al., *Cell*, **1997**, 91, 335-345

c) J. M. Miwa et al., *Neuron*, **1999**, 23, 105-114

crystallographic structure and the number of restraints per residue for an NMR structure are indicative of its accuracy. If the model is to be used to analyze the geometry of the active site of an enzyme, it is preferable to use a high-resolution template. Furthermore the use of several templates approximately equidistant from the target sequence generally increases the model accuracy⁷⁹.

The second step in model building is generating a correct target-template alignment. Most fold assignment methods produce an alignment between the target sequence and template structures. However, this alignment is often not the optimal target-template alignment for comparative modeling. Searching methods are usually tuned for detection of remote relationships, not for optimal alignments. Therefore, once templates have been selected, a specialized method should be used to align the target sequence with the template structures⁸⁰. For closely related protein sequences with identity higher than 40%, the alignment is almost always correct. Regions of low local sequence similarity become common when the overall sequence identity is below 40%⁸¹. The alignment becomes difficult in the twilight zone of less than 30% sequence identity⁸². As the sequence similarity decreases, alignments contain an increasingly large number of gaps and alignment errors, regardless of whether they are prepared automatically or manually. For example, only 80% of the residues are likely to be correctly aligned when two proteins share 30% sequence identity⁸³. Maximal effort to obtain the most accurate alignment possible is needed because no current comparative modeling method can recover from an incorrect alignment. In the more difficult alignment cases, it is frequently beneficial to rely on multiple structure and sequence information⁸⁴.

First, the alignment of the potential templates is prepared by superposing their structures. Next, the sequences that are clearly related to the templates and are easily aligned with them are added to the alignment. The same is done for the target sequence. Finally, the two profiles are aligned with each other, taking structural information into account as much as possible⁸⁵.

79 N. Srinivasan and T. L. Blundell, *Protein Eng.*, **1993**, *6*, 501-512

80 T. F. Smith, *Structure Fold Des.*, **1999**, *7*, R7-R12 and ref cited therein

81 M. A. Saqi et al., *Protein Eng.*, **1998**, *11*, 627-630

82 B. Rost, *Protein Eng.*, **1999**, *12*, 85-94

83 M. S. Johnson and J. P. Overington, *J. Mol. Biol.*, **1993**, *233*, 716-738

84 W. R. Taylor et al., *Protein Sci.*, **1994**, *3*, 1858-1870 and ref cited therein

85 Sali, A., Fiser, A., Sanchez, R., Marti-Renom, M. A., Jerkovic, B., Badretdinov, A., Melo, F., Overington, J., and Feyfant, E. MODELLER, A Protein Structure Modeling Program, Release 6v2. **2002**. <http://guitar.rockefeller.edu/modeller/>.

Third step is generating models for target structure, and a variety of methods can be used to construct a 3D model for the target protein. The original and still widely used method is modeling by rigidbody assembly⁸⁶. Another family of methods, modeling by segment matching, relies on the approximate positions of conserved atoms in the templates⁸⁷. The third group of methods, modeling by satisfaction of spatial restraints, uses either distance geometry or optimization techniques to satisfy spatial restraints obtained from the alignment⁸⁸, and this latter is the one used by Modeller6V2, however accuracies of the various model building methods are relatively similar when used optimally⁸⁹. Other factors, such as template selection and alignment accuracy, usually have a larger impact on the model accuracy, especially for models based on less than 40% sequence identity to the templates.

Last but not least in homology modelling is the model evaluation. The first step in model evaluation is to determine if the model has the correct fold⁹⁰. A model will have the correct fold if the correct template is picked and if that template is aligned at least approximately correctly with the target sequence. The confidence in the model fold is generally increased by a high sequence similarity to the closest template, a pseudo-energy Z-score⁹¹, and conservation of the key functional or structural residues in the target sequence. Once the fold of a model is accepted, a more detailed evaluation of the overall model accuracy can be obtained based on the similarity between the target and template sequences⁹⁰. Sequence identity above 30% is a relatively good predictor of the expected accuracy. The reasons are the well known relationship between structural and sequence similarities of two proteins⁹², the geometrical nature of modeling that forces the model to be as close to the template as possible⁹³, and the inability of any current modeling procedure to recover from an incorrect alignment⁷⁸. The dispersion of the model-target structural overlap increases with the decrease in sequence identity. If the target-template sequence identity falls below 30%, the sequence identity becomes unreliable as a measure of expected accuracy of a single model. Models that deviate significantly

86 J. Greer, *Proteins*, **1990**, 7, 317-334 and ref cited therein

87 M. Levitt, *J. Mol. Biol.*, **1992**, 226, 507-533 and ref cited therein

88 A. Kolinski et al., *Proteins*, **2001**, 44, 133-149 and ref cited therein

89 Marti-Renom et al., *Structure*, **2002**, 10, 435-440

90 R. Sanchez and A. Sali, *Proc Natl Acad Sci U S A*, **1998**, 95, 13597-13602

91 M. J. Sippl, *Proteins*, **1993**, 17, 355-362

92 C. Chothia and A. M. Lesk, *EMBO J.*, **1986**, 5, 823-826

93 A. Sali and T.L. Blundell, *J. Mol. Biol.*, **1993**, 234, 779-815

from the average accuracy are frequent. It is in such cases that model evaluation methods are particularly useful. A basic requirement for a model is to have good stereochemistry. Some useful programs for evaluating stereochemistry are PROCHECK⁹⁴, PROCHECK-NMR and AQUA , SQUID⁹⁵, and WHATCHECK⁹⁶. The features of a model that are checked by these programs include bond lengths, bond angles, peptide bond and sidechain ring planarities, chirality, mainchain and sidechain torsion angles, and clashes between non-bonded pairs of atoms. There are also methods for testing 3D models that implicitly take into account many spatial features compiled from high resolution protein structures. These methods are based on 3D profiles and statistical potentials of mean force⁹⁷. Programs implementing this approach include VERIFY3D⁹⁸ and PROSAIL⁹¹. The programs evaluate the environment of each residue in a model with respect to the expected environment as found in the high-resolution X-ray structures.

In the present work the catalytic domain was then modelled from high homologue PDB files 1AGW chain A (FGFR K) and 1VR2(VEGFRK) as templates, using the program Modeller6V2. A strength of this program is the ability to consider multiple templates alignments as input, and thus generating more significative models compared with those generated using single templates. Templates were identified using the SEQ_SEARCH routine as implemented in modeller. Several models were generated and checked with the program PROCHECK⁹⁴. The best model was then validated trying to reproduce the theoretical binding mode proposed by Palmer et al for compound **22**⁹⁹ depicted in Figure 9.

94 Laskowski et al., *Curr. Opin. Struct. Biol.*, **1998**, 8, 631-639

95 T. J. Oldfield, *J. Mol. Graph.*, **1992**, 10, 247-252

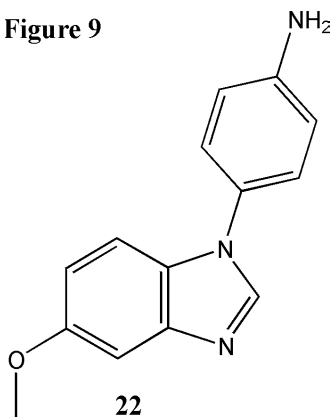
96 R. W. Hooft et al., *Proteins*, **1996**, 26, 363-376

97 M. J. Sippl, *J. Mol. Biol.*, **1990**, 213, 859-883

98 R. Luthy et al., *Nature*, **1992**, 356, 83-85

99 Brian D. Palmer et al., *J. Med. Chem.*, **1999**, 42, 2373-2382

Figure 9



The docking run provided doubtful results, because more than 2 possible orientations were predicted and two of them gave paragonable results. In order to discriminate the most favored orientation both complexes (called hear for semplicity dock1 and dock2) were minimized using Parm99¹¹¹ and GAFF¹⁰⁵ forcefields with the program Sander included in the Amber7 package and a short molecular dynamic simulation was performed using

the Generalized Born Solvation Model¹¹² in order to include solvent effects. Resulting structures were minimized again to a gradient of 0.1. Energy of both conformations was then evaluated semiempirically at PM5¹⁰⁰ theory level using the program MOPAC2002. The algorithm MOZYME implemented in MOPAC2002 is able to solve SCF large systems in a reasonable time, by the way of a linear scaling method. In this method, the time required for calculating the SCF increases linearly with the size of the system. The memory demand is also considerably reduced (for the larger systems run, by 97 to 98 percent of what would be needed conventionally). This allows systems of many thousands of atoms to be calculated rapidly¹⁰¹.

PM5 calculations predicted an energy difference $E_{g_{dock1}} - E_{g_{dock2}}$ of 12.348 Kcal/mol in favor of the dock2 complex, that was choosen as docking model. Compound 22 was then docked to this structure and a single conformation was predicted, with a binding mode in agreement with litterature results. All 2-pyridineacetamides reported in figure 1 has then been docked to PDGFRK model and results are summarized in Table 2 and represented graphically in Graph2.

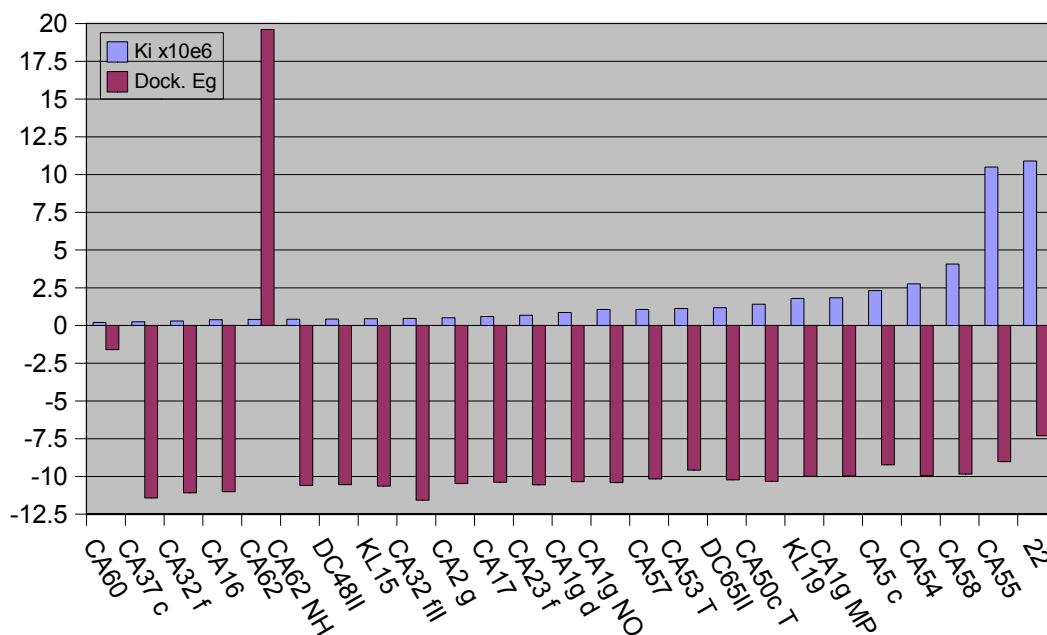
100J. J. P. Stewart, *Meth. J. Comput. Chem.*, **1989**, 10, 209

101J. J. P. Stewart, Mopac2002 program manual.

Table 2: *Docking of 2-Pyridinacetamides to PDGFRK; energy results and scoring*

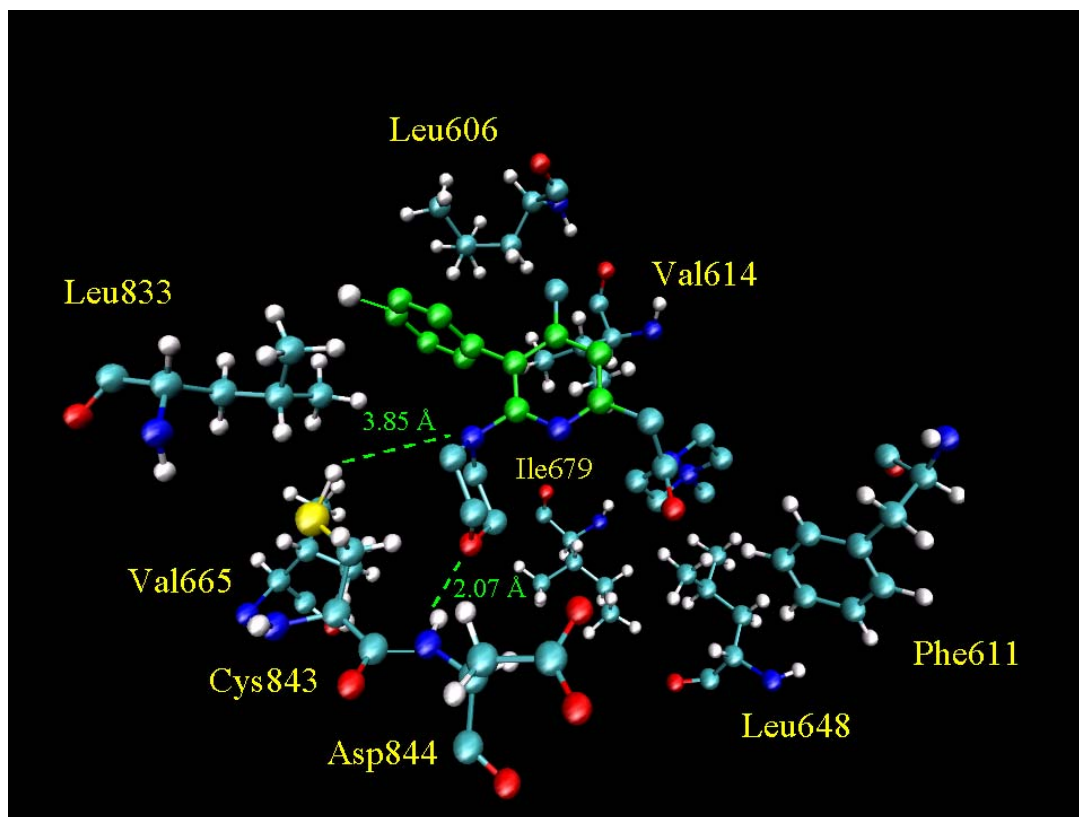
	Ki x10e6	Dock. Eg	Mol/clust	clust/rank
CA60	0.2	-1.6	21	1
CA37c	0.25	-11.42	27	3
CA32 f	0.3	-11.08	46	1
CA16	0.38	-11.01	43	1
CA62	0.4	19.61	6	24
CA62_NH	0.41	-10.6	10	2
DC48II	0.43	-10.54	10	1
KL15	0.45	-10.64	42	2
CA32fII	0.47	-11.57	3	8
CA2 g	0.52	-10.47	26	2
CA17	0.6	-10.38	23	6
CA23 f	0.68	-10.55	23	5
CA1g d	0.86	-10.34	29	2
CA1g NO	1.06	-10.4	35	5
CA57	1.06	-10.16	17	4
CA53 T	1.12	-9.58	18	2
DC65II	1.18	-10.23	10	11
CA50c t	1.41	-10.32	11	1
KI19	1.79	-9.99	11	14
CA1g MP	1.83	-9.97	19	4
CA5 c	2.32	-9.23	23	2
CA54	2.76	-9.94	14	8
CA58	4.07	-9.84	25	4
CA55	10.5	-9.02	9	17
22	10.9	-7.3	34	1

Graph 2: Docking of 2-Pyridinacetamides to PDGFRK; energy results and scoring



Results in this case are less clean, compared to those obtained from EGFRK. It can be noted from Table 2 that number of conformations per cluster are lower and cluster ranking is higher, however few compounds provided even better results: docking of CA32 f, CA16 and KL15 resulted in more than 40 conformations per cluster with an optimal ranking, while the same provided respectively 21, 12 and 25 conformations per cluster when docked to EGFRK . Furthermore all compounds having a significative clustering (e. g. more than 25 conformations/cluster) show the same binding mode, as represented in Figure 10 for compound CA32 f.

Figure 10: *Proposed binding mode for 2-Pyridinacetamides to PDGFRK.
Compound CA32 f is shown as example*



Observed interactions are:

- H-bond between C-6 linked morpholine oxygen and Asp844
- Electrostatic interaction between C-6 linked morpholine nitrogen and Cys843
- Hydrophobic interactions between aromatic C-5 substituent and aminoacids Leu606, Leu833 and Val665 forming an hydrophobic pocket.
- Hydrophobic interactions between Val614 and pyridine nucleus
- Hydrophobic interactions between the amidic substituent and a lipophilic pocket formed by Phe611, Leu648 and Ile679

Electrostatic interactions appear to be pretty weak, considering the relative long distance between morpholine oxygen and amidic N-H of Asp844 (2.07 Å) and the greater distance between morpholine nitrogen and the S-H moiety of Cys843 (3.85 Å). However hydrophobic interactions seems to be more important, as it can be better appreciated by the molecular surface representations reported in Figures 11 and 12, respectively inherent to docked literature compound 22 and compound CA32 f. Hydrophobic pocket formed by aminoacids Leu606, Leu833 and Val665 it's well evident on the left side of the pictures below, while Phe611, Leu648 and

Ile679 form the cavity hosting the amidic substituent of compound CA32 f and visible on the right.

Figure 11: *Literature compound 22 docked into the PDGFRK cavity.
A molecular surface representation*

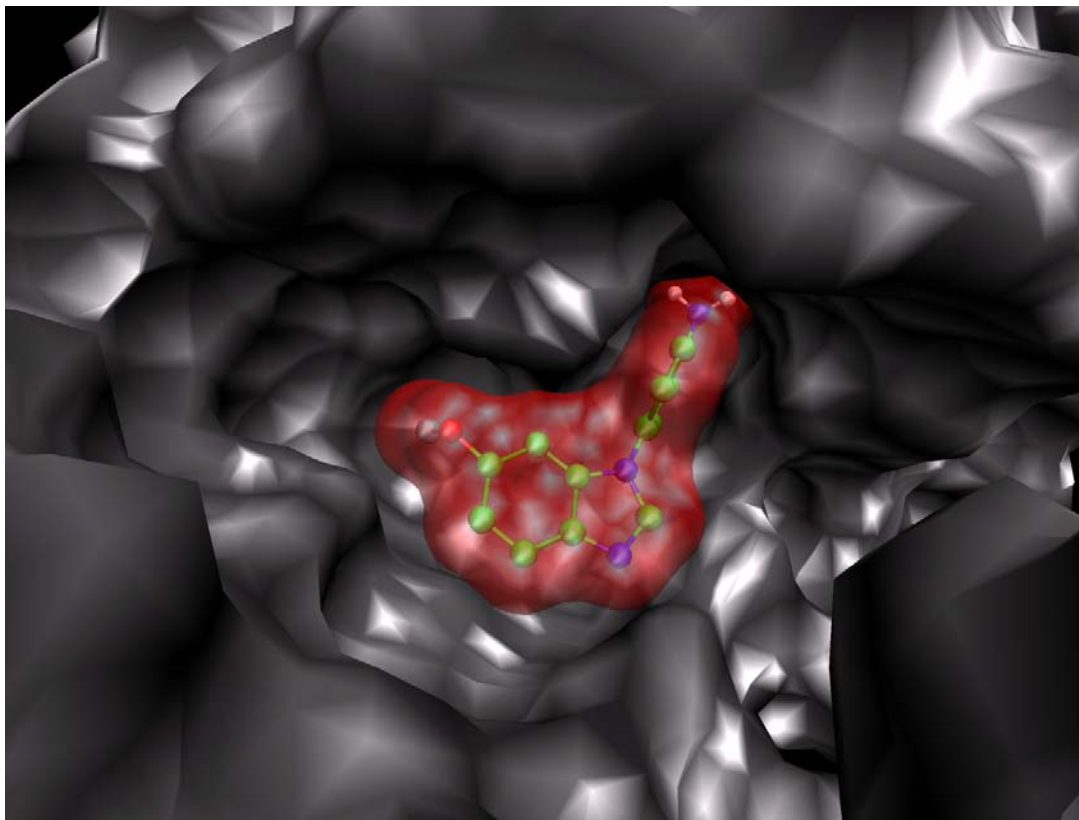
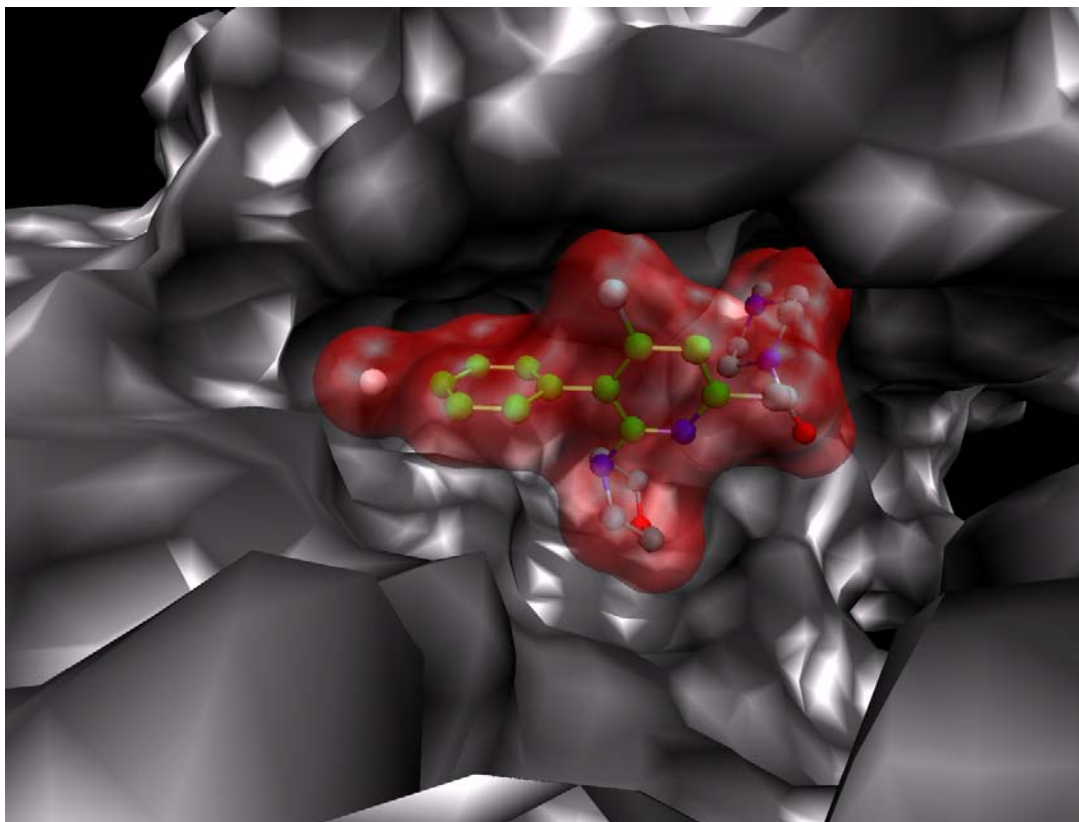


Figure 12: *Compound CA32 f docked into the PDGFRK cavity.*
A molecular surface representation



It could be noticed from *Figures 11* and *12* that compound CA32 f fits much better inside the binding site, assuming a conformation similar to an “embrace” that fill properly both right and left hydrophobic pockets respectively with the halosubstituted phenyl ring and the amidic N-methyl piperazine. This could explain the much lower K_i and docking energy values predicted by AutoDock if compared with the benzoimidazol derivative **22** represented in *Figure 9*.

However it could also be noticed that the C-4 methyl substituent and the C-4 itself seem to cause a steric clash with the upper part of the cavity. It could be interesting, in this case, to explore the docking behavior of a five membered ring pyridine bioisoster, such as a pyrrole, applying a classical QSAR technique for lead optimization.

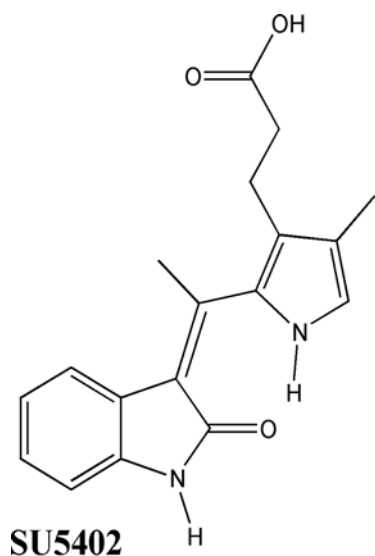
Docking of 2-Pyridineacetamides to VEGFRK

On the basis of sequence homology and overall domain structure, VEGFR belong to the platelet derived growth factor receptor family (PDGFR). CrYstal structure of VEGFR 2 has been resolved⁴¹ with a resolution of 2.4 Å and deposited as PDB file 1VR2. The crystal structure has been determined in an unligated but phosphorylated state. Analogous to other protein kinases VEGFR2 is folded into two lobes, with the active site placed in a cleft between the two lobes. Like other kinases, VEGFR2 contains other functionally important loop regions: the nucleotide binding loop (residues 841-846), the catalytic loop (residues 1026-1033) and the activation loop (residues 1046-1075). However authors state that the kinase activation loop phosphorylated on tyrosine 1059 was disordered and thus not properly resolved. Furthermore it can be noticed that a portion of it occupies a position inhibitory to substrate binding. Litterature does not report detailed binding mode for any known inhibitor, however authors report that crystal structure of VEGFR2 resembles most closely that of the catalitic domain of FGFR1 resolved by Hubbard et al. in complex with adenylyl methylenediphosphate (AMP-PCP)¹⁰² and in another work complexed to known inhibitors SU4984 and SU5402¹⁰³. VEGFR2 and FGFR1 share approximately 55% sequence identity, and a least square superposition of 82 C α positions of strands (β 1- β 5) of the N-terminal lobe or 152 C α positions of helices (α D, α E, α F, α G, α H, α I) of the C-terminal lobe between FGFR1 and crystal structure of VEGFR2 result in respective root mean square deviation (r.m.s.d.) values of 0.40 Å and 0.52 Å.

102M. Mohammadi, J. Schlessinger, S.R. Hubbard, *Cell.*, **1996**, 86, 577.

103S.R. Hubbard, J. Schlessinger et al., *Science*, **1997**, 276, 955-960

Figure 13



Hubbard reports that SU5402 is a selective inhibitor of FGFR1, because the hydrogen bond between the side chain amide of asparagine 568 in the hinge region of FGFR1 and the carboxyethyl group of SU5402, represented in *Figure 13*, confer this specificity. In PDGFRK the residue at the position corresponding to Asn568 is an aspartic acid, which at neutral pH will not form hydrogen bonds with the carboxyethyl group. However Hubbard reports also that VEGFR has an asparagine in this position and that SU5402 is a potent VEGFR

inhibitor in living cells.

For the reasons stated above we used molecular modelling and molecular dynamics tools to describe the binding mode of SU5402 to the active site of VEGFR2. This must be done in order to obtain informations useful to validate any result produced by docking of our 2-pyridineacetamides to VEGFR 2 kinase.

As the VEGFR2K cristal structure resolved by McTigue presented many disordered residues we constructed a complete homology model based on templates 1VR2 (VEGFR 2K) and 1AGW (FGFR1K) with the program Modeller6V2 using alignments generated with the program T-COFFEE as previously described for PDGFR model. A least square superposition of C α atoms of both reported cristal structures 1VR2 and 1AGW with our model resulted in respective root mean square deviation values of 0.54 Å and 1.15 Å, while a superposition of C α atoms of 1VR2 and 1AGW resulted in rmsd value of 0.99 Å, confirming that the generated model conserved properly the conformation of templates.

Ligand SU5402 was extracted from the PDB file (1FGI), hydrogens were added using Autodock Tools and molecular mechanics parameters were derived using with the program Antechamber¹⁰⁴ included in the Amber7 package⁵⁴, in conjunction

¹⁰⁴P. A. Kolman et al. "Antechamber, an Accessory Software Package for Molecular Mechanical Calculations", manuscript in preparation

with the GAFF force field¹⁰⁵. The AM1-BCC¹⁰⁶ procedure was employed for generating atomic charges. This model marries complementary features of already existing and readily available methods, namely AM1 atomic charges, the BCI approach¹⁰⁷, and ESPmethodologies¹⁰⁸. AM1 atomic charges are population quantities based directly on the occupancies of the atomic orbitals. They are not meant to reproduce the ESP or even the multipole moments of the subject molecule, and therefore they perform poorly in condensed-phase simulations if compared to ESP-derived charges¹⁰⁸. On the other hand, they can be calculated very quickly and they capture underlying features of the electron distribution of a molecule, including net charge and π -delocalization. Bond charge corrections (BCCs), which have been parameterized using standard least-squares fitting procedures¹⁰⁹ to reproduce the HF/6-31G ESP of a training set of molecules, are then added in order to emulate the HF/6-31G ESP. The parameterization algorithm used here is formally identical to that developed by Bush et al. in the consensus fitting of BCIs to HF/6-31G ESPs¹¹⁰. The AM1-BCC model uses few atom types because it takes advantage of the AM1 atomic charges to express subtle chemical variations of electron distribution, thus reducing the degrees of freedom in the parameterization obtaining a great numerical stability. The philosophy adopted is correcting semiempirical charges to reproduce desired properties. Charge is partitioned across bonds to correct for deficiencies encountered in the simple atomic population charges derived from the AM1 wave function. AM1-BCC uses a simple formal bond order derived from the bond topology of the molecule. In AM1-BCC, fitting directly to the short-range sampling of the ESP captures features of higher order electric multipoles important to characterize shorrange strong hydrogen bonding. Fitting directly to the HF/6-31G ESP as in AM1-BCC uses much more information per molecule, as well as embedding the necessary overpolarization of the ab initio wave function. This also allows the bond charge corrections the opportunity to make up for any systematic intrinsic deficiency in the semiempirical wave function compared to the ab initio 6-31G wave function. The AM1-BCC method thus combines the speed of a

105P.A. Kollman et al. "Development of General AMBER Force Field (GAFF)", manuscript in preparation

106A. Jayaram, B.L. Bush, D.B. Jack and C.I. Bayly, *J. Comput. Chem.*, **2000**, *21*, 132-146

107T. A. Halgren, *J. Comput. Chem.*, **1996**, *17*, 616

108U.C. Singh and P. A. Kollman, *J. Comput. Chem.*, **1984**, *5*, 129

109B.H. Besler, K.M. Merz and P. A. Kollman, *J. Comput. Chem.*, **1990**, *11*, 431

110B. L. Bush, C. I. Bayly and T. A. Halgren, *J. Comput. Chem.*, **1999**, *20*, 1495

semiempirical calculation with the efficiency of the BCI approach, aiming to achieve the quality of HF/6-31G ESP-fit charges.

The SU5402 ligand file parametrized in this manner was manually docked to VEGFRK keeping the same orientation described by Hubbard for FGFR1, and the complex was minimized with the program Sander included in the Amber7 package using parm99 force field¹¹¹. The minimized structure was then submitted to a short molecular dynamics run (100 ps). The generalized Born solvation model¹¹² was used in order to consider the solvent contributions. Authors report that this model could be less accurate if compared to explicit solvent boxes, but can achieve some advantages: it generally speed-up the simulation, certain processes may occur more quickly probably due to the lack of solvent frictional forces, and generalized Born simulations are also independent of the shape of the system and could thus be used to study various conformations of a molecule that cannot otherwise be addressed by explicit solvent simulations. An additional advantage of continuum models lies in the implicit averaging over the solvent degrees of freedom, so that this averaging does not need to be done by sampling the solute configurations explicitly. This greatly simplifies calculations of thermodynamic parameters, and can be used to examine free energy differences between different conformations of a molecule, or to obtain binding free energies.

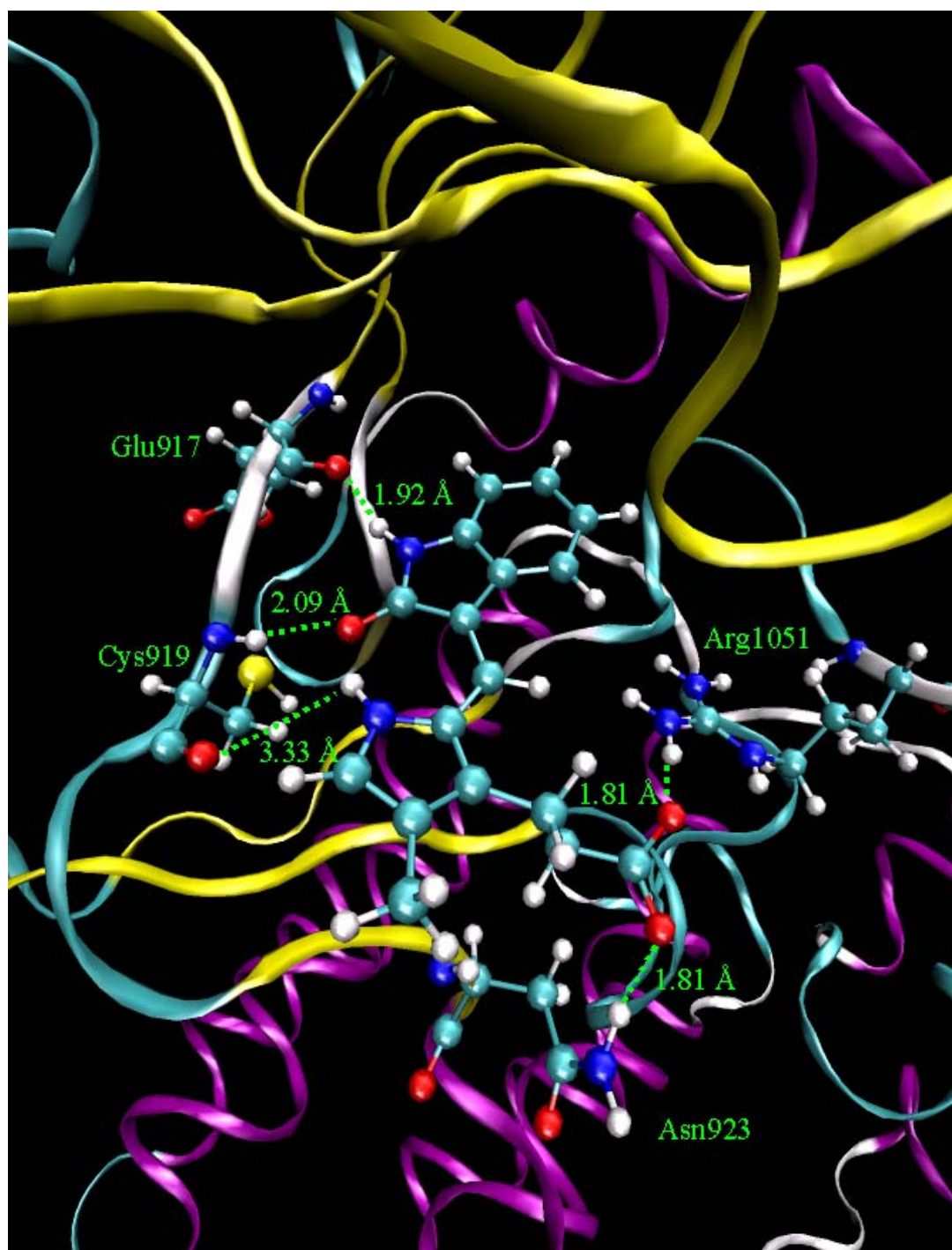
The final conformation obtained was then minimized again to a rmsd of 0.15.

Figure 14 depict resulted binding mode for SU5402 to VEGFR2K.

111P. A.Kollman et al., *J. Comput. Chem.*, **2000**, *21*, 1049-1074

112V. Tsui and D. A. Case, *Biopolymers (Nucl. Acid. Sci.)*, **2001**, *56*, 275-291

Figure 14: *Proposed binding mode for SU5402 to the active site of VEGFR2K*



Main interactions found resemble closely those described by Hubbard for FGFR1. In fact VEGFR2K presents a glutamic acid residue (Glu917) in the same position as found in FGFR1K (Glu562) forming an H-bond with SU5402. A similar H-bond

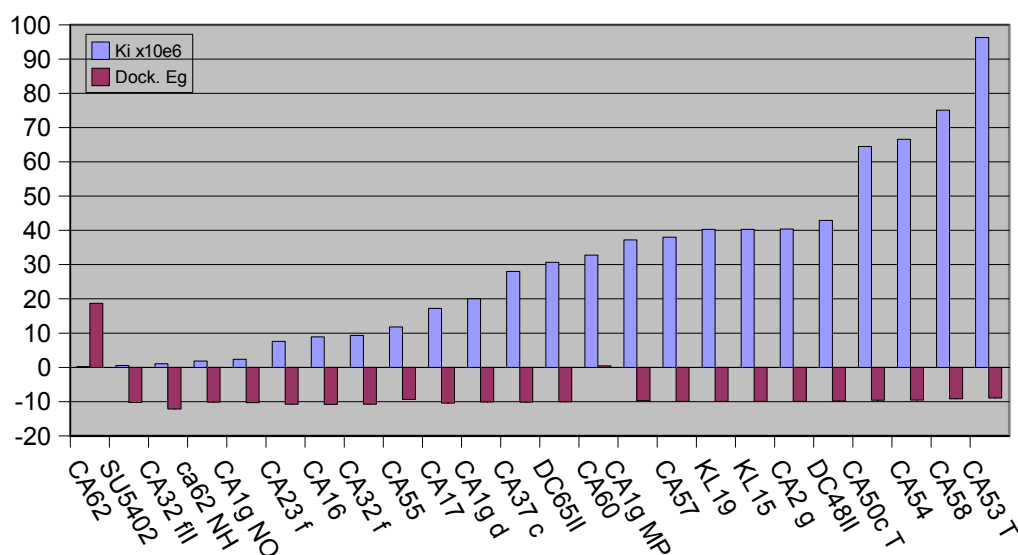
is present between the oxindole N-H and Glu917; alanine 564 of FGFR1K is replaced by a cysteine in VEGFR2K (Cys919) which likewise forms an H-bond between the N-H and the oxindole carbonyl and another H-bond between the amidic carbonyl and pyrrole N-H. Finally, VEGFR2K presents an asparagine residue in the same position as found in FGFR1K and as expected an H-bond is formed between the sidechain NH₂ and the ethylcarboxyl moiety of SU5402. Another H-bond not reported for FGFR1K seems to be formed between the ethylcarboxyl moiety of SU5402 and Arginine 1051 present in the activation loop of VEGFR2K, but such bond seems to be due to the particular conformation assumed by the activation loop in our model. At the same position of Arginine 1051 FGFR1K has a lysine residue. Those observations allowed us to choose SU5402 as reference inhibitor for docking of 2-pyridineacetamides to VEGFR2K.

Receptor was prepared as usual from the PDB file 1VR2; hydrogens were added to the receptor using Leap, included in the Amber7 package. The backbone was restrained in order to keep the original conformation, especially in the active site position. Structure minimization was then performed to a r.m.s.d. of 0.15 using the Generalized Born solvation model as implemented in the program Sander from AMBER package using the Amber99 force field. Resulted geometry was then processed with the program AutoDock Tools in order to merge non-polar hydrogens, add solvation parameters and generate pdbqs file requested by AutoDock3. Results are collected in *Table 3* and represented graphically in *Graph3*.

Table 3: *Docking of 2-Pyridinacetamides to VEGFR2K; energy results and scoring*

	Ki x10e6	Dock. Eg	Mol/clust	clust/rank
CA62	0.22	18.72	7	1
SU5402	0.56	-10.23	40	1
CA32 fII	1.08	-12.16	7	1
CA62 NH	1.86	-10.16	16	3
CA1g NO	2.4	-10.29	24	3
CA23 f	7.63	-10.76	12	1
CA16	8.91	-10.8	10	1
CA32 f	9.34	-10.74	13	1
CA55	11.8	-9.37	22	4
CA17	17.2	-10.4	23	1
CA1g d	20	-10.08	20	1
CA37 c	28	-10.17	8	9
DC65II	30.7	-10.04	13	4
CA60	32.8	0.46	4	4
CA1g MP	37.2	-9.74	12	1
CA57	38	-9.91	7	1
KL19	40.3	-9.92	9	6
KL15	40.3	-9.92	13	7
CA2 g	40.4	-9.9	9	8
DC48II	42.9	-9.83	16	3
CA50c T	64.5	-9.56	5	10
CA54	66.6	-9.54	11	2
CA58	75.1	-9.17	17	6
CA53 T	96.3	-8.92	8	6
CA5 c	122	-8.74	13	2

Graph 3: Docking of 2-Pyridinacetamides to VEGFR2K; energy results and scoring

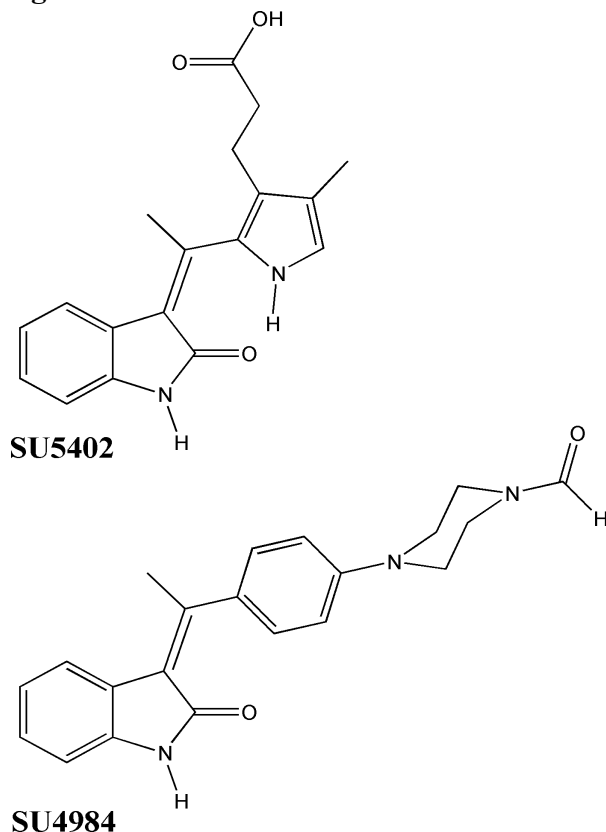


Observing results represented in the above *Table* and *Graph 3* it's pretty evident that 2-pyridineacetamides does not dock properly to the VEGFR2K active site. In fact compound CA62 wich is scored as first on the basis of predicted Ki (0.22×10^{-6}) is the worst considering docking energy (18.72 Kcal/mol), a value that suggest that the interaction is totally unfavored. Compounds CA32 fII, CA62 NH and CA1g NO are scored properly, but the number of conformations per cluster is pretty low and we were not able to describe a common binding mode after visual inspection of results. However SU5402 is predicted to be from 10 to 1000 fold more potent than our 2-pyridine acetamides, suggesting that the pharmacological activity of the latter could be due only in minimal part to VEGFR2K inhibition.

Docking of 2-Pyridineacetamides to FGFRK

FGFRK crystal structures bound to inhibitors SU5402 and SU4984 has been resolved by Hubbard¹⁰³ and deposited at the Protein Data Bank respectively as 1FGI and 1AGW. SU5402 and SU4984 are represented in *Figure 15* and present a pharmacophore moiety based on a 2-indolinone nucleus.

Figure 15



Authors report that autophosphorylation of FGFR1 induced by FGF was inhibited by the two compounds with IC_{50} s of 20 to 40 μ M for SU4984 and 10 to 20 μ M for SU5402. These two compounds also inhibited (with similar IC_{50} s) FGF-induced tyrosine phosphorylation of a 90-kD phosphoprotein (pp90) and mitogen-activated protein (MAP) kinases (ERK1 and ERK2), two intracellular events that are dependent on the kinase activity of FGFR1.

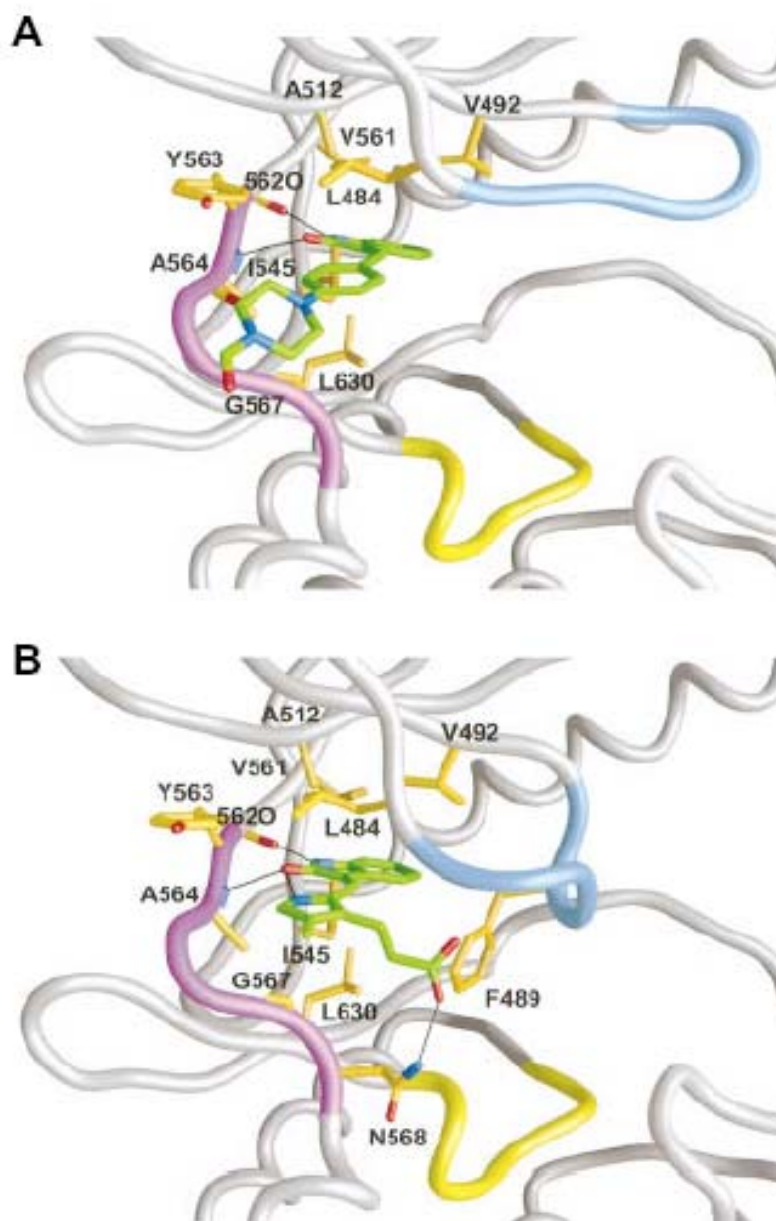
Both compounds also inhibited [³H]thymidine incorporation in response to FGF stimulation¹¹³. In similar experiments, SU4984 inhibited tyrosine phosphorylation of the platelet-derived growth factor (PDGF) receptor and of the insulin receptor¹¹⁴. In contrast, SU5402 did not inhibit tyrosine phosphorylation of the insulin receptor and was only a weak inhibitor of phosphorylation of the PDGF receptor. Neither compound inhibited the kinase activity of the epidermal growth factor (EGF) receptor, even at an inhibitor concentration of 200 nM.

113M. Mohammadi et al., *Mol. Cell. Biol.*, **1996**, 16, 977.

114S.J. Isakoff et al., *J. Biol. Chem.*, **1996**, 271, 3959.

Authors describe accurately the binding mode for both inhibitors and a schematic representation is depicted in *Figure 16*. **A** represent the observed binding mode for SU4984 while **B** represent SU5402 bound to the active site.

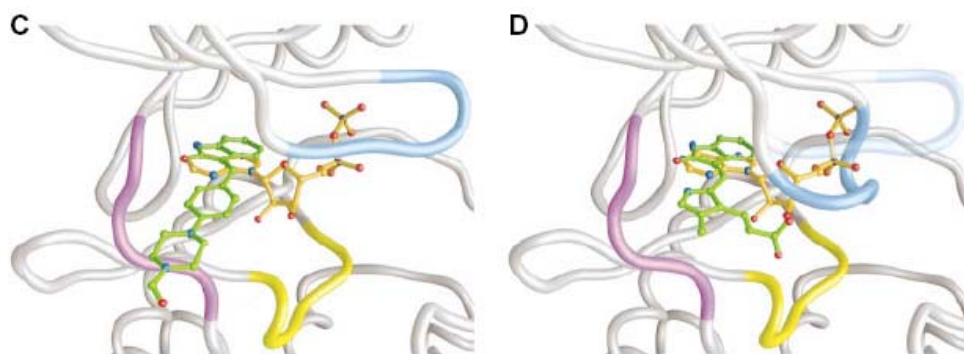
Figure 16



The inhibitors bind to FGFR1K in the same general region as ATP. The oxindole of the inhibitors occupies the same site as the ATP adenine, although the orientations

of the bicyclic ring systems differ by nearly 180°. The chemical groups attached to C-3 of the oxindole emerge from the cleft at approximately right angles to the direction taken by the rest of the ATP molecule. Neither inhibitor binds near the putative substrate peptide binding site in the COOH-terminal lobe of the kinase, indicating that these inhibitors do not compete with substrate peptide. The oxindole makes two hydrogen bonds to the protein backbone of FGFR1K: between N-1 of the oxindole and the carbonyl oxygen of Glu562, and between O-2 of the oxindole and the amide nitrogen of Ala564. Glu562 and Ala564 reside in the hinge region, the segment between $\beta 5$ and αD (residues 563 through 568) that connects the two lobes of FGFR1K. These same two backbone groups of FGFR1K make hydrogen bonds to N-1 and N-6 of the ATP adenine¹⁰². *Figure 17* shows superpositions of SU4984 (C) and SU5402 (D) with ATP.

Figure 17



The cavity in which the oxindole (or adenine) binds is lined with numerous hydrophobic residues including Val492, Ala512, Ile545, Val561, Ala564, and Leu630. In addition, Leu484 and Tyr563 provide a hydrophobic environment for the ring proximal to the oxindole a phenyl in SU4984 and a pyrrole in SU5402. The remainder of the interactions between the two inhibitors and FGFR1K differ. The phenyl ring of SU4984 makes an oxygen-aromatic contact with the carbonyl oxygen of Ala564. The piperazine ring of SU4984 is in van der Waals contact with Gly567, a highly conserved residue in protein kinases. The terminal formyl group of SU4984 seems to be not important for inhibition, as authors state that a compound lacking the formyl group is as potent as SU4984. In the FGFR1K-SU5402 structure, N-19 of the pyrrole ring makes an intramolecular hydrogen bond with O-2 of the oxindole. The methyl group of the pyrrole ring is in van der Waals contact with Gly567, and the carboxyethyl group attached to C-3' of the pyrrole ring is

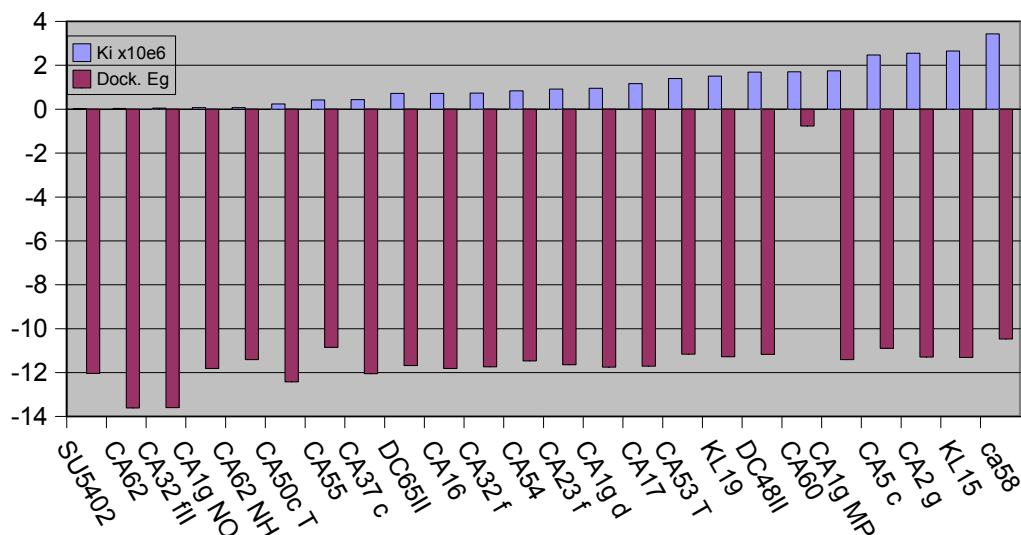
hydrogen-bonded to the side chain of Asn568, the last residue in the hinge region. The interactions between SU4984 and FGFR1K observed in the crystal structure would not appear to confer specificity: hydrogen bonds are made to backbone groups, and many of the hydrophobic interactions are with conserved residues in the PTK family. Consistent with the structural results, SU4984 exhibited rather broad specificity. In contrast, SU5402 showed specificity for FGFR1. The hydrogen bond between the side chain amide of Asn568 in the hinge region and the carboxyethyl group of SU5402, and the conformational change in the nucleotide-binding loop stabilized by such interaction confer this specificity. However, as stated above, the vascular endothelial growth factor (VEGF) receptor has an asparagine at this position and SU5402 is a potent inhibitor of VEGFR.

Due to its quite absolute specificity for FGFR1K and to the major potency if compared with other inhibitors SU5402 was chosen as reference compound for docking of 2-pyridinacetamides to FGFR1K, and consequently 1FGI chain A was used as PDB receptor file. Results are then reported in *Table 4* and *Graph 4*.

Table 4: *Docking of 2-Pyridinacetamides to the FGFRK active site:
energy results and scoring*

	Ki x10e6	Dock. Eg	Mol/clust	clust/rank
SU5402	0.03	-12.04	39	1
CA62	0.03	-13.61	5	3
CA32 flI	0.05	-13.6	8	12
CA1g NO	0.07	-11.81	19	1
CA62 NH	0.07	-11.41	13	11
CA50c T	0.24	-12.42	5	1
CA55	0.42	-10.85	8	4
CA37 c	0.44	-12.05	19	4
DC65II	0.72	-11.68	11	7
CA16	0.72	-11.81	14	10
CA32 f	0.74	-11.74	15	10
CA54	0.84	-11.47	11	1
CA23f	0.91	-11.64	10	10
CA1g d	0.95	-11.75	23	3
CA17	1.16	-11.71	20	4
CA53 T	1.4	-11.16	11	4
KL19	1.51	-11.28	16	8
DC48II	1.69	-11.17	14	10
CA60	1.7	-0.77	11	15
CA1g MP	1.75	-11.41	21	4
CA5 c	2.47	-10.89	9	3
CA2 g	2.55	-11.29	20	7
KL15	2.65	-11.31	16	8
CA58	3.43	-10.47	11	9
CA57	4.92	-10.95	13	10

Graph 4: Docking of 2-Pyridinacetamides to the EGFRK active site:
energy results and scoring



Observing results represented in the above *Table 4* and *Graph 4*, as expected, it's we can state that 2-pyridineacetamides does not dock properly to the FGFR1K active site, behaving quite similar as in the VEGFR2K case. In fact compound CA62 is still scored well on the basis of predicted Ki (0.03×10^{-6}) and in this case also considering docking energy (-13.61 Kcal/mol). Compound CA32FII is scored even better by docking energy (-13.66 Kcal/mol) and shows a predicted Ki of 0.05×10^{-6} . Even other 2-pyridinacetamides present correct values of predicted Ki and docking energy, however they show particularly low values of Molecules/Cluster and most significative cluster ranking. Furthermore a visual inspection of results with Autodock Tools revealed that all 2-pyridineacetamides does not dock inside the FGFR1K active site, but tend to bind to the activation loop portion, except for CA62 wich superpose the N-benzylpiperazino moyety with the oxindole ring of SU5402 and seems to form an H-bond of about 2.34 Å with Alanine 564. However, results obtained by docking of 2-pyridineacetamides to FGFR1K (1FGI) suggest that FGFR1K inhibition give probably just a small contribution to the overall pharmacological activity of our compounds.

3. Experimental

Preparation of receptor's files:

When available, crystal structures have been used for docking, otherwise homology models have been generated.

Crystal structures of EGFRK (PDB code 1M17), VEGFRK (PDB code 1VR2) and FGFRK (PDB code 1FGI) were downloaded from the Protein Data Bank⁶⁰. If multiple files were available, it has been chosen the one with the best crystallographic resolution. A careful analysis of the PDB files is necessary in order to evidence eventual errors, missing aminoacids or mutated residues. Ligands were removed from the file and if dimers were present only one chain was considered. All waters present in the file were controlled, evaluating their position and any eventual interaction with the active site aminoacids. If a critical water was found, this was considered as a part of the active site. Two test runs were then made, including or not including water, using reference compound having known binding mode to assess the real importance of water during docking runs.

All hydrogens were added to the receptor using the program Leap, included in the Amber7⁵⁴ package. Restraints (20kcal/mol) were added to the backbone in order to keep the original conformation. Structure minimization was then performed to a r.m.s.d. of 0.15 using the Generalized Born solvation model¹¹² as implemented in the program Sander from Amber7 package. parm99¹¹¹ force field was used for minimization. Amber charges were then used for all receptors during docking runs. Resulted geometries were then processed with the program AutoDock Tools in order to merge non-polar hydrogens, add solvation parameters and generate pdbqs file requested by AutoDock3⁵⁰.

The crystal structure of PDGFRK has not been resolved yet, so the receptor was constructed by homology modelling with the program Modeller6V2⁶¹. Suitable templates have been individuated using the routine "SEQ_SEARCH" as implemented in Modeller6v2. PDB files 1VR2 and 1AGW chain A has been chosen as templates for the catalytic domain, because it was our interest to study the kinase receptor in its activated form, while the SH2 domain of c-SRC has been used as template for the long interlobar insertion. 25 models were generated and models were checked using program Procheck⁹⁴. The best model was chosen and has been treated like other PDB files. Since the first docking run with a known inhibitor

provided two binding modes (reference compound 22), resulted complexes were submitted to a 50ps molecular dynamic simulation. Parm99¹¹¹ force field was used for the protein while GAFF¹⁰⁵ force field was used for benzoimidazole **22**⁹⁹. Missing parameters were derived with the BCC¹⁰⁶ procedure using program Antechamber¹⁰⁴ from the Amber7 package. The final model was minimized to a r.m.s.d. of 0.15 and used for docking.

An analogue procedure was employed for constructing the model of VEGFR2K from template PDB files 1VR2 and 1AGW; the model has been used for description of the binding mode of SU5402 to the active site of VEGFR2K, while 1VR2 was used for docking purposes.

Preparation of ligand's files:

Ligands were constructed using program LinMopac from Fujitsu and minimized at the semi empirical AM1⁶⁴ level of theory to a gradient norm of 0.01. Charges derived from electrostatic potential¹⁰⁸ were then calculated *ab-initio* at the RHF/6-31G* level of theory using the program GAMESS²¹ following the Merz-Kollman procedure⁶⁵, where the electrostatic potential is calculated on the Conolly surface and point charges are then fitted in order to reproduce the total charge using the program Resp from the Amber7 package. Structures obtained were then treated with the program Autotors implemented in AutoDock Tools package, in order to merge non polar hydrogens and to select bonds allowed to rotate. Every selection was left active, including amidic bonds. *Ab-initio* calculations and protein molecular mechanics minimizations were performed on a HP64000 machine at CILEA²⁴; semi empirical calculations were performed with the commercial package MOPAC2002 from Fujitsu on a PC-Linux workstation. File conversions between different formats has been done using VEGA¹¹⁵, Babel¹¹⁶ or Molden¹¹⁷

Autodock parameters:

Grids for docking evaluation were computed using the program AutoGrid3 included in the Autodock3 distribution. Grid center was centered on the active site and 80x80x80 grids with a spacing of 0.275 were calculated. Atomic affinity maps were computed for all atoms potentially present in ligands, including carbon, aromatic carbon, nitrogen, oxygen, sulfur, phosphorus, bromine, chlorine and fluorine.

115A. Pedretti, L. Villa, G. Vistoli, *J. Mol. Graph.*, **2002**, 21, 47-49

116P. Walters and M. Stahl, <http://smog.com/chem/babel>

117G. Schaftenaar and J.H. Noordik, *J. Comput.-Aided Mol. Design*, **2000**, 14, 123-134

Floating point electrostatic potential grid maps were also computed, and a distance dependent dielectric constant was chosen.

Autodock3 parameters were set in order to obtain greater accuracy. Hybrid GA-LS Lamarckian genetic algorithm was chosen and following parameters were modified from defaults: population size was set to 100 (ga_pop_size 100), 2.5×10^6 energy evaluations were requested (ga_num_evals 2500000) and 50 trials per run were set (ga_run 50). Pseudo-Solis & Wets parameters were used for local search and 300 iterations of Solis & Wets local search were imposed (sw_max_its 300). Other parameters were used as default for AutoDock Tools.

Both Autogrid and Autodock computations were performed on a HP64000 machine at CILEA.²⁴

Analysis of results and visual inspection of docked conformation were performed with AutoDock Tools or with the program VMD¹¹⁸ on a PC-Linux workstation.

¹¹⁸W. Humphrey, A. Dalke and K. Schulten, *J. Molec. Graphics*, **1996**, *14*, 33-38

Chapter 4

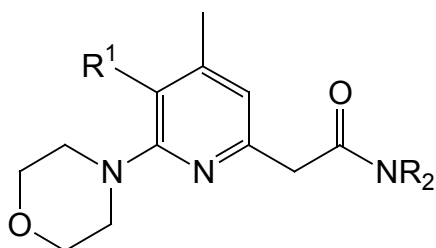
Conclusions

Conclusions

On the basis of results obtained by this research project we can conclude that:

1. The reactivity of amidino derivatives of the triacetate lactone has been thoroughly explored, leading to the design, realization and validation of a new synthetic path for the preparation of pyridine amido derivatives. The key step is the selective nucleophilic attack at the C-2 position of the amidino-pyrone leading to ring opening followed by a rearrangement controlled by the amidinic carbanion to afford 2-pyridineacetamides. The reaction is economic and widely applicable as demonstrated by the large number of derivatives prepared, generally with good yields. Quantum mechanical calculation based on the evaluation of the electrostatic potential of the amidino-pyrone reactant confirmed the observed synthetic behavior.

The general formula of 2-pyridineacetamides synthesized is represented below



2. Results from a pharmacological screening conducted on 2-pyridine acetamides synthesized inside this project revealed an inhibitory activity toward proliferation of rat's aorta smooth muscular cells. The response to the drug seems to be higher if cellular proliferation is induced by growth factors, in particular EGF and PDGF. All active compounds are able to raise the SMC's doubling time and to inhibit the incorporation of [³H] thymidine, confirming that the pharmacological effect is due to reduced DNA synthesis and not to cell death. Time course experiments evidence that the antiproliferative effect is manifested during the first moments of the G₁ phase, underlining both cycle and phase specificity and thus supporting an interference with biochemical paths controlled by growth factors as EGF and PDGF.
3. Structure-activity relationships have been evaluated. Both R¹ and NR₂ substituents have been shown to be critical for pharmacological activity. The

contribution to the potency by R¹ and NR₂ can be summarized as

R¹: $p\text{-Br-Ph} \geq 2,4\text{ diCl} > p\text{-CH}_3\text{O-Ph} > p\text{-Cl-Ph} > p\text{-F-Ph} > \text{Ph}$

NR₂: diethylamine > morpholine > N-methylpiperazine > piperidine

The potential binding mode of 2-pyridineacetamides has been investigated and proposed on the basis of docking and molecular modeling calculations, suggesting that preferred targets are the tyrosine kinase receptors EGFR and PDGFR, where our amides dock correctly in the ATP binding site. Estimated K_is and docking energies are aligned to those for known literature compounds. Calculations conducted on kinases different from the above mentioned didn't furnish acceptable results, suggesting a certain selectivity toward EGFR and PDGFR.

Acknowledgments

Thanks to all the people that directly or indirectly have been involved in the realization of this doctoral thesis. In particular I'm grateful to:

- Prof. P. Trimarco for supporting and leading me during this research experience.
- Prof. A. Corsini for pharmacological experiments.
- Prof. L. Scapozza, Prof. G. Folkers and the all group for allowing me to perform part of this research project at **ETH**, *Department of Applied Biosciences*, Zürich (CH)
- Dr. A. Cavalli and Dr. Stefano Moro for useful discussions
- Dr. A. Pedretti and Dr. G. Vistoli
- CILEA for computational time and technical support for parallel calculations
- MIUR “Progetto Giovani” for financial support.
- Authors of software: Amber, AutoDock, GAMESS, Gaussian98, gOpenMol, Modeller, Molden, Mopac, VEGA, VMD and OpenOffice. Thanks to Linus Torwald and all the developers of Linux operating system and special thanks to all the people and companies involved in the Open Sources projects.